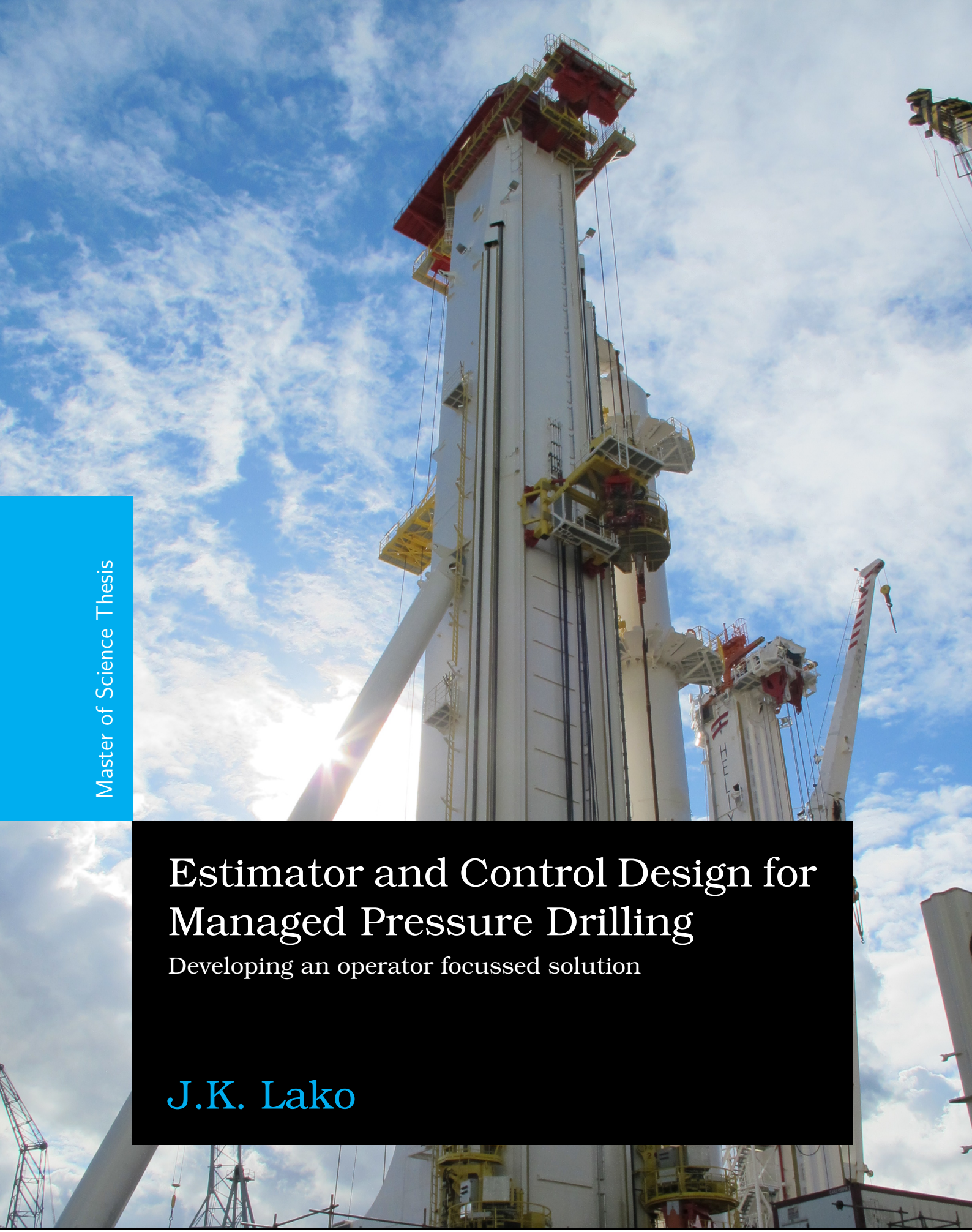

Master of Science Thesis

Estimator and Control Design for Managed Pressure Drilling

Developing an operator focussed solution

J.K. Lako

TU Delft Delft University of Technology

Delft Center for Systems and Control

Estimator and Control Design for Managed Pressure Drilling

Developing an operator focussed solution

Master of Science Thesis

For the degree of Master of Science in Systems and Control at Delft University of Technology

J.K. Lako

January 20, 2017

Faculty of Mechanical, Maritime and Materials Engineering (3mE) · Delft University of Technology

The work in this thesis was supported by Huisman Equipment. Their cooperation is hereby gratefully acknowledged.

Copyright © Delft Center for Systems and Control (DCSC)
All rights reserved.

Abstract

Managed Pressure Drilling (MPD) is a new drilling technique that originated from conventional drilling. This technique offers a solution to drill challenging wells and to increase drilling efficiency. It is a drilling process to precisely control the annular hydraulic pressure profile and to keep the bottomhole pressure (BHP) within its limits. Bottomhole measurements are not available, therefore, other methods have to be found to acquire bottomhole information in order to control the BHP.

For these reasons, the objective of this thesis is to develop an automated control system that is able to estimate and control the BHP. This system should be able to deal with nonlinearities as well as unmeasured and varying parameters. In addition, it should only use surface measurements, since transmission of downhole measurements is either expensive or too slow. Furthermore, the system should be easy to use for the operators working on the rig site.

In order to attain this objective, the MPD process, current control solutions and challenges were investigated during a literature study. Afterwards, during the research phase, a model of the well is developed and an additional validation model is designed. Furthermore, a case study is presented in order to evaluate the performance of the control system. Two estimators are designed based on the well model in order to estimate the BHP and other unmeasured parameters, namely an adaptive observer and an Extended Kalman-Bucy filter. Subsequently, the estimated BHP is used in the next phase to develop a controller. Two practical control solutions, a PI and LQR controller, are implemented on the MPD system.

Finally, the performance of the MPD control system is evaluated using the developed validation model. This report concludes that the developed control system, suitable for operator usage, is able to control the BHP and secondly, that this can be done by using only surface measurements.

Table of Contents

List of Figures

Preface

This Master of Science graduation thesis was conducted at Huisman Equipment B.V. in the pas eleven months. The current state of practice for MPD was evaluated and possible opportunities for Huisman were discussed. This research was possible because of the request for research in this subject by dr.ir. Jelmer Braaksma and Huisman Equipment. Therefore I would like to thank Huisman for the opportunity to work on such an innovative project and providing me with the required information.

I would like to thank my daily supervisor from Huisman Equipment, ir. Wouter Rijkee, for providing his knowledge, helping me the structure the research and reviewing my work critically. I would also like to thank my academic supervisors at Delft University of Technology prof.dr. Robert Babuška and prof.dr.ir. Nathan van de Wouw for their assistance during this research.

Delft, University of Technology — J.K. Lako
January 20, 2017

Chapter 1

Introduction

As living standards improve and countries develop, energy demand grows rapidly. This forces engineers and specialists to discover new ways to produce energy or better methods to recover depleted wells. Many current hydrocarbon resources are economically undrillable using conventional drilling methods [6]. MPD offers a solution for drilling in such challenging wells to improve economic benefits and safety. Furthermore, it provides an increase in efficiency in regular wells compared to conventional drilling. MPD is a drilling process to precisely control the hydraulic pressure profile and to keep the BHP within its limits. Bottomhole measurements are difficult and expensive, and even if bottomhole information is available via mud-pulse telemetry it contains a lot of noise and has a large time delay. Therefore, other methods have to be found to acquire bottomhole information in order to control the BHP. So far, different hydraulic pressure models have been proposed to describe the drilling system and studies have been performed on different methods to control the BHP. Also, research has been done on which components can be used in a MPD control system and how the most essential actuator, the choke valve, can be controlled adapting to nonlinear behaviour of the flow and the valve. Despite of all the studies that have been carried out, MPD is still not widely used and non-productive time (NPT) due to drilling problems is still increasing drilling costs. Moreover, in unfortunate cases, a kick can occur, meaning that oil, gas or water enters the well during drilling because mud pressure is below the pore pressure. This can even lead to a blow-out, which happened on the BP Deepwater Horizon and had catastrophic results [7]. Applying MPD in drilling processes has only just started and therefore, a lot of research is left on how to apply the process in practice.

The research of this thesis is performed in cooperation with Huisman Equipment. Huisman is currently developing a control solution that makes use of a complex hydraulic pressure model to precisely predict the BHP. Huisman will focus on applying the MPD process in easily accessible wells like onshore wells in order to improve efficiency in these drilling operations (compared to conventional drilling). This particular research, aimed at designing a control system that is easy to operate, so that little or no information is required from the operator, might therefore be an interesting alternative for Huisman Equipment.

A summary on the fundamentals of MPD is presented in this introduction. In addition, the challenges that are encountered in the design of an observer and controller for the MPD are described in Section 1-2. The objectives of this thesis are presented and in the end, an outline of the report is given.

1-1 Fundamentals of managed pressure drilling

The International Association of Drilling Contractors describes MPD as follows: "An adaptive drilling process used to precisely control the annular pressure profile throughout the wellbore. The objectives are to ascertain the downhole pressure environment limits and to manage the annular hydraulic pressure profile accordingly. MPD is intended to avoid influx of formation fluid to the surface." [8].

Before explaining the principles of MPD it is essential to explain the terms mentioned in this citation. The meaning of the adaptive drilling process is that there is no standard technique on how to apply MPD and it varies per application. Drilling experts decide on how to perform the MPD process by looking at the objectives of the well and other influencing factors like rig type, field geology, reservoir type, pressure profile and costs [9]. The annular pressure profile is the pressure in the wellbore from the bottomhole up to the annulus. The downhole pressure environment limits, also known as the drilling window, is described as the area between the fracture pressure and the pore pressure or the well-bore stability as can be seen in Figure 1-1.

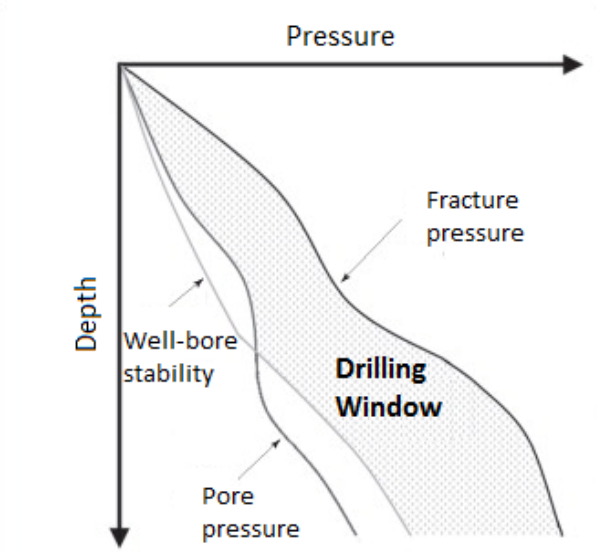

Figure 1-1: Drilling window where the upper limit is the fracture pressure and the lower limit is either the pore pressure or the well-bore stability [1].

Definitions of the pore- and fracture pressure and well-bore stability will now be explained. The fracture pressure forms the base for the highest practical annular pressure and can be described as the pressure a formation can endure before it fails or splits. If the rocks fractures, the mud flows into the rock formation, which is called loss. The lower critical pressure is often

determined by the pore pressure (the pressure of fluid in pore spaces) but in directional wells, the well-bore stability, being a function of stress and well direction, can also define the lower critical pressure [1]. If the pressure in the annulus or BHP is below the pore pressure, gas bubbles can flow into the mud stream which is called reservoir influx and can eventually cause a kick or a blow-out. A bottomhole or annular pressure below the well-bore stability can cause the well to collapse.

The drilling window, represented in Figure 1-1, has even more narrow margins when in deep-water since seawater overburdens the well [10]. Also, in more mature fields, the drilling windows becomes narrower since pore pressure, fracture pressure and overburden profiles will change due to production and depletion. These aspects make it harder to stay within the drilling window while still preventing lost circulation or influx.

Typical MPD wells make use of three devices, normally not used with conventional drilling; the rotating control device (RCD), a backpressure pump and the multiphase separator. The RCD is placed below the drill floor and above the blowout preventer (BOP) to close the system, whereas conventional drilled wells are open systems. The RCD functions as a seal around the drillpipe and simultaneously diverts formation and lets drilling fluid flow to the multiphase separator. The backpressure pump is used for additional (back)pressure to balance the annular pressure to maintain constant BHP. The multiphase seperator is used to seperate the particles from the mud, whereafter the mud can be re-used. Transferring from a conventional drilling set-up to a MPD system is relatively easy since the RCD is installed on top of the BOP, and the backpressure pump and multiphase separator can be installed parallel to the regular choke manifold. A simplified graphical flow scheme of MPD can be seen in Figure 1-2.

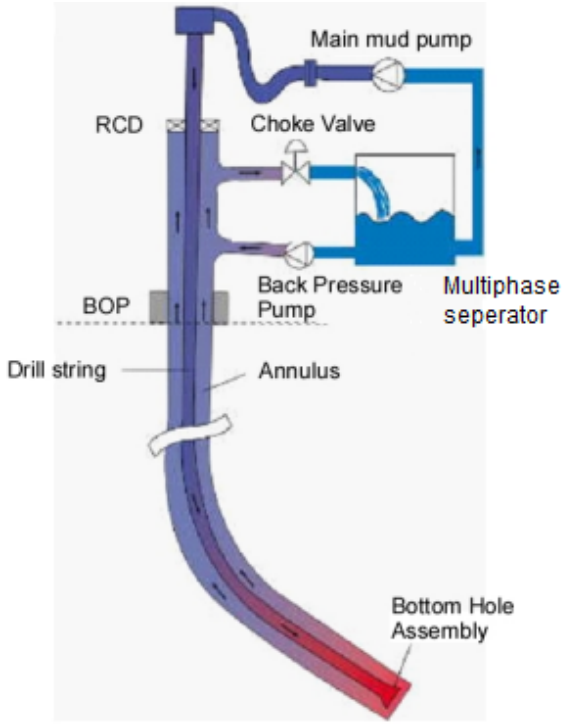

Figure 1-2: Schematic overview of flow in a managed pressure drilling system [2].

During MPD, the mud or another drilling fluid (fluid used to drill the wellbore) is pumped into the top of the drillstring from where it flows through the drilling bit in the open well bore. Partitions of the formation (cuttings) are transported up to the surface through the annulus along with the mud. When the surface is reached, the mud exists the annulus through the choke, below the RCD [11], and mud is then is separated from the particles in the multiphase separator. The purified mud flows to the storage tanks from where it is recirculated into the drill string. The pressure at the bottomhole varies during normal drilling operations but even higher variations are created during special operations such as tripping (upward or downward pipe movement) and making new drillstring connections. So during these operations, the BHP should be precisely monitored.

From the information described above, it can be summarized that the benefits of controlling the pressure in the well, compared to conventional drilling are:

- Improved drillability, by improving the accuracy of the drilling process, offering a solution for many challenging wells that are undrillable with conventional drilling [12].
- Lower costs, by improving the efficiency of the drilling process and creating the opportunity to drill in more (difficult) wells, thus to increase oil production.
- Higher safety, by reducing the operator workload, risks for blow-outs or kicks and moving (most of) the workforce to a control panel instead of working on the rig.

1-2 Challenges in managed pressure drilling

The MPD technique evolved from conventional drilling in order to control BHP and pressure throughout the wellbore as described in the section above. Controlling the BHP is throughout the MPD process is not as straightforward as it seems, in practice, some challenges arise that will be tackled in this research.

From literature available, it can be deduced that the MPD control problem can be split up into two problems; retrieving bottomhole information so that the BHP can be estimated and controlling the actuators, in particular the choke valve, to control the BHP.

The first problem deals with receiving downhole information. A common problem in MPD is that bottomhole information is not directly available and even when it is available (through e.g. mud-pulse telemetry), it contains a lot of measurement noise and has a large time delay, therefore these bottomhole measurements can not be used in real-time in the control system. Measurement systems that can be used in real-time to control the BHP, such as wired drillpipe, are too complex and expensive and will thus not be considered in this research. Therefore the control system to be designed must not rely on bottomhole measurements and an observer/estimator shall be used instead to estimate the BHP.

To control the actuators, a control system will be designed in order to keep the BHP within the drilling window. The choke valve is used as an actuator to control the BHP. Optionally, other actuators such as the backpressure pump can be involved in the control system.

1-3 Thesis objectives

The aim of this research project is to develop a controller for the MPD system. The objective is to control the BHP and the pressure throughout the wellbore with a control system that is easy to use for the operators. In order to achieve this goal in a structured way, the objective is split up into sub-objectives:

- Designing a hydraulic well model that accurately simulates the well dynamics.
- Developing an observer/estimator as a solution to overcome the problem of having no real-time bottomhole measurements.
- Designing a control system to actuate the choke valve in order to control the BHP. The system should be easy to operate, thus little or no input parameters should be required from the operator.
- Simulating the control system, including the BHP estimator, to decide on which observer-controller combination performs best.
- Validating the observer and controller on a validation model to examine performance and robustness.

1-4 Approach and outline

In order to achieve the objectives described above, the following outline is chosen. First of all, modelling is done in Chapter 2, where a well model suited for observer design and a validation model will be defined. Furthermore, a case study will be specified in order to test the control system on different aspects and analyze its performance. Then, in Chapter 3, two estimators for the BHP will be presented. Subsequently, the design of a controller will be described in Chapter 4 and the usability for the operators will be discussed. In Chapter 5, the control system will be validated using a validation model and results will be discussed. The final chapter discusses the conclusions and suggests recommendations for further research or improvements.

In Figure 1-3 it is shown how the chapters are connected.

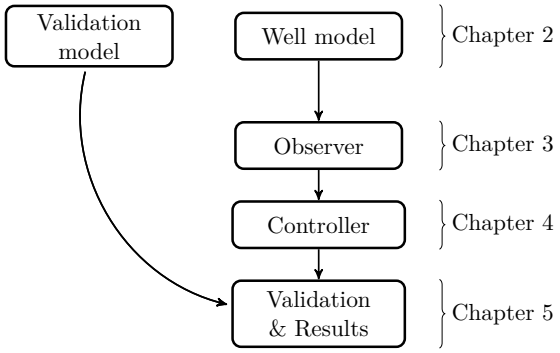

Figure 1-3: Structure of the thesis.

Chapter 2

Modelling

In order to understand the MPD process and to design a suitable control solution, a model that describes the dynamics of the well is required. Different approaches on modelling the well can be found in literature.

In this thesis, a lumped parameter model (one dimensional state space) will be used, consisting of a set of Ordinary Differential Equations (ODE's). The well can also be described as a distributed parameter model (infinite dimensional state space) but, due to complexity in setting up and calibrating this model, it is outside the scope of this project. A lumped parameter model for the hydraulics of the well is derived from standard Partial Differential Equations (PDE's) which are based on mass and momentum balances. The PDE's can be simplified to sets of ODE's. This chapter describes an approach for a simple lumped parameter model in Section 2-1. Furthermore, in Section 2-2, a validation model is developed, which is divided into multiple compartments and has increased complexity in describing the systems dynamics. These models are simulated in MATLAB/SIMULINK. The simpler version of the lumped parameter model, consisting of only three equations, is used as a base for designing the observer and controllers. The more complex lumped parameter model will be used to validate the designed (MPD) control system.

Simplifications in modelling the well will be made for two reasons. Firstly, the focus of Huisman will be on designing a system that is used to improve the efficiency of drilling relatively easy accessible wells, therefore a relatively simple well is assumed. Secondly, the system to be designed should be easy to implement and to use, hence the observer should only require the most essential dynamics of the system and simplifications are done regarding flow and fluid properties. The following assumptions are made (for both the simple and the validation model):

- Drilling is done onshore (no heave is simulated).
- Wells are drilled vertical (directional drilling is disregarded).
- Temperature and viscosity effects are neglected.

- The flow is one dimensional (from inlet to outlet) and radially homogeneous.
- The fluid accelerates as a stiff mass.
- The flow is turbulent throughout the well.

In order to make estimations of the BHP, the well models make use of parameters that are unmeasured or uncertain, this estimation problem is outlined in Section 2-3. Furthermore, possible situations during drilling need to be simulated in a later stage to examine the performance of the MPD control system. These situations are defined in Section 2-4.

2-1 Well model

2-1-1 Fundamental equations

A lumped parameter hydraulic model was developed by Kaasa [13] and contains only the dominant dynamics of the system, it simplifies the well model into two sections; the drillstring and the annulus. The fundamental equations from [13] that describe the hydraulics of the well are defined as follows:

Equation of state: The density of a fluid, ρ, can be described as a function of pressure, p, and temperature, T. For liquids, pressure and temperature changes are small, and therefore it is common to use the following linearised equation:

$$\rho = \rho_0 + \frac{\rho_0}{\beta}(p - p_0) - \rho_0\alpha(T - T_0), \tag{2-1}$$

where ρ_0, p_0 and T_0 determine the reference points for linearisation. Also, α is the cubical expansion coefficient and β is the isothermal bulk modulus.

Since temperature dynamics in MPD operations are neglected, as stated earlier, a simple model for the pressure transients can be derived so the density from (2-1) is written in the following differential form:

$$d\rho = \frac{\rho_0}{\beta}dp. \tag{2-2}$$

Conservation of mass: To formulate the conservation of mass equation, the density, ρ, and control volume, V, are required. The control volume is a section of the well over which the density and pressure is calculated. The conservation of mass equation is composed as follows:

$$\frac{d}{dt}(\rho V) = \rho_{in}q_{in} - \rho_{out}q_{out}, \tag{2-3}$$

where q_{in} and q_{out} are respectively flow in and flow out and ρ_{in} and ρ_{out} are respectively the density of the mud flowing in and out the wellbore.

Since it is more convenient to have the pressure as main variable, the mass equation can be rewritten into:

$$\rho_0\frac{V}{\beta}\frac{dp}{dt} = -\rho\frac{dV}{dt} + \rho_{in}q_{in} - \rho_{out}q_{out}. \tag{2-4}$$

Conservation of momentum: To determine the conservation of momentum equation, one needs to know that the flowrate is $q = v_s A_s$ where v_s is the velocity of the flow and A_s is the cross sectional area (assumed constant). As stated, the flow is one-dimensional along the main flow path and with $q = v_s A_s$, the partial differential equation of momentum can be written as:

$$\rho \frac{\partial v_s}{\partial t} = \frac{\rho}{A} \frac{\partial q}{\partial t} = -\frac{\partial \rho}{\partial x_s} - \frac{\partial \tau}{\partial x_s} + \rho g \cos \gamma. \tag{2-5}$$

The spatial coordinate of the flow is described as x_s, τ is a lumped friction term, the angle of the flow relative to the vertical is represented by γ (since a vertical well is assumed, γ=0) and the acceleration of gravity is g.

Making use of (2-5) and the assumption that that the fluid accelerates as a stiff mass, the following equations for the average flow rate dynamics are formulated:

$$M(l_1, l_2) \frac{dq}{dt} = p_1 - p_2 - \Delta p_f(l_1, l_2, q, \mu) + G(l_1, l_2, \rho), \tag{2-6}$$

$$M(l_1, l_2) = \int_{l_1}^{l_2} \frac{\rho}{A_s} \, dx_s, \tag{2-7}$$

$$\Delta p_f(l_1, l_2, q, \mu) = \int_{l_1}^{l_2} \frac{\partial \tau(\frac{q}{A_s}, \mu)}{\partial x_s} \, dx_s, \tag{2-8}$$

$$G(l_1, l_2, \rho) = \int_{l_1}^{l_2} \rho g \cos \gamma \, dx_s. \tag{2-9}$$

The parameter M is the integrated density per cross section over the flow path, Δp_f is the friction along the flow path and G is the full amount of gravity affecting the fluid. Furthermore, l_1 and l_2 are the spacial coordinates of the flow path where q represents the average flow rate of the fluid in the control volume between these coordinates, p_1 is the pressure at l_1 and p_2 is the pressure at l_2.

Friction A closer look is taken at (2-8), which describes the pressure drop due to friction in the drillstring and annulus. For simplicity reasons, it is assumed that the mud is a Newtonian fluid, flowing through a smooth pipe. A Newtonian fluid has a linear relationship between shear stress and shear rate, meaning that the viscosity of the fluid will not change. This choice has been made since equations for other fluids contain parameters that are not measured in the set-up proposed by Huisman, such as the yield point and the pipe roughness. Furthermore, the equations for a Newtonian fluid in a smooth pipe can easily be differentiated with respect to the flow, which will appear to be necessary in the stage of observer design. In later stages of this research, these assumptions regarding the frictional pressure drop will be put to the test by varying the frictional pressure drop.

To calculate the frictional pressure drop in the drillstring for a Newtonian fluid, the Reynolds number, Re, is calculated as:

$$Re = \frac{\rho v_s d_{di}}{\mu}, \tag{2-10}$$

where ρ is the density of the mud, v_s the velocity of the mud flowing through the pipe ($v_s = \frac{q}{A_s}$) and d_{di}, is the inside diameter of the drillstring. The dynamic viscosity is denoted as μ.

In the annulus, the Reynold number is calculated as:

$$Re = 0.816\frac{\rho v_s(d_{ai} - d_{do})}{\mu}, \tag{2-11}$$

where d_{ai} is the inside diameter of the annulus, d_{do} is the outside diameter of the drillpipe and 0.816 is a factor corresponding to the shape of the annulus [14], namely two concentric circles.

The (Blasius) friction factor, f_b, for a smooth pipe and turblent flow is calculated with the following formula [14]:

$$f_b = \frac{0.079}{Re^{0.25}}, \tag{2-12}$$

where the Reynolds number is taken from Equations (2-10) and (2-11).

Subsequently, the frictional pressure drop per volume is calculated as [14]:

$$\Delta p_f = \frac{f_b \rho v_s^2}{519d} h_{bit}, \tag{2-13}$$

where d is the diameter of the section, $\bar{v}_s$ is the average velocity of the fluid ($\frac{q}{A_s}$) and h_{bit} is the vertical depth of the well.

Since $v_s = \frac{q}{A_s}$, (2-13) becomes:

$$\Delta p_f = \frac{f_b \rho (\frac{q}{A_s})^2}{519d} h_{bit}. \tag{2-14}$$

As is described in Chapter 1, the flow through the bit is unmeasured. Furthermore, the density in the annulus, ρ_a, is an uncertain parameter in this model since an uncertain amount of cuttings might increase the annular density. For observer design, the frictional pressure drop will be expressed as a known parameter multiplied by the unknown q_{bit} and ρ. To be consistent with literature about the frictional pressure drop in managed pressure drilling, as in [15] and [13], simplification is done when it comes to expressing the frictional pressure drop w.r.t. q_{bit} so it depends on q_{bit}^2 (and not q_{bit}^3 that is actually in the equation when Re and f_b are fully written in (2-13)):

$$\Delta p_f = \frac{f_b}{519dA_s^2} h_{bit} \cdot \rho q_{bit}^2. \tag{2-15}$$

In order to formulate this equation, a generalized Reynolds number is assumed to calculate f_b from Equation (2-12). An average flow of 1000 l/min is used. To simplify this equation, the known parameters will be jointly combined in one parameter as a new friction factor, F:

$$F = \frac{f_b}{519dA_s^2} h_{bit}. \tag{2-16}$$

If the generalized f_b is filled into (2-16), a friction factor for both the drillstring and the annulus can be determined and the equations for the pressure drop will be as follows:

$$\begin{aligned} \Delta p_{fd} &= F_d \rho_d q_{bit}^2, \\ \Delta p_{fa} &= F_a \rho_a (q_{bit} + q_{res})^2, \end{aligned} \tag{2-17}$$

where F_d and F_a are calculated from (2-16) for the drillstring and the annulus respectively. Δp_{fd} and Δp_{fa} denote subsequently the pressure drop in the drillstring and in the annulus. For the annular pressure drop the (possible) reservoir influx, q_{res} must be added up to the flow in the bit to obtain the total annular flow. To summarize, the frictional pressure drop is now calculated assuming a turbulent Newtonian fluid in a smooth pipe with a generalized Reynolds number calculated at a flowrate of 1000 l/min.

Gravity As mentioned earlier, a vertical well is assumed which implies $\gamma = 0$ thus (2-9) is simplified to:

$$G = (\rho_d - \rho_a) g h_{bit}, \tag{2-18}$$

where ρ_d and ρ_a are the densities of the mud in the drillstring and the annulus respectively and h_{bit} is the measured depth of the borehole.

Pressure pulse propagation Propagation of pressure pulses are also incorporated in this model. If pressure pulses travel from the mud pump to the bit it does not affect the BHP immediately. Pressure waves propagate as sound waves and move with the speed of sound, which is the distance travelled per unit time by a sound wave through an elastic medium. Since the bulk modulus of drilling mud is higher than air and water, the flowrate (flowing with the speed of sound) of drilling mud will be higher. The speed of sound is calculated as [13]:

$$c = \sqrt{\frac{\beta}{\rho}}, \tag{2-19}$$

where c is the speed of sound, β is the bulk modulus and ρ is the density. With the parameters defined in the base case in Appendix A, a speed of sound of approximately 1000 m/s is derived with (2-19). In this model, the speed is also influenced by M (the integrated mass density per cross section) since this affects the compressibility of the model and thus the flowrate in the well.

To visualize this pulse propagation, pump shut down is simulated at t=100 s and the flows at the pump, bit and choke are examined during this simulation. A zoomed-in plot at the moment the transient response takes place is shown in Figure 2-1.

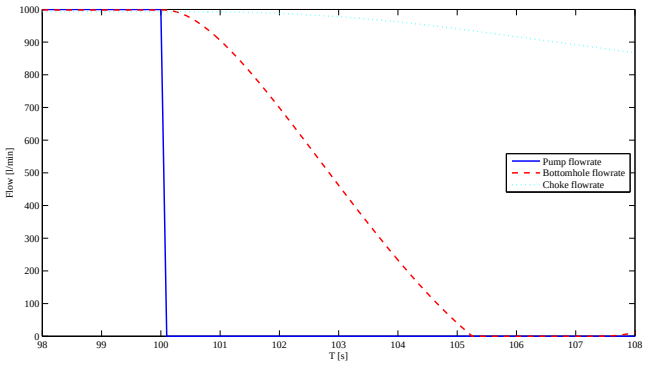

Figure 2-1: Pulse propagation in flow after pump shut down.

2-1-2 Drillstring and annulus model

Making use of the fundamental equations described in Section 2-1-1, a simplified hydraulic pressure model is derived. For simplification the assumption can be made that: $\rho = \rho_0 = \rho_{in} = \rho_{out}$. The well is divided into two control volumes; the drill string and the annulus. All the fundamental equations will be discretised into ODE's and applied to these two control volumes. A graphical interpretation of the drilling system divided into two control volumes is shown in Figure 2-2.

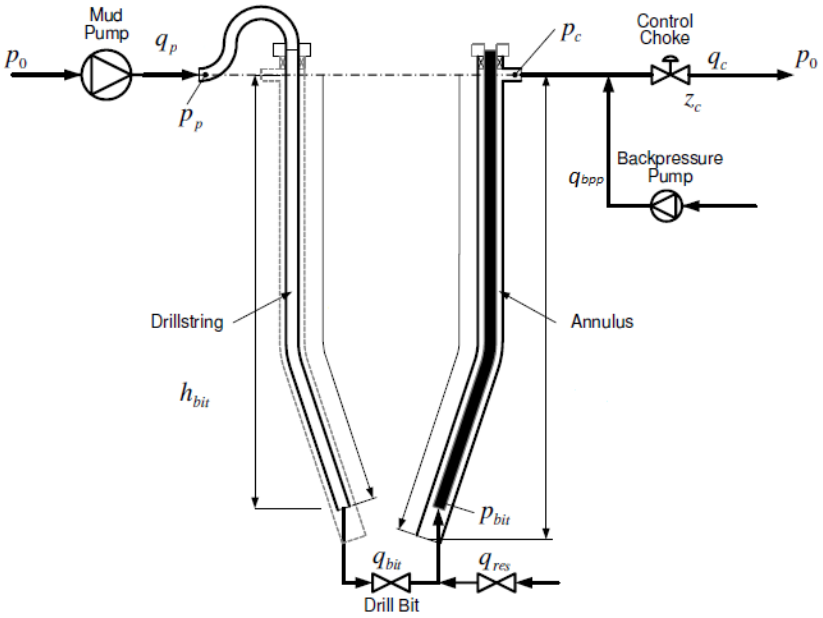

Figure 2-2: Control volumes for the drillstring and the annulus [3].

The pressure of the mud pump, denoted as p_p, and the pressure of the choke, denoted as p_c, are according to (2-4) written as:

$$\dot{p}_p = \frac{\beta_d}{V_d}(q_p - q_{bit}), \tag{2-20}$$

$$\dot{p}_c = \frac{\beta_a}{V_a}(q_{bit} + q_{res} + q_{bpp} - q_c), \tag{2-21}$$

where β_d and V_d are the bulk modulus and volume of the mud in the drillstring and β_a and V_a are the bulk modulus and volume of the mud in the annulus. Further, q_p is the mud pump flow rate, q_{bit} is the flow rate through the drill bit, q_{res} is the reservoir influx, q_c is the flow through the choke and q_{bpp} is the flow from the backpressure pump.

The bottomhole flow, in literature referred to as q_{bit}, can be calculated using Equations (2-6) to (2-9):

$$\dot{q}_{bit} = \frac{1}{M}(p_p - p_c - F_d\rho_d q_{bit}^2 - F_a\rho_a(q_{bit} + q_{res})^2 + (\rho_d - \rho_a)gh_{bit}), \tag{2-22}$$

where $M = M_a + M_d$. It must be noted that only pressure drops in the drillstring and in the annulus are taken into account and that pressure drop in the nozzles is neglected.

The three states that describe the dominant dynamics of the whole system can now be denoted as follows:

$$\begin{bmatrix} \dot{p}_p \\ \dot{p}_c \\ \dot{q}_{bit} \end{bmatrix} = \begin{bmatrix} \frac{\beta_d}{V_d}(q_p - q_{bit}) \\ \frac{\beta_a}{V_a}(q_{bit} + q_{res} + q_{bpp} - q_c) \\ \frac{1}{M}(p_p - p_c - F_d\rho_d q_{bit}^2 - F_a\rho_a(q_{bit} + q_{res})^2 + (\rho_d - \rho_a)gh_{bit}) \end{bmatrix}. \tag{2-23}$$

An estimation for the BHP, in literature referred to as the bit pressure, p_{bit}, is now made by making use of the states described in (2-23):

$$p_{bit} = \begin{cases} p_p + \rho_d g h_{bit} - F_d\rho_d q_{bit}^2 & \text{Considering pressure in drillstring} \\ p_c + \rho_a g h_{bit} + F_a\rho_a(q_{bit} + q_{res})^2 & \text{Considering pressure in annulus,} \end{cases} \tag{2-24}$$

which is true when the system is in steady state and no reservoir influx is present. In this project, the pressure and dynamics in the annulus will be used to determine the BHP since reservoir influx is taken into account, therefore in the well model the BHP is denoted as:

$$p_{bit} = p_c + \rho_a g h_{bit} + F_a\rho_a(q_{bit} + q_{res})^2. \tag{2-25}$$

In Appendix A, all input parameters and initial conditions that are used in this simplified well model are presented and values for a base case are defined.

Choke valve A standard expression for the choke valve is included in the model in order to find a relationship between the position of the choke and the flow through the choke [13]:

$$q_c = C_v(z)\sqrt{\frac{p_c - p_0}{SG}}, \tag{2-26}$$

where C_v is a valve sizing coefficient depending on the valve's position, z, p_0 is the atmospheric pressure and SG is the specific gravity of the fluid.

In order to model choke valve dynamics that are similar to practice, a nonlinear C_v-curve needs to be introduced, that is used for C_v in (2-26). This curve is made based on measured data from the AXON Chokemaster 3" valve [4], which will be used in the Huisman set-up. The nonlinear C_v-curve, as seen in Figure 2-3, is implemented in the SIMULINK model as a look-up table which contains input-output data points spread over a desired region. When an input is fed to the look-up table, the according output is given.

Note that the C_v-curve is in inches, so during modelling in MATLAB/SIMULINK, the curve is rescaled to S.I. units.

Check-valve In common drilling set-ups, a check-valve is placed in the drill bit to prevent mud/drilling fluid from flowing back into the drillstring. Thus, the mud only flows in one direction through the bit. This can be implemented in the model by replacing the bit flow equation from (2-23) with:

$$\dot{q}_{bit} = \begin{cases} \frac{1}{M}(p_p - p_c - F_d\rho_d q_{bit}^2 - F_a\rho_a(q_{bit} + q_{res})^2 + (\rho_d - \rho_a)gh_{bit}) & q > 0 \\ \max[0, \frac{1}{M}(p_p - p_c - F_d\rho_d q_{bit}^2 - F_a\rho_a(q_{bit} + q_{res})^2 + (\rho_d - \rho_a)gh_{bit})] & q = 0 \end{cases}. \tag{2-27}$$

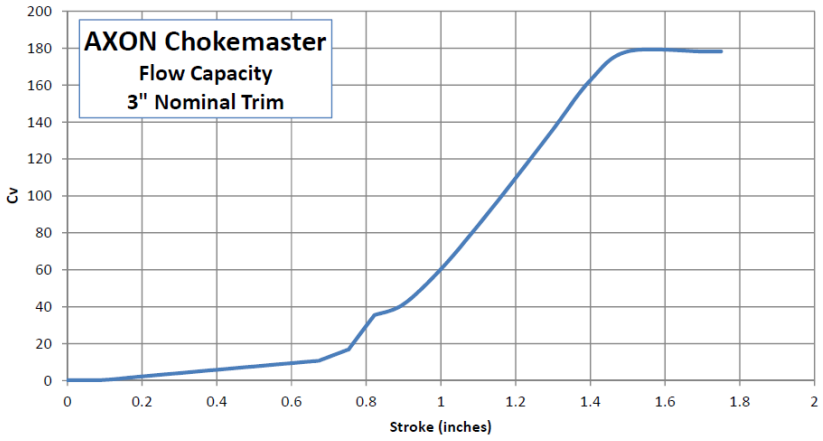

Figure 2-3: The nonlinear C_v-curve of the choke valve [4].

Rescaling To make the system analytically and numerically more comprehensible, scaling is applied to the parameters of the system. The necessity follows from the the fact that for instance the magnitude of the pressure (in Pa) is in the order of 10^7 whilst the flow (in m^3/s) is in the order of 10^{-2}. In order to rescale the parameters, arbitrary scaling factors can be chosen. The notation S will be used to represent the scaling factors:

- S_p for pressure, $p = S_p p_n$
- S_q for flow, $q = S_q q_n$
- S_m for integrated mass, $M = S_m M_n$
- S_ρ for density, $\rho = S_\rho \rho_n$
- S_β for bulk modulus, $\beta = S_\beta \beta_n$.

Here the subscript $_n$ denotes a 'new' (scaled) parameter or variable. This can be implemented in (2-23) as:

$$\begin{aligned}
\dot{p}_{pn} S_p &= \frac{\beta_{dn} S_\beta}{V_d}(q_{pn} S_q - q_{bitn} S_q), \\
\dot{p}_{cn} S_p &= \frac{\beta_{an} S_\beta}{V_a}\left(q_{bitn} S_q + q_{resn} S_q + q_{bppn} S_q - C_v(z)\sqrt{\frac{p_{cn} S_p - p_{0n} S_p}{SG_n S_\rho}}\right), \\
\dot{q}_{bitn} S_q &= \frac{1}{M_n S_m}\left(p_{pn} S_p - p_{cn} S_p - F_d \rho_{dn} S_\rho q_{bitn}^2 S_q^2 - F_a \rho_{an} S_\rho (q_{bitn} + q_{resn})^2 S_q^2 + (\rho_{dn} - \rho_{an}) S_\rho g h_{bit}\right).
\end{aligned} \tag{2-28}$$

Firstly, all scaling factors are moved to the right-hand side of the equation. Secondly, the scaling factors should be chosen. In order to keep the equations organized, it is chosen that $S_q = 1$ (so the flow will still be in m^3/s) and $S_p = S_M = S_\rho = S_\beta = 10^5$. Note that the

pressure in is now divided by 10^5 which makes it scaled to the unit of bar. The equations are now reduced to:

$$\begin{aligned}
\dot{p}_{pn} &= \frac{\beta_{dn} S_\beta}{V_d S_p}(q_{pn} - q_{bitn}),\\
\dot{p}_{cn} &= \frac{\beta_{an} S_\beta}{V_a S_p}\left(q_{bitn} + q_{resn} + q_{bppn} - C_v(z)\sqrt{\frac{p_{cn} - p_{0n}}{SG_n}}\right),\\
\dot{q}_{bitn} &= \frac{S_p}{M_n S_m}\left(p_{pn} - p_{cn} - F_d \rho_{dn} q_{bitn}^2 - F_a \rho_{an}(q_{bitn} + q_{resn})^2 + (\rho_{dn} - \rho_{an}) g h_{bit}\right).
\end{aligned} \tag{2-29}$$

Using the knowledge that $S_p = S_M = S_\rho = S_\beta$ the scaling parameters are eliminated and the system is again in its original form, this time with new rescaled parameters. In Appendix A, the base case is defined with the systems original parameters and the newly defined rescaled parameters. From here on, it must be assumed that in the MATLAB and SIMULINK simulations, the scaled units will be used. In this report the parameters will be denoted in S.I. units, unless stated otherwise.

2-1-3 Open-loop analysis

In order to understand the dynamics and stability of the model, a brief open-loop analysis is presented in this section. This analysis is done by performing a stability check in the pole-zero map and executing a frequency domain analysis in a Bode plot. In the analysis, the system is linearised in a steady-state condition around the states; $p_p = 80$ bar, $p_c = 50$ bar and $q_{bit} = 1000$ l/min, and different choke position inputs, z, will be used. It is investigated that the system behaviour of the linearised system is the same when linearising around other operating points (other pressures and flows within operating region). A pole-zero map for the linearised model was created, by examining the poles and zeros for the model with the choke position as input and the BHP as output. Stability of the linearised model can be inferred from the pole-zero plot in Figure 2-4. The poles and zeros all lie in the left half-plane and the model is therefore locally stable (around the linearised states). It can be seen that the more the choke valve is closed, the more the single real pole moves towards the (unstable) right half-plane. This observation can be used in the stadium of controller design by noticing that the single real poles near zero indicate slowly decaying components.

A Bode plot is generated to analyze the frequency dynamics from the input (the choke position) to the output (the BHP). In Figure 2-5 it is visible that, at low frequencies, amplification of the input signal is higher when z is lower. This is coherent with the fact that a small choke opening will lead to higher pressures in the well and putting a sine wave on the choke opening will lead to a larger variation in the pressure. Thus, a smaller choke opening leads to a higher BHP and larger variations and as a result, amplification of the input signal is larger. A bigger choke opening, on the other hand, results in a lower BHP with less variation if a sine wave is applied, and is thus less amplified. Furthermore, it is seen that amplification at higher frequencies is reduced earlier for smaller choke openings. If a high frequency sine signal will be used in small choke opening the variations in Δp will be too big for the system too follow. When the choke opening is bigger the variations of Δp are smaller and thus the BHP can be controlled up to higher frequencies when the choke opening is larger. The controller to be designed should therefore not operate at high frequencies when the choke valve is almost closed.

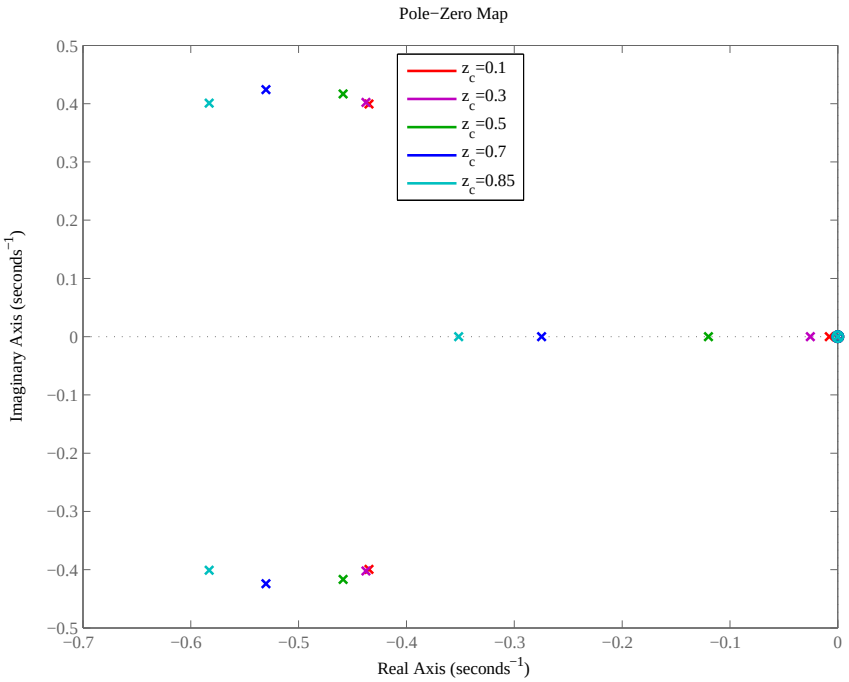

Figure 2-4: A pole-zero plot for the linearised simplified MPD model at $p_p = 80$ bar, $p_c = 50$ bar and $q_{bit} = 1000$ l/min.

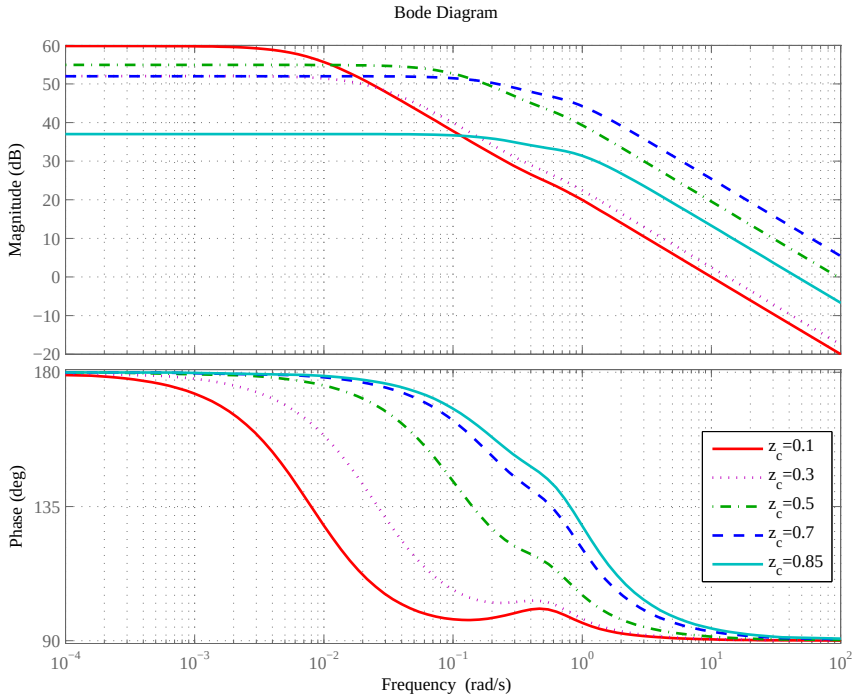

Figure 2-5: Bode plot for the linearised simplified MPD model from choke position to the bottomhole pressure at $p_p = 80$ bar, $p_c = 50$ bar and $q_{bit} = 1000$ l/min.

2-2 Validation model

For validation purposes, another lumped parameter model is designed that more accurately represents the transient responses in each section of the well during drilling. For this purpose, the annulus and drillstring are divided into multiple compartments, also called control volumes. This is illustrated in Figure 2-6 and the fundamental equations from Section 2-1 are integrated over each of these control volumes as is similarly done in [5] and [16]. The result is a set of ODE's that represent the pressure and flow at each section in the drillstring and in the annulus.

In this multiple compartment model, the well is divided into N compartments for the drillstring and annulus and the pressures and flow are calculated from the following equations:

$$\begin{aligned}
\dot{p}_{1d} &= \frac{\beta_d}{V_{1d}}(q_p - q_{1d}) \\
\dot{p}_{id} &= \frac{\beta_d}{V_{id}}(q_{(i-1)d} - q_{id}) \\
\dot{p}_{Nd} &= \frac{\beta_d}{V_{id}}(q_{(N-1)d} - q_{bit}) \\
\dot{q}_{id} &= \frac{1}{M_{id}}(p_{id} - p_{(i+1)d} - \Delta p_{fid} - \rho_d g \Delta h_{id}) \\
\dot{p}_{1a} &= \frac{\beta_a}{V_{1a}}(q_{bit} + q_{res} - q_{1a}) \\
\dot{p}_{ia} &= \frac{\beta_a}{V_{ia}}(q_{(i-1)a} - q_{ia}) \\
\dot{p}_{Na} &= \frac{\beta_a}{V_{ia}}(q_{(N-1)a} - q_c + q_{bpp}) \\
\dot{q}_{ia} &= \frac{1}{M_{ia}}(p_{ia} - p_{(i+1)a} - \Delta p_{fia} - \rho_a g \Delta h_{ia}) \\
\dot{q}_{bit} &= \frac{1}{M_{bit}}(p_{Nd} - p_{1a} - \Delta p_{fbit} - (\rho_d - \rho_a) g \Delta h_{ia}).
\end{aligned} \tag{2-30}$$

From here, the pressure at the bit is calculated as:

$$p_{bit} = p_{1a} + \rho_a g h_{ia} + \Delta p_{f1a}, \tag{2-31}$$

where, i=1,..,N, refer to the compartment number and the subscripts a and d represent the annulus and the drillstring. For the annulus, control volume 1 represent the lowest compartment (above the bit) and N represents the top compartment where the choke pressure, p_c is calculated. For the drillstring, the compartments are reversed, so 1 represents the compartment where the pump pressure is calculated and N serves as the lowest compartment close to the bit. The flows are calculated at each boundary whilst the pressures are calculated in the middle of each control volume. The height of each control volume is denoted by Δh. β, V, M, and Δp_f represent the bulk modulus, volume, integrated mass per density and frictional pressure drop in each section.

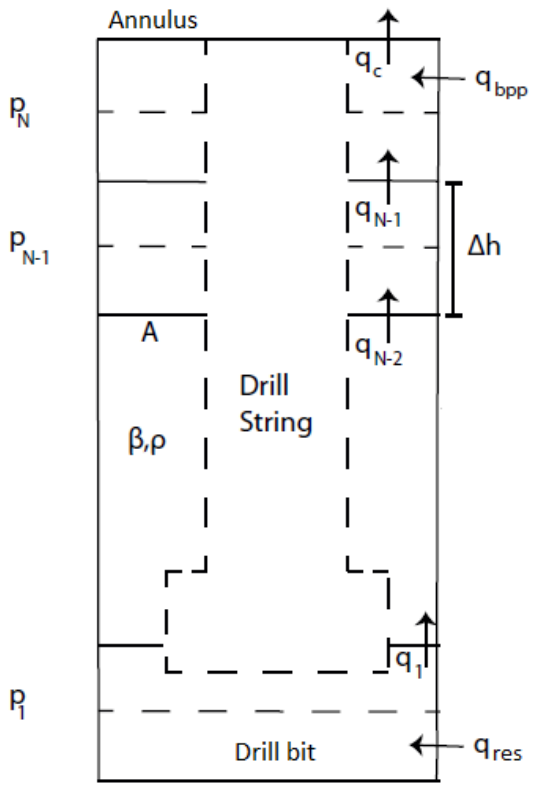

Figure 2-6: The well divided into multiple compartments [5].

To use this model in the continuation of this research, an appropiate N should be chosen since the number of control volumes influences the accuracy of the model. It is evident that a higher number of control volumes improves the accuracy of the well model, however, it also increases the computation time. In [5] simulations with different numbers of control volumes, $N = 5$, $N = 10$, $N = 50$, are compared to full-scale test data. It is found that the most significant pressure changes are even captured by the lowest number of control volumes, $N = 5$, and little gain is achieved by increasing the number of control volumes. Since the well parameters of the base case well in this research are approximately in the same range as the parameters used in [5], the same number of control volumes is used to represent this multiple compartment model for validation purposes.

A visualization of the pulse propagation through the sections is shown in Appendix B. Furthermore, a more detailed description of how the pressure is distributed over the depth in the drillstring and the annulus is presented.

2-3 The estimation problem

This research aims to design a control system in order to control the BHP. Techniques are available to measure the BHP but these are either very expensive (wired drillpipe) or have a large time delay (mud-pulse telemetry). Therefore, an observer/estimator is required to make estimations of the BHP. In order to do so, real-time information from the mud pump and the

Table 2-1: Percentage and cause of uncertainty per parameters

Parameter	Unit	Value	Uncertainty range	Cause of uncertainty
C_v	-	$4.1 \cdot 10^{-5}$	5%	Unmeasured, valve behaviour might differ from input signal
F_a	-	$4.75 \cdot 10^{5}$	30%	Calculated, depending on several unsure parameters such as pipe roughness, viscosity, temperature etc.
F_d	-	$5.63 \cdot 10^{6}$	30%	Calculated, depending on several unsure parameters such as pipe roughness, viscosity, temperature etc.
h_{bit}	m	2000	0.50%	Measurement error in depth measurement
ρ_a & SG	kg/m^3	1490/1.49	10%	Unmeasured, unknown amount of cuttings in annulus can lead to a higher density compared to drillstring
ρ_d	kg/m^3	1490	1%	Measurement error in density measurement
q_p	m^3/s	$1.67 \cdot 10^{-2}$	5%	Unmeasured, flow through pump might differ from input signal
q_{res}	m^3/s	$3.33 \cdot 10^{-2}$	100%	Unmeasured, though it can be safe to assume that it varies between 0 and 0.0033 m^3/s (approx. 200 l/min)

choke and information about known parameters is necessary to make estimations for q_{bit} and p_{bit}. In this section, other uncertain or unknown variables will be identified that influence the BHP and hence should also be estimated.

In order to see which parameters have the biggest influence on the BHP, a sensitivity analysis is performed. In first place, it was determined which parameters have direct influence on the BHP in steady state. Parameters only influencing the dynamics (the transient responses) do not play a part in this sensitivity analysis. In second place, research was performed on the cause of uncertainty per parameter and the corresponding range of uncertainty was investigated. The percentage of uncertainty and the cause for the uncertainty per parameter are listed in Table 2-1. Here, the specific gravity from the choke valve equation is considered together with the annulus density since $SG{=}\rho_a/\rho_w$ (ρ_w is the density of water and is always equal to $\pm$ 1000 kg/m^3).

The effect of these uncertainties is examined by keeping the parameters at a constant value as defined in the base case (Appendix A), simultaneously the parameters defined in Table 2-1 are varied in their range of uncertainty. This is plotted in Figure 2-7, where the line in the middle defines the nominal value of the BHP in steady state and the bars represent the lowest and highest BHP outcome per parameter.

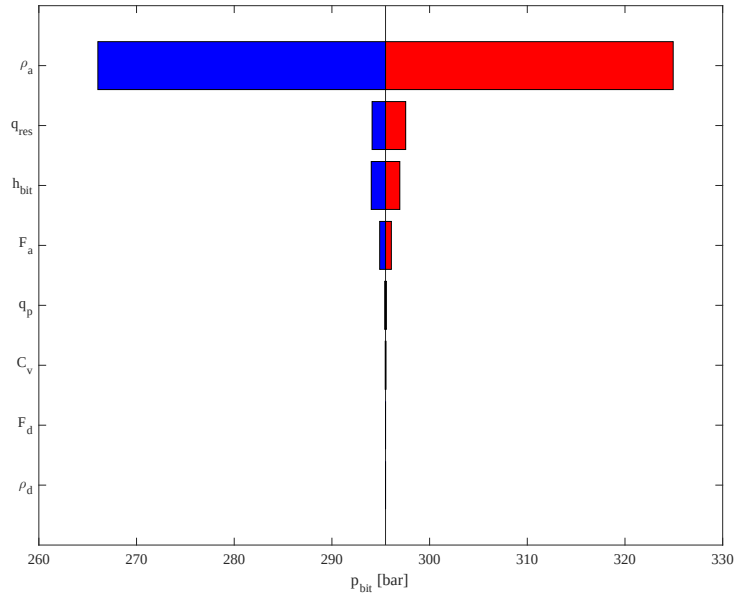

Figure 2-7: A sensitivity analysis on the three-state model, the line in the middle indicates the nominal p_{bit}. Bars to the left indicate the minimum p_{bit} per uncertainty (lower bound of uncertainties), bars to the right indicate the maximum p_{bit} per uncertainty (upper bound of uncertainties).

From Figure 2-7 it is clearly visible that the uncertainty of the density in the annulus, ρ_a, causes the biggest variation in BHP. Furthermore, the unmeasured reservoir influx might also influence the BHP, if it is a big as 0.0033 m^3/s (or 200 l/min).

In later stages of this research an observer will be proposed that should estimate the uncertain or unmeasured variables. From the sensitivity test it is clear that the reservoir influx and annulus density have the highest influence on estimating the BHP. Therefore, the following state and parameters must be estimated by the observer to be designed:

- flow through the bit, q_{bit}
- reservoir influx, q_{res}
- annulus density, ρ_a

2-4 Case study simulations

To test the performance and robustness of the observer and controller that will be designed in this research, several simulations are created in this section that might occur during the drilling process and will be simulated in MATLAB/SIMULINK.

2-4-1 Drilling situations

Firstly, situations will be defined that could actually happen during the drilling process, these are:

- Shutting of the pump without backpressure flow and turning the pump back on. This is considered to be important since the pump will be turned off when making new drillstring connections or when tripping. It will be simulated as:
  - q_p will be turned of in 10 seconds at t=200 s and turned on in 10 seconds at t=290 s.
  - In an open-loop case when testing the observer, z will be closed from 30% open to 0% open in 10 seconds at t=200 s and opened from 0% to 30% in 10 seconds at t=290 s.
- Shutting of the pump with backpressure flow and turning the pump back on while reducing backpressure flow, again to simulate making new drillstring connections or tripping. The backpressure pump is added since it provides extra flow through the choke, therefore the valve doesn't need to be closed completely and the pressure can be trapped in the well making it easier to follow the setpoint of the BHP since there is less pressure loss. It will be simulated to see the difference in pump shut-off with and without the backpressure pump.
  - q_p will be turned of in 10 seconds at t=400 s and turned on in 10 seconds at t=490 s. Simultaneously, the backpressure flow will be turned on in 10 seconds at t=400 s to 200 l/min and turned of at t=490 s to 0 l/min.
  - In an open-loop case when testing the observer, z will be closed from 30% open to 10% open in 10 seconds at t=400 s and opened from 10% to 30% in 10 seconds at t=490 s.
- Occurrence of reservoir influx during the MPD process. It is important for the observer and controller to recognize the reservoir influx and handle it since neglecting reservoir influx might cause a blow-out. Reservoir influx is simulated as:
  - Between 200 $<t<$400 [s] reservoir influx will be simulated by imposing q_{res} is 200 l/min.
- Taking up cuttings in the mud stream during the drilling process. If cuttings come up together with the mud in the annulus, the density of the mud in the annulus will rise. According to [17], the cuttings can take up to 7% of the total mud volume. Based on a cuttings density of 2200 kg/m^3 the density in the annulus, being a mixture of cuttings and drilling mud, is assumed to potentially rise to 1540 kg/m^3. Since the annular density can not be measured, it is relevant to see how the observer handles this situation.
  - At t=800 s the presence of cuttings is simulated in the annular mud flow by raising ρ_a from 1490 to 1540 kg/m^3 in 40 seconds. The moment where no cuttings are drilled anymore is simulated at t=860 s by decreasing the annular density again to 1490 kg/m^3 in 40 seconds.

In order to visualize these drilling simulations and to compare the dynamics of the simplified and the multiple compartment model, the situations described above are simulated on both models. Furthermore, to asses the quality of the simplified model compared to the multiple compartment model, the variance accounted for (VAF) is used. The VAF is defined as [18]

$$\text{VAF}(y(k),\hat{y}(k)) = \max\left(0,\left(1-\frac{\frac{1}{N_v}\sum_{k=1}^{N_v}\|y(k)-\hat{y}(k)\|_2^2}{\frac{1}{N_v}\sum_{k=1}^{N_v}\|y(k)\|_2^2}\right)100\%\right). \tag{2-32}$$

Here, the multiple compartment model or validation model serves as the true model and the simplified model represents the estimations. Hence in this cost function the calculated BHP by the multiple compartment model will be filled in for y and the calculated BHP from the simplified model will be used for $\hat{y}$ in order to compare the models. k represents each time step that is used to calculate the VAF and N_v represents the number of data samples used to calculate the VAF. The results of the simulations are shown in Figure 2-8.

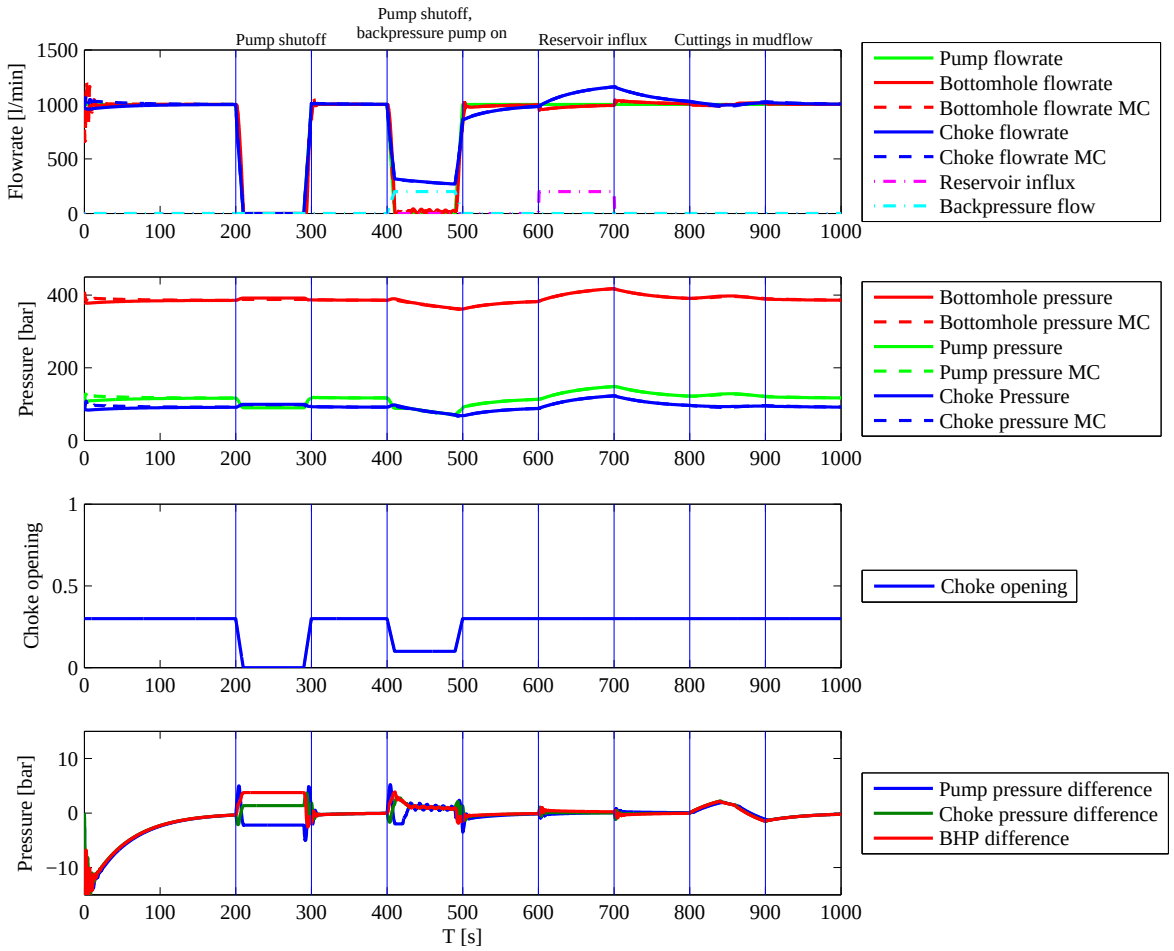

Figure 2-8: Comparison of the simplified model and the validation model during drilling situations.

In this figure, MC is used to indicate the multiple compartment model. It is clear that the dynamics of both well models are approximately the same. During all situations, the behaviour is resembling and no big differences can be detected. What must be noted is that the multiple compartment model behaves differently during transient responses but in steady state the difference is approximately zero. A VAF value of 97% of the BHP is achieved, using (2-32). A high VAF indicates high similarity between the outcomes of both models and thus model resemblance is high. This VAF value needs to be considered when examining the control systems performance, since the VAF of the BHP by both models is not 100% (caused by transient responses), indicating that there is a model discrepancy that will influence the observer/controller performance.

2-4-2 Noise

Furthermore, noise simulations will be done to see how well the observer is able to handle process and measurement noise, which is considered an important property. Since process and measurement noise might disturb the systems result, this is considered separately from the situations described above.

- In order to resemble true drilling conditions, process noise is simulated on the main mud pump. During drilling operations, the mud flow from the pump will not flow continuously but it will follow the strokes of the mud pump. The process noise on the main mud pump is simulated as:
  - A sinusoid is imposed on q_p with an amplitude of 50 l/min and a frequency of 3.33 Hz between 200 $<t<$400 [s].
- Another issue that can occur in practice during a MPD operation is measurement noise on the sensors. Information from both the pump and choke pressure sensor is used in real time for BHP estimation. Since the sensors are roughly the same (similar pressure sensors are placed in the mud pump and in the choke), it is arbitrary chosen to simulate random measurement noise on the sensor of the pump pressure to examine the control systems robustness to noise. It is simulated as:
  - A random Gaussian white noise signal is added to p_p with a standard deviation of 0.02 bar between 600 $<t<$800 [s].

2-4-3 Varying friction

At last, in order to test the performance of the observer, it is chosen to replace the fluid model that is used in the simplified well model (the drillstring and annulus model). Two other fluid types are used to simulate the pressure drop due to friction, to test the assumption that the fluid is a turbulent Newtonian fluid in a smooth pipe. The newly introduced fluid types are both Newtonian, one assuming a rough pipe (instead of a smooth pipe) and one includes higher pressures losses to account for drillstring rotation.

Friction model 2, Newtonian fluid in a rough pipe In this Newtonian fluid, a rough pipe is assumed. In (2-16), the friction factor was simplified by assuming a smooth pipe and a generalized Reynolds number in turbulent flow. The equation for the Reynolds number for a Newtonian fluid was given in (2-10), but is repeated here

$$Re = \frac{\rho v_s d}{\mu}. \tag{2-33}$$

The friction factor for a rough pipe is calculated using Chen's friction factor, f_c (Chen's friction factor):

$$f_c = \left(-4 \log_{10} \left(\frac{\epsilon}{3.7065} - \frac{5.0452}{Re} \log_{10} \left(\frac{\epsilon^{1.1098}}{2.8257} + \frac{7.149}{Re^{0.8981}} \right) \right) \right)^{-2}, \tag{2-34}$$

where $\epsilon = \frac{\delta}{d}$ is the relative roughness and δ is the absolute roughness.

The pressure drop is subsequently calculated as also done in (2-13):

$$\Delta p_f = \frac{f_c \rho v_s^2}{519 d} h_{bit}. \tag{2-35}$$

Equations (2-33) to (2-35) are general equations for pressure drop as a result of friction in a pipe for a turbulent Newtonian fluid (in a rough pipe). Note that the annulus is not a standard pipe since it consists of two concentric circles and the equations need to be adjusted to the shape of the annulus just as is done earlier for Newtonian fluids.

Friction model 3, Newtonian fluid with drillstring rotation In order to account for pressure loss due to drillstring rotation, or other factors that might increase the pressure loss, an offset of 30% is added to the pressure loss term used in the simplified model. Note that this is a simplification and that in practice, pressure loss due to drillstring rotation will probably not simply result in a proportional 30% increase.

$$\begin{cases} \Delta p_{fd} &= F_d \rho_d q_{bit}^2 \cdot 1.3 \\ \Delta p_{fa} &= F_a \rho_a (q_{bit} + q_{res})^2 \cdot 1.3. \end{cases} \tag{2-36}$$

A comparison of the three rheology models (Newtonian fluid in a smooth pipe, Newtonian fluid in a rough pipe and Newtonian fluid with drillstring rotation) is visualized to get a concise idea of the differences. The pressure drop per flowrate is shown in Figure 2-9.

As is seen, the frictional pressure drop for a smooth or rough pipe Newtonian fluid is approximately the same. The pipe roughness does not have a large effect with these well parameters. For the fluid flow when drillstring rotation is taken into account, the pressure loss in the drillstring will be approximately 6 bar higher and in the annulus approximately 1 bar higher at a flowrate of 1000 l/min (steady-state condition).

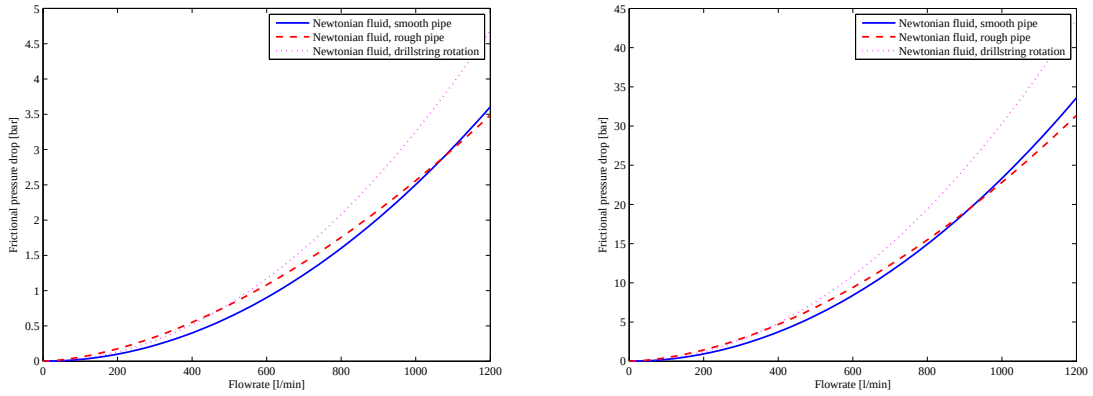

(a) Frictional pressure drop in the annulus.

(b) Frictional pressure drop in the drillstring.

Figure 2-9: Frictional pressure drop in both the annulus and the drillstring for a Newtonian fluid assuming smooth pipe, rough pipe and a 30% offset.

2-5 Summary and concluding remarks

In this chapter, two models were introduced that represent the MPD system. The first one, being a simplified model, divides the well into the drillstring and annulus and examines pressures and flow in these two compartments. The second one, consists of multiple compartments to represent the flow and pressure in each section of the well. The simplified model is used as a base for designing the observer and controller. The multiple compartment model will be used to validate the model.

Furthermore, the estimation problem was presented by identifying the unmeasured or uncertain state/variables. This should be taken to the next chapter, where an estimator will be proposed to estimate the unknown variables and the BHP.

At last, several drilling situations were introduced and a description was given on how these situations are simulated in MATLAB and SIMULINK. The same was done for noise and varying frictional pressure drops. These drilling simulations will be used in a later stage of this project to test the performance and robustness of the MPD control system.

Chapter 3

Estimator design

Now a model for the system has been introduced in Chapter 2, this chapter shows the design of an estimator to estimate the unmeasured/uncertain variables determined in Section 2-3. Two estimators are designed in order to deal with the estimation problem. These are an Extended Kalman-Bucy filter (EKBF), outlined in Section 3-1, and an adaptive observer, outlined in Section 3-2.

Both observers will be tested using the drilling situations and noise from the case study simulations described in Section 2-4. For the observer to be designed, the following requirements are formulated:

- The error in estimated BHP should be below 1%.
- The time it takes for the estimated values to convergence to steady state should be less then 100 seconds.

With these demands in mind, the observer will be designed and the performance will be examined.

3-1 Extended Kalman-Bucy Filter

The Kalman filter is a widely used algorithm in estimation and control processes. It uses measurements from the plant which may contain noise or uncertainties and applies linear quadratic estimation to produce estimates based on these measurements. It is done by combining previous measurements which makes the resulting estimates usually more accurate and reliable than those based on only a single measurement. In case of a continuous-time process, a Kalman-Bucy filter can be used, developed by the authors of [19], which serves as the continuous-time counterpart to the discrete-time Kalman Filter.

The Kalman-Bucy filter algorithm, or continuous-time Kalman filter, works with a combined prediction-update step. In the prediction-update step, the current state variables and their

uncertainties are estimated and updated by using the next measurement and the estimate with a weighted average. Weighted averages have to be assigned to both prediction and measurement uncertainties. The mathematical steps of the Kalman-Bucy filter will now be explained.

First, the state space model needs to be determined:

$$\begin{aligned} \dot{x} &= Ax + Bu + w \\ y &= Cx + v, \end{aligned} \tag{3-1}$$

where x is the state vector, y is the output vector and u is the control vector. Further, A is the state matrix, B is the input matrix, C is the measurement matrix, w is the process noise and v is the measurement noise.

When the measurement output is available, the prediction-update step takes place, according to:

$$\begin{aligned} K_e &= PC^T R^{-1} \\ \dot{\hat{x}} &= A\hat{x} + Bu + K(y - C\hat{x}) \\ \dot{P} &= AP + PA^T - KRK^T + Q. \end{aligned} \tag{3-2}$$

Here, K_e denotes the Kalman-Bucy gain, Q and R are respectively the covariance matrices of the process and measurement noise and P is the covariance of the estimation error.

Since the simplified well model of this research is nonlinear, the previously described Kalman-Bucy filter cannot be used. Therefore a filter is necessary that handles nonlinear systems, which is the Extended Kalman filter that uses a Jacobian with partial derivatives of the nonlinear system. Since the system is considered a *nonlinear continuous-time* process, an Extended Kalman-Bucy filter (EKBF) is required, which has proven to work in [20] and [21].

Another advantage of the EKBF is that it is capable of estimating parameters for the nonlinear system so it does not assume the system matrices to be known (as is the case with the (linear) Kalman filter). To understand the mathematical equation for the EKBF, a nonlinear state space system needs to be defined first:

$$\begin{aligned} \dot{x} &= f(x, u) + w \\ y &= h(x) + v, \end{aligned} \tag{3-3}$$

where f represents the nonlinear system dynamics depending on the states, x, and the input, u. h is the (nonlinear) output function and w and v are again respectively the process noise and the measurement noise (independent white noise).

Since f and h are possible nonlinear functions, calculation of the covariance of the outcome as in (3-2) is no longer possible. Therefore, f and h are approximated by taking the Jacobian and filling it in to calculate the new covariance of the measurement error, P.

The equations for the EKBF are given below:

$$\begin{aligned}
\dot{\hat{x}} &= f(\hat{x}, u) + K(y - \hat{y}) \\
\hat{y} &= h(\hat{x}) \\
K_e &= PH^T R^{-1} \\
\dot{P} &= FP + PF^T - K_e R K_e^T + Q, \\
F &= \left.\frac{\partial f}{\partial x}\right|_{\hat{x},u} \\
H &= \left.\frac{\partial h}{\partial x}\right|_{\hat{x}}
\end{aligned} \tag{3-4}$$

The most important differences compared to the continuous-time Kalman filter (Kalman-Bucy filter) are the use of F and H instead of A and C and the fact that the prediction is done with a nonlinear model. Note that the EKF will not perform optimally if the model is highly uncertain; then other methods such as the (computationally more expensive) Unscented Kalman filter (UKF) are required [22], [23]. The simplified well model from this research is only slightly nonlinear so therefore the decision is made to use the EKF for the estimation problem in this research.

3-1-1 Estimator design

Now that the general theory of the EKBF is explained, the simplified well model needs to be implemented in the equations to use the EKBF as an estimator for unknown well parameters and variables.

The well model was given in Section 2-1, containing the states p_p, p_c and q_{bit}. The other two uncertain parameters that influence the BHP, as defined in Section 2-3, namely q_{res} and ρ_a, should be added as states. Also, it is assumed that q_{res} and ρ_a are bounded signals. The extended model thus becomes:

$$\dot{x} = \begin{bmatrix} \dot{p}_p \\ \dot{p}_c \\ \dot{q}_{bit} \\ \dot{q}_{res} \\ \dot{\rho}_a \end{bmatrix} = \begin{bmatrix} \frac{\beta_d}{V_d}(q_p - q_{bit}) \\ \frac{\beta_a}{V_a}(q_{bit} + q_{res} + q_{bpp} - q_c) \\ \frac{1}{M}\left(p_p - p_c - F_d \rho_d q_{bit}^2 - F_a \hat{\rho}_a (q_{bit} + q_{res})^2 + (\rho_d - \rho_a) g h_{bit}\right) \\ 0 \\ 0 \end{bmatrix}. \tag{3-5}$$

Note that the pump and choke pressure, p_p and p_c, are the only measurement outputs and are thus the only variables that occur in the measurement matrix, h. A prediction of the system's states can be made by the EKBF using the equations from (3-4) as follows:

$$\dot{\hat{x}} = \begin{bmatrix} \dot{\hat{p}}_p \\ \dot{\hat{p}}_c \\ \dot{\hat{q}}_{bit} \\ \dot{\hat{q}}_{res} \\ \dot{\hat{\rho}}_a \end{bmatrix} = \begin{bmatrix} \frac{\beta_d}{V_d}(q_p - \hat{q}_{bit}) \\ \frac{\beta_a}{V_a}(\hat{q}_{bit} + \hat{q}_{res} + q_{bpp} - q_c) \\ \frac{1}{M}\left(\hat{p}_p - \hat{p}_c - F_d \rho_d \hat{q}_{bit}^2 - F_a \hat{\rho}_a (\hat{q}_{bit} + \hat{q}_{res})^2 + (\rho_d - \hat{\rho}_a) g h_{bit}\right) \\ 0 \\ 0 \end{bmatrix} + K\left(\begin{bmatrix} p_p \\ p_c \end{bmatrix} - \begin{bmatrix} \hat{p}_p \\ \hat{p}_c \end{bmatrix} \right), \tag{3-6}$$

$$\hat{y} = \begin{bmatrix} 1 & 0 & 0 & 0 & 0 \\ 0 & 1 & 0 & 0 & 0 \end{bmatrix} \begin{bmatrix} \hat{p}_p \\ \hat{p}_c \\ \hat{q}_{bit} \\ \hat{q}_{res} \\ \hat{\rho}_a \end{bmatrix}. \tag{3-7}$$

The Jacobian, $F = \frac{\partial f}{\partial x}\Big|_{\hat{x},u}$, is determined as:

$$F = \begin{bmatrix} 0 & 0 & -\frac{\beta_d}{V_d} & 0 & 0 \\ 0 & 0 & \frac{\beta_a}{V_a} & \frac{\beta_a}{V_a} & 0 \\ \frac{1}{M} & -\frac{1}{M} & -\frac{2}{M}\Big(F_d\rho_d\hat{q}_{bit} + F_a\hat{\rho}_a(\hat{q}_{bit}+\hat{q}_{res})\Big) & -\frac{2}{M}F_a\hat{\rho}_a(\hat{q}_{bit}+\hat{q}_{res}) & -\frac{1}{M}\Big(F_a(\hat{q}_{bit}+\hat{q}_{res})^2 + gh_{bit}\Big) \\ 0 & 0 & 0 & 0 & 0 \\ 0 & 0 & 0 & 0 & 0 \end{bmatrix}. \tag{3-8}$$

The covariance matrices of the EKBF are given in Table 3-1.

Table 3-1: Covariance matrices of the Extended Kalman-Bucy filter.

Parameter	Value
Q	$\text{diag}\begin{pmatrix} 0.1 & 0.1 & 0.5 & 0.5 & 0.5 \end{pmatrix}$
R	$\text{diag}\begin{pmatrix} 100 & 1 \end{pmatrix}$
P_0	$\text{diag}\begin{pmatrix} 10^{-3} & 10^{-3} & 10^{-3} & 10^{-3} & 10^{-3} \end{pmatrix}$

As stated earlier, Q defines the covariance matrix of the process noise and R defines the covariance matrix of the measurement noise. A remark should be made here that a higher weighting on a Q or R value indicates more uncertainty, a lower value indicates more certainty about the measurement (R) or modelled state (Q), according to [24]. The R matrix is determined by examining the measurement noise. In the case study, only noise is imposed on the mud pump pressure sensor and not on on the choke pressure sensor. Therefore, the pump pressure measurement requires a higher weighting factor since this measurement is more uncertain. Hence, p_c will be given a weighting factor of 1 whilst the weighting factor of the measurement of p_p will be larger since measurement noise on this sensor is introduced. Determining the Q matrix is not straightforward but it is constructed intuitively. The Q matrix includes parametric uncertainties and unmodeled dynamics, a higher value in the Q matrix indicates more uncertainty about unknown noise and/or model errors and low Q indicates certainty in the modelled state. Therefore, the measured parameters p_p and p_c are given a lower weighting than the unmeasured state q_{bit} and the unmodeled states q_{res} and ρ_a. Moreover, it should be noted that the values of R a now given a relatively higher weighting than the values of Q since the measurements are considered more certain than the (linearised) modelled states.

From the predicted states, the BHP can be calculated as well. The estimated BHP is defined by using (2-25) in the EKBF as:

$$\hat{p}_{bit} = p_c + F_a\hat{\rho}_a(\hat{q}_{bit}+\hat{q}_{res})^2 + \hat{\rho}_a g h_{bit}. \tag{3-9}$$

Finally, a block scheme was created for the EKBF described in this section. The block scheme, including the drilling well model and the EKBF is shown in Figure 3-1.

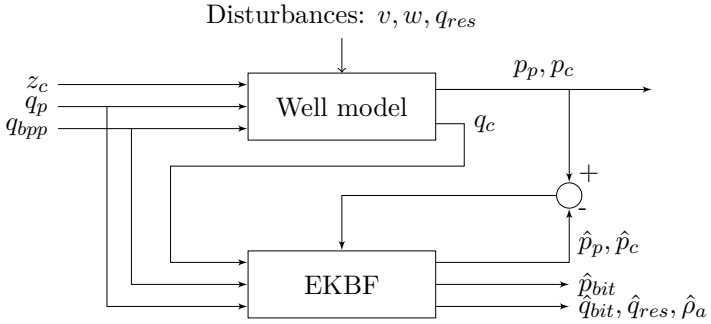

Figure 3-1: Block scheme of the Extended Kalman-Bucy filter.

3-1-2 Local stability analysis

The estimated parameters will only converge to steady state values if the EKBF is stable and the estimation error is bounded. This imposes a problem since proof of stability or boundedness of estimation errors for nonlinear filters is hardly present in current literature. Even in research where boundedness of the estimation errors and convergence is proven for the extendend Kalman filter by [25], this is only true under very strict conditions, rarely satisfied in practice and impossible to verify beforehand. Therefore, in this research only local boundedness and stability of estimations errors will be shown.

First, to show boundedness of the estimation error, the extended system that is used in the EKBF, namely $f(\hat{x}, u)$, has to be locally *detectable and observable* according to [26]. A system is observable if and only if the observability matrix is full column rank for the linearised state space. The observability matrix is expressed as:

$$Ob = \begin{bmatrix} C \\ CA \\ CA^2 \\ CA^{(n-1)} \end{bmatrix}. \tag{3-10}$$

Detectability is a weaker annotation, it implies that the unobservable state should be stable (converge to equilibrium). For a Kalman Filter (F, H) should be observable and (F, QQ^T) should be detectable. In our case, the Jacobian, F, and measurement matrix, H, replace respectively the A and C matrix in the observability condition. Note that the Jacobian F is not constant and need to be linearised around operating points. Calculation in MATLAB leads to full rank observability matrices during normal drilling conditions. (F, QQ^T) has 2 unobservable states, namely q_{res} and ρ_a so these have to be stable which is shown in the verification section that follows next. Here it is seen that both estimated parameters converge to an equilibrium state. Thus, during common drilling conditions the EKBF extended system is locally stable. Nevertheless, in aberrant situations, for instance if there is no flow ($q_{bit} = 0$), the Jacobian will not be equal to (3-8) and in that case, the estimator model will neither be observable nor detectable and thus might not be stable. In these situations the EKBF is no longer able to make reliable estimations of the BHP.

As mentioned above, if the system is in normal operating regions, and the system is detectable and observable, according to [26], without the presence of process and measurement noise;

$w = 0$ and $v = 0$, the system will converge to its true values. When noise is present, the estimations will logically not converge to a steady state. Nevertheless, if the kalman filter is stable the noise will not drive the state far and the variance of the states remain bounded. Here, it is assumed that the process and measurement noise is bounded and Gaussian white noise. If the system is not stable, the variance of the estimation error will not be bounded anymore and could even diverge. Therefore, it must be ensured that the control loop to be designed including the plant, observer and feedback controller, remains stable during various situations.

Verification of convergence Here, it will be shown that, under common drilling conditions without the presence of noise, the observer is stable and the unknown parameters will converge. In this simulation, the choke position input was held constant at 30% open and the mud pump flow was held constant at 1000 l/min. From Figure 3-2 it is clear that the estimated parameters converge to steady-state values and this confirms the theory described above. Nevertheless, it is seen that convergence of the estimated density in the annulus and the bottomhole flowrate is a little slow and it takes approximately 50 seconds to converge. Convergence of the BHP takes longer due to initial conditions but is also shown in this graph.

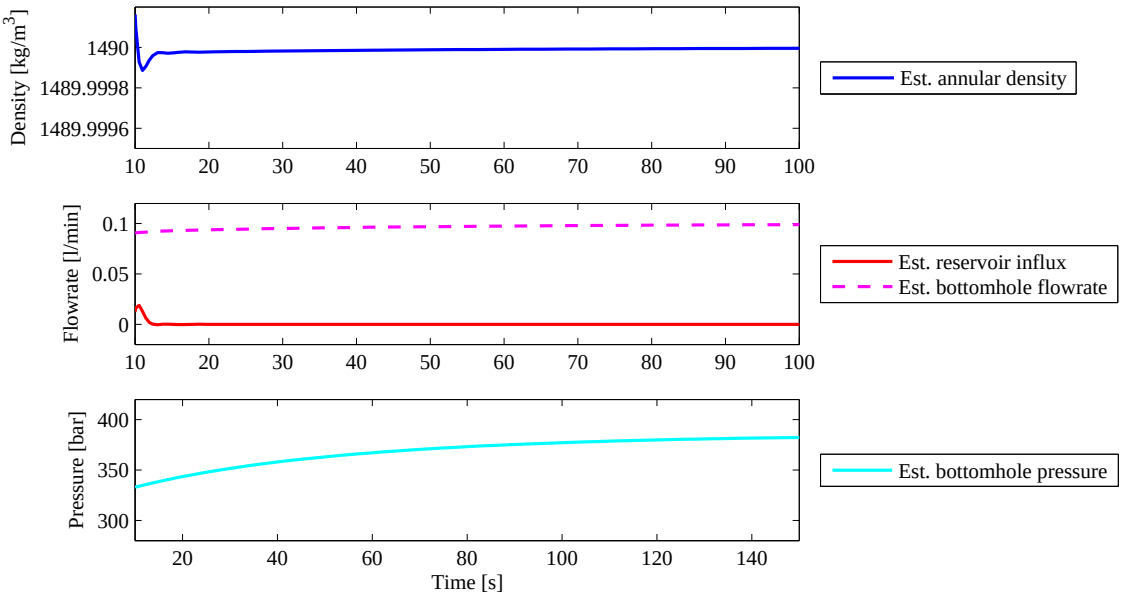

Figure 3-2: Convergence of the uncertain parameters for the adaptive observer, the bottomhole flowrate is scaled to 0.1 l/min for figure readability.

3-2 Adaptive observer

Besides the EKBF, another estimation method that handles nonlinearities, unmeasured states and unknown parameters is proposed: an adaptive observer. Practical application of this method was found in [27] and [28] and applied by Stamnes on a similar estimation problem in MPD [15], [29], [30]. In this research, the same observer structure will be used, but the extended model of the system dynamics is different, meaning that other parameters are considered uncertain or unmeasured. As defined in Section 2-3, the density in the annulus is considered highly uncertain in this project and will be estimated together with the unmeasured flow through the bit and reservoir influx.

The adaptive observer uses a change of coordinates to estimate an unmeasured/unknown state, in this case the flow through the bit. As only the flow through the bit is estimated and not the pump and choke pressure, this observer is a reduced-order observer. Since the bit flow depends on other unknown parameters, a second change of coordinates has to be implemented, in order to estimate the unknown parameters. Throughout this section, the unknown parameters will be denoted as:

$$\begin{bmatrix}\theta_1\\ \theta_2\\ \theta_3\end{bmatrix} = \begin{bmatrix}\frac{(\rho_a-\rho_d)g}{M}\\ \frac{F_a\rho_a}{M}q_{res}\\ \frac{F_a\rho_a}{M}q_{res}^2\end{bmatrix}. \tag{3-11}$$

3-2-1 Observer design

A description of the adaptive observer is already presented in literature [15], but since a different estimation problem is solved here, the design will be explained in this section.

To improve readability, the simplified well model defined in Chapter 2, is repeated here.

$$\begin{aligned}\begin{bmatrix}\dot{p}_p\\ \dot{p}_c\\ \dot{q}_{bit}\end{bmatrix} &= \begin{bmatrix}\frac{\beta_d}{V_d}(q_p - q_{bit})\\ \frac{\beta_a}{V_a}(q_{bit}+q_{res}+q_{bpp}-q_c)\\ \frac{1}{M}(p_p - p_c - F_d\rho_d q_{bit}^2 - F_a\rho_a(q_{bit}+q_{res})^2 + (\rho_d-\rho_a)gh_{bit})\end{bmatrix}\\ p_{bit} &= p_c + \rho_a g h_{bit} + F_a\rho_a(q_{bit}+q_{res})^2,\end{aligned} \tag{3-12}$$

with $q_c = C_v(z)\sqrt{\frac{p_c-p_0}{SG}}$. For design of this adaptive observer it is assumed that all signals from (3-12) are bounded.

The set of equations from (3-12), is filled into the nonlinear canonical form from [28] in order to create the adaptive observer. Note that a reduced-order observer for the flow through the bit, q_{bit}, will be designed:

$$\dot{x}_r = f(x,u) - \Theta^T\phi, \tag{3-13}$$

where the subscript $_r$ indicates the state of the reduced-order observer, Θ is a vector of unknown variables and ϕ is the regressor, based on information about known parameters. The form of (3-13) is obtained by denoting the unknown parameters, as: $\Theta = \begin{bmatrix}\theta_1 & \theta_2 & \theta_3\end{bmatrix}^T$ and $\theta_1 = \frac{(\rho_a-\rho_d)g}{M}$, $\theta_2 = \frac{F_a\rho_a}{M}q_{res}$ and $\theta_3 = \frac{F_a\rho_a}{M}q_{res}^2$. The regressor is denoted as $\phi = \begin{bmatrix}h_{bit} & 2q_{bit} & 1\end{bmatrix}^T$. Since a reduced-order observer will be designed for the flow through the bit, only q_{bit} will be denoted in the form of (3-13), i.e. $x_r = q_{bit}$:

$$\begin{aligned}\dot{x}_r = \dot{q}_{bit} &= \frac{1}{M}\Big(p_p - p_c - (F_d\rho_d + F_a\rho_a)q_{bit}^2\Big) - \begin{bmatrix}\frac{(\rho_a-\rho_d)g}{M} & \frac{F_a\rho_a}{M}q_{res} & \frac{F_a\rho_a}{M}q_{res}^2\end{bmatrix}\begin{bmatrix}h_{bit}\\2q_{bit}\\1\end{bmatrix}\\ &= f(x,u) - \Theta^T\phi,\end{aligned} \tag{3-14}$$

To design the adaptive observer, the assumption is done that $q_{bit} > 0$ and $q_{bit} + q_{res} \geq 0$. This is true knowing that a non-return valve has been implemented in the model and that reservoir outflux (negative q_{res}) is never larger than the flow through the bit. The equation for dynamics of the flow through the bit can now denoted as:

$$\begin{aligned}\dot{q}_{bit} &= \frac{1}{M}\Big(p_p - p_c - F_d\rho_d q_{bit}^2 - F_a\rho_a(q_{bit}+q_{res})^2 - (\rho_a-\rho_d)gh_{bit}\Big)\\ &= \frac{1}{M}\Big(p_p - p_c - (F_d\rho_d + F_a\rho_a)q_{bit}^2\Big) - \theta_1\phi_1 - \theta_2\phi_2 - \theta_3\phi_3\\ &= \frac{1}{M}\Big(p_p - p_c - (F_d\rho_d + F_a\rho_a)q_{bit}^2\Big) - \Theta^T\phi,\end{aligned} \tag{3-15}$$

where $\rho_a = \theta_1\frac{M}{g} + \rho_d$. According to the authors of [27], an unmeasured state can be estimated by applying a change of coordinates, which uses a positive gain constant and a measured (or known) state. In this case, the unmeasured state is q_{bit} and p_p will be used as a measured state. Furthermore, the positive gain constant is called L and the new coordinate is called ξ, obtained by applying a change of coordinates:

$$\xi = q_{bit} + Lp_p. \tag{3-16}$$

The dynamics of ξ can be found by using (3-15) and by using the equations for the dynamics of the pump pressure from (3-12):

$$\begin{aligned}\dot{\xi} &= \dot{q}_{bit} + L\dot{p}_p\\ &= \frac{1}{M}\Big(p_p - p_c - (F_d\rho_d + F_a\rho_a)q_{bit}^2\Big) - \Theta^T\phi + L\frac{\beta_d}{V_d}(q_p - q_{bit}).\end{aligned} \tag{3-17}$$

Using (3-17), the reduced-order observer is designed as

$$\dot{\hat{\xi}} = \frac{1}{M}\Big(p_p - p_c - (F_d\rho_d + F_a\hat{\rho}_a)\hat{q}_{bit}^2\Big) - \hat{\Theta}^T\hat{\phi} + L\frac{\beta_d}{V_d}(q_p - \hat{q}_{bit}), \tag{3-18}$$

$$\hat{q}_{bit} = \hat{\xi} - Lp_p, \tag{3-19}$$

where $\hat{\rho}_a$ depends on $\hat{\theta}_1$.

3-2-2 Adaptive law

Since the reduced-order observer from (3-18) estimates the flow through the bit but not the unknown parameters represented by Θ, the problem on estimating these still remains. Therefore, a second change of coordinates, σ, is introduced:

$$\sigma = \Theta + \Gamma\eta(\hat{q}_{bit}, h_{bit}), \tag{3-20}$$

where η is a new function depending on known parameters from the regressor that was determined in Section 3-2-1 and Γ is a symmetric and positive definite adaptation gain matrix (serving the same purpose as L in (3-16)). Following the same procedure as in (3-17), and assuming that the reservoir influx is a constant, which implies $\dot{\Theta} = 0$, the dynamics of σ can be represented as:

$$\begin{aligned}\dot{\sigma} &= \dot{\Theta} + \Gamma\dot{\eta}(\hat{q}_{bit}, h_{bit}) \\ &= \frac{\partial \eta}{\partial \hat{q}_{bit}}\dot{\hat{q}}_{bit} + \frac{\partial \eta}{\partial h_{bit}}\dot{h}_{bit}.\end{aligned} \tag{3-21}$$

Since it is assumed that there is no vertical motion, $\dot{h}_{bit}$ can be regarded as zero. Note that the derivative of the height due to drilling and lengthening the drillstring are very small. Using (3-19) and the state equation for p_p, the dynamics of σ and the resulting estimate of Θ will be:

$$\begin{aligned}\dot{\sigma} &= \frac{\partial \eta}{\partial \hat{q}_{bit}}(\dot{\hat{\xi}} - L\dot{p}_p) \\ &= \frac{\partial \eta}{\partial \hat{q}_{bit}}\dot{\hat{\xi}} - \frac{\partial \eta}{\partial \hat{q}_{bit}}L\frac{\beta_d}{V_d}(q_p - q_{bit}),\end{aligned} \tag{3-22}$$

and

$$\hat{\Theta} = \hat{\sigma} - \Gamma\eta(\hat{q}_{bit}, h_{bit}). \tag{3-23}$$

Analogously to Equations (3-18) and (3-19), the adaptive observer (or adaptive equation) for the unknown parameters shall now be set up:

$$\dot{\hat{\sigma}} = \frac{\partial \eta}{\partial \hat{q}_{bit}}\dot{\hat{\xi}} - \frac{\partial \eta}{\partial \hat{q}_{bit}}L\frac{\beta_d}{V_d}(q_p - \hat{q}_{bit}), \tag{3-24}$$

$$\hat{\Theta} = \hat{\sigma} - \Gamma\eta(\hat{q}_{bit}, h_{bit}). \tag{3-25}$$

The error dynamics of the unknown parameters, $\tilde{\Theta} = \Theta - \hat{\Theta}$, following from Equations (3-22), (3-24) and (3-25) shall now be determined:

$$\tilde{\Theta} = \sigma - \Gamma\eta(\hat{q}_{bit}, h_{bit}) - \Big(\hat{\sigma} - \Gamma\eta(\hat{q}_{bit}, h_{bit})\Big) = \tilde{\sigma}, \tag{3-26}$$

$$\dot{\tilde{\Theta}} = \dot{\tilde{\sigma}} = L\frac{\beta_d}{V_d}\frac{\partial \eta}{\partial \hat{q}_{bit}}\tilde{q}_{bit} = L\frac{\beta_d}{V_d}\frac{\partial \eta}{\partial \hat{q}_{bit}}\Big(\xi - Lp_p - (\hat{\xi} - Lp_p)\Big) = L\frac{\beta_d}{V_d}\frac{\partial \eta}{\partial \hat{q}_{bit}}\tilde{\xi}, \tag{3-27}$$

where $\tilde{q}_{bit} = q_{bit} - \hat{q}_{bit}$ and $\tilde{\xi} = \xi - \hat{\xi}$. In order to stabilize the error dynamics of Θ, an adaptive law is required that uses the adaptation gain matrix, Γ, and the regressor, ϕ. The adaptive The error dynamics is chosen to be equal to:

$$\dot{\tilde{\Theta}} = \Gamma\hat{\phi}\tilde{\xi}. \tag{3-28}$$

A remark should be made here that this adaptive law will be further explained in Section 3-2-3 (Equation (3-39)).

Substituting Equation (3-27) in (3-28) results in:

$$L\frac{\beta_d}{V_d}\frac{\partial \eta(\hat{q}_{bit}, h_{bit})}{\partial \hat{q}_{bit}} = \Gamma\hat{\phi}. \tag{3-29}$$

The regressor $\phi = \begin{bmatrix} h_{bit} & 2\hat{q}_{bit} & 1 \end{bmatrix}$ shall now be used to integrate (3-29).

$$\begin{aligned} \frac{\partial \eta(\hat{q}_{bit}, h_{bit})}{\partial \hat{q}_{bit}} &= \Gamma \begin{bmatrix} \frac{h_{bit}}{L\frac{\beta_d}{V_d}} \\ \frac{2\hat{q}_{bit}}{L\frac{\beta_d}{V_d}} \\ \frac{1}{L\frac{\beta_d}{V_d}} \end{bmatrix}, \\ \eta(\hat{q}_{bit}, h_{bit}) &= \Gamma \begin{bmatrix} \frac{h_{bit}\hat{q}_{bit}}{L\frac{\beta_d}{V_d}} \\ \frac{\hat{q}_{bit}^2}{L\frac{\beta_d}{V_d}} \\ \frac{\hat{q}_{bit}}{L\frac{\beta_d}{V_d}} \end{bmatrix}. \end{aligned} \tag{3-30}$$

Now a function, η, of known parameters has been determined, it can be substituted in (3-24) and (3-25), to find the unknown parameters. Subsequently, (3-25) should be used in Equations (3-18) and (3-19) to find an estimate of flow through the bit. It should be noted that this adaptive observer has 4 tuning parameters, namely the gain constant, L, and the three parameters of the gain matrix, Γ. The gain constants L and Γ can be set to how fast the estimated parameters are required to converge. These constant are tuned in Section 3-2-4. Tests are performed to examine the suitability of these gains for other well parameters. It was found that this set of gains are suited to estimate the unknown values within a large range of well parameters.

A control scheme of the adaptive observer described above in shown in Figure 3-3.

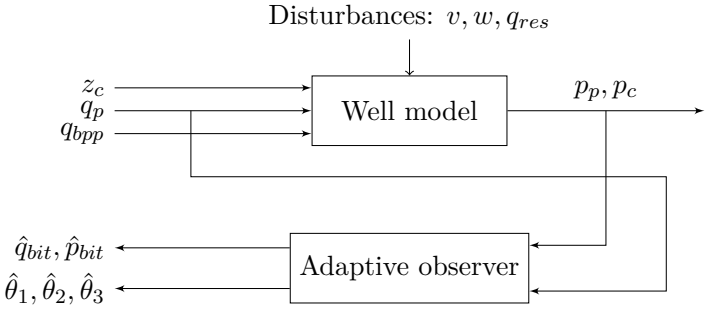

Figure 3-3: Block scheme of the adaptive observer.

3-2-3 Convergence analysis

An adaptive observer, based on a reduced-order observer and an adaptive law, has been designed. In this section it will be examined if the estimations of this observer will converge to (true) steady-state values. This proof was shown on a similar estimation problem in [29] and [30]. The proof will be adjusted to the estimation problem defined in this research and will be presented here. Convergence of $\tilde{q}_{bit} = q_{bit} - \hat{q}_{bit} \to 0$ will be shown by performing a Lyapunov analysis.

First, the error dynamics of the change of coordinates, $\tilde{\xi} = \xi - \hat{\xi}$, is determined from Equations (3-17) and (3-18)

$$\dot{\tilde{\xi}} = -\frac{F_d\rho_d}{M}(q_{bit}^2 - \hat{q}_{bit}^2) - \frac{F_a}{M}(\rho_a q_{bit}^2 - \hat{\rho}_a \hat{q}_{bit}^2) - 2(\theta_2 q_{bit} - \hat{\theta}_2 \hat{q}_{bit}) - (\theta_3 - \hat{\theta}_3) - (\theta_1 - \hat{\theta}_1)h_{bit} - L\frac{\beta_d}{V_d}(q_{bit} - \hat{q}_{bit}) \tag{3-31}$$

where $\hat{\rho}_a$ depends on the constant $\hat{\theta}_1$. In order to further derive the error dynamics of ξ it is necessary to define the following error terms, depending on q_{bit}:

$$\rho_a q_{bit}^2 - \hat{\rho}_a \hat{q}_{bit}^2 = \rho_a q_{bit}^2 - (\rho_a - \tilde{\rho}_a)\hat{q}_{bit}^2 = \rho_a(q_{bit}^2 - \hat{q}_{bit}^2) + \tilde{\rho}_a \hat{q}_{bit}^2, \tag{3-32}$$

$$q_{bit}^2 - \hat{q}_{bit}^2 = (q_{bit} + \hat{q}_{bit})(q_{bit} - \hat{q}_{bit}) = (q_{bit} + \hat{q}_{bit})\tilde{q}_{bit}, \tag{3-33}$$

$$\theta_2 q_{bit} - \hat{\theta}_2 \hat{q}_{bit} = \theta_2(q_{bit} - \hat{q}_{bit}) + (\theta_2 - \hat{\theta}_2)\hat{q}_{bit} = \theta_2 \tilde{q}_{bit} + \tilde{\theta}_2 \hat{q}_{bit}, \tag{3-34}$$

where $\tilde{\rho_a} = \rho_a - \hat{\rho}_a$.

Furthermore, it is necessary to know that:

$$\tilde{\xi} = \xi - \hat{\xi} = q_{bit} + Lp_p - (\hat{q}_{bit} + Lp_p) = \tilde{q}_{bit}. \tag{3-35}$$

Now using Equations (3-32), (3-33) and (3-34), deriving the error dynamics from (3-31) continues:

$$\begin{aligned}
\dot{\tilde{\xi}} &= -\frac{F_d\rho_d}{M}(q_{bit}^2 - \hat{q}_{bit}^2) - \frac{F_a}{M}(\rho_a(q_{bit}^2 - \hat{q}_{bit}^2) + \tilde{\rho}_a \hat{q}_{bit}^2) - 2\theta_2 \tilde{q}_{bit} - 2\tilde{\theta}_2 \hat{q}_{bit} - \tilde{\theta}_3 - \tilde{\theta}_1 h_{bit} - L\frac{\beta_d}{V_d}(q_{bit} - \hat{q}_{bit}) \\
&= -\frac{F_d\rho_d + F_a\rho_a}{M}(q_{bit} + \hat{q}_{bit})\tilde{q}_{bit} - \frac{F_a}{M}\tilde{\rho}_a \hat{q}_{bit}^2 - 2\theta_2 \tilde{q}_{bit} - \tilde{\Theta}^T \hat{\phi} - L\frac{\beta_d}{V_d}\tilde{q}_{bit} \\
&= -\frac{F_d\rho_d + F_a\rho_a}{M}(q_{bit} + \hat{q}_{bit})\tilde{\xi} - \frac{F_a}{M}\tilde{\rho}_a \hat{q}_{bit}^2 - 2\theta_2 \tilde{\xi} - \tilde{\Theta}^T \hat{\phi} - L\frac{\beta_d}{V_d}\tilde{\xi}.
\end{aligned} \tag{3-36}$$

Now, a Lyapunov function candidate, V_l, is chosen as

$$V_l(\tilde{\xi}, \tilde{\Theta}) = \frac{1}{2}\tilde{\xi}^2 + \frac{1}{2}\tilde{\Theta}^T \Gamma^{-1} \tilde{\Theta}, \tag{3-37}$$

where Γ is again the positive definite adaptation gain matrix. The time derivative of V_l is determined as:

$$\dot{V}_l = -\frac{F_d\rho_d + F_a\rho_a}{M}(q_{bit} + \hat{q}_{bit})\tilde{\xi}^2 - \frac{F_a}{M}\tilde{\rho}_a \hat{q}_{bit}^2 \tilde{\xi} - 2\theta_2 \tilde{\xi}^2 - L\frac{\beta_d}{V_d}\tilde{\xi}^2 + \tilde{\Theta}^T \Gamma^{-1}(\dot{\tilde{\Theta}} - \Gamma \hat{\phi}\tilde{\xi}). \tag{3-38}$$

This suggest that an adaptation gain should be chosen that satisfies

$$\dot{\tilde{\Theta}} = \Gamma \hat{\phi}\tilde{\xi}, \tag{3-39}$$

As one might have noticed, this is the adaptive law that was used in (3-28). This results in

$$\dot{V}_l = -\frac{F_d\rho_d + F_a\rho_a}{M}(q_{bit} + \hat{q}_{bit})\tilde{\xi}^2 - \frac{F_a}{M}\tilde{\rho}_a \hat{q}_{bit}^2 \tilde{\xi} - 2\theta_2 \tilde{\xi}^2 - L\frac{\beta_d}{V_d}\tilde{\xi}^2. \tag{3-40}$$

It is known that F_d, F_a, ρ_d, ρ_a, g and M (defined in the base case in Appendix A) are all positive values. In order to continue, the following assumptions need to be made: $q_{bit} > 0$,

$\hat{q}_{bit} > 0$ and $q_{bit} > 2\,|q_{res}|$, and if $\tilde{\rho}_a \hat{q}_{bit}^2 \geq 0$. $q_{bit} > 0$ can be assumed to be true since a non-return valve is implemented. Furthermore, in regular drilling conditions, reservoir influx is only a fraction of the flow through the well, so $q_{bit} > 2\,|q_{res}|$ should be accepted. $r\hat{h}o_a \geq 0$ is true since $\hat{\Theta}$, $\hat{\theta}$ and $\hat{\rho}_a$ are all bounded signals and $\hat{q}_{bit} > 0$ will be proven next. Now $\dot{V}_l$ satisfies

$$\dot{V}_l \leq -L\frac{\beta_d}{V_d}\tilde{\xi}^2. \tag{3-41}$$

It can thus be concluded that $\lim_{t\to\infty} -L\frac{\beta_d}{V_d}\tilde{\xi} = 0$ and that $\tilde{\xi} \to 0$ as $t \to \infty$. As a result $q_{bit} - \hat{q}_{bit} \to 0$. Furthermore, it implies that $\hat{q}_{bit}$ and $\hat{\theta}$ are bounded. Note that it does not guarantee $\lim_{t\to\infty}(\hat{\Theta} - \Theta) = 0$.

The earlier made assumption that $\hat{q}_{bit} > 0$ can now be proven to be true if the following equation is used:

$$\dot{\hat{q}}_{bit} = \frac{1}{M}\Big(p_p - p_c - (F_d\rho_d + F_a\hat{\rho_a})\hat{q}_{bit}^2\Big) - 2\hat{\theta}_2\hat{q}_{bit} - \hat{\theta}_3 - \hat{\theta}_1 h_{bit} + L\frac{\beta_d}{V_d}(q_{bit} - \hat{q}_{bit}). \tag{3-42}$$

$\hat{q}_{bit} > 0$ is correct when $\hat{q}_{bit}(0) > 0$ and $p_p > p_c + \frac{\hat{\theta}_1}{M}h_{bit} + \frac{\hat{\theta}_3}{M}$. Also, it is required that $\frac{F_a}{M}\hat{\rho}_a\hat{q}_{bit}^2 + 2\hat{\theta_2}\hat{q}_{bit} > 0$ which is true since $\hat{q}_{bit} > 0$ and $\hat{\rho}_a$ and $\hat{\theta}_2$ are bounded signals.

The question whether the BHP is estimated correctly still remains. Or, in other words, it still needs to be shown that $\hat{p}_{bit}$ will converge to p_{bit}. Firstly, the estimate of the BHP is noted as:

$$\begin{aligned}\hat{p}_{bit} &= p_c + F_a\hat{\rho}_a(\hat{q}_{bit} + \hat{q}_{res})^2 + \hat{\rho}_a g h_{bit} \\ &= p_c + F_a\hat{\rho}_a\hat{q}_{bit}^2 + 2M\hat{\theta}_2\hat{q}_{bit} + M\hat{\theta}_3 + (M\hat{\theta}_1 + \rho_d g)h_{bit}.\end{aligned} \tag{3-43}$$

For solving this issue, $F_a\hat{\rho}_a$ was left in its original form on purpose and not rewritten to $F_a(M\hat{\theta}_1 + \rho_d g)$. Now the estimation error of the BHP, $\tilde{p}_{bit} = p_{bit} - \hat{p}_{bit}$, can be expressed as:

$$\begin{aligned}\tilde{p}_{bit} &= F_a(\rho_a q_{bit}^2 - \hat{\rho}_a\hat{q}_{bit}^2) + 2M(\theta_2 q_{bit} - \hat{\theta}_2\hat{q}_{bit}) + M\tilde{\theta}_3 + M\tilde{\theta}_1 h_{bit} \\ &= F_a\Big(\rho_a(q_{bit}^2 - \hat{q}_{bit}^2) + \tilde{\rho}_a\hat{q}_{bit}^2\Big) + M\left(2\Big(\theta_2(q_{bit} - q_{\hat{bit}}) + \tilde{\theta}_2\hat{q}_{bit}\Big) + \tilde{\theta}_3 + \tilde{\theta}_1 h_{bit}\right) \\ &= F_a\Big(\rho_a(q_{bit}^2 - \hat{q}_{bit}^2) + \tilde{\rho}_a\hat{q}_{bit}^2\Big) + M\Big(2\theta_2(q_{bit} - q_{\hat{bit}})\Big) + M(2\tilde{\theta}_2\hat{q}_{bit} + \tilde{\theta}_3 + \tilde{\theta}_1 h_{bit}).\end{aligned} \tag{3-44}$$

By means of (3-41) it was proven that $q_{bit} - \hat{q}_{bit} = q_{\tilde{bit}} \to 0$ as $t \to \infty$. Therefore, $q_{bit}^2 - \hat{q}_{bit}^2$ will also converge to 0 as $t \to \infty$. The estimation error is now reduced to:

$$\begin{aligned}\tilde{p}_{bit} &= F_a\tilde{\rho}_a\hat{q}_{bit}^2 + M(2\tilde{\theta}_2\hat{q}_{bit} + \tilde{\theta}_3 + \tilde{\theta}_1 h_{bit}) \\ &= F_a\tilde{\rho}_a\hat{q}_{bit}^2 + M(\tilde{\Theta}^T\hat{\phi}) \\ &= F_a M\tilde{\theta}_1\hat{q}_{bit}^2 + M(\tilde{\Theta}^T\hat{\phi}) \\ &= M(F_a\tilde{\theta}_1\hat{q}_{bit}^2 + \tilde{\Theta}^T\hat{\phi}).\end{aligned} \tag{3-45}$$

The extended Barbalat's Lemma is now introduced, applying it as in [31] and [32]. The Lemma will be used to show that $\lim_{t\to\infty} F_a\tilde{\theta}_1\hat{q}_{bit}^2 + \tilde{\Theta}^T\hat{\phi} = 0$ and thus $\lim_{t\to\infty}\tilde{p}_{bit} = 0$. First, a function f will be defined:

$$f = \tilde{\Theta}^T\hat{\phi} + F_a\tilde{\theta}_1\hat{q}_{bit}^2. \tag{3-46}$$

The derivative, $\dot{f}$, is now determined.

$$\begin{aligned}\dot{f} &= \dot{\tilde{\Theta}}^T\hat{\phi} + \tilde{\Theta}^T\dot{\phi} + F_a\tilde{\theta}_1\dot{\hat{q}}_{bit}^2 \\ &= \Gamma\hat{\phi}\tilde{\xi}\hat{\phi} + (2\tilde{\theta}_2\dot{\hat{q}}_{bit} + \tilde{\theta}_3 + \tilde{\theta}_1 h_{bit}) + F_a\tilde{\theta}_1\hat{q}_{bit} \\ &= \Gamma\hat{\phi}\tilde{\xi}\hat{\phi} + 2\tilde{\theta}_2\hat{q}_{bit}\dot{q}_{bit} + F_a\tilde{\theta}_1\hat{q}_{bit}\dot{q}_{bit} \\ &= \Gamma\hat{\phi}\tilde{\xi}\hat{\phi} + 2(\tilde{\theta}_2 + F_a\tilde{\theta}_1\hat{q}_{bit})\dot{q}_{bit}.\end{aligned} \tag{3-47}$$

Here $g_1 = 2(\tilde{\theta}_2 + F_a\tilde{\theta}_1\hat{q}_{bit})\dot{q}_{bit}$ is a uniformly continuous function, since $\hat{\theta}$ and $\hat{q}_{bit}$ are bounded. Also, $\lim_{t\to\infty} g_2 = \Gamma\hat{\phi}\tilde{\xi}\hat{\phi} = 0$ as a result of $\tilde{\xi} \to 0$ (3-41). Therefore $\lim_{t\to\infty} f(t) = 0$. It is deduced that

$$\tilde{p}_{bit} = M(F_a\tilde{\theta}_1\hat{q}_{bit}^2 + \tilde{\Theta}^T\hat{\phi}), \tag{3-48}$$

satisfies Barbalat's Lemma and will converge to zero. As a result, it can be concluded that $\lim_{t\to\infty}[p_{bit} - \hat{p}_{bit}] = 0$ and hence it is proven that the BHP is estimated correctly (and converges over time).

Lemma 1. *([33], Lemma A.21) Extended Barbalat's Lemma: If a given differentiable function f(t): $R_+ \to R$ has a limit as $t \to \infty$ and if $f(t)$ has a time derivative, defined as $\dot{f}(t)$, that can be written as the sum of two functions, denoted by $g_1(t)$ and $g_2(t)$, as follows*

$$\dot{f}(t) = g_1 + g_2, \tag{3-49}$$

where $g_1(t)$ is a uniformly continuous function and $\lim_{t\to\infty} g_2(t) = 0$ then $\lim_{t\to\infty} \dot{f}(t) = 0$ and $\lim_{t\to\infty} g_1(t) = 0$.

Verification of convergence The proof of convergence will be supported here by showing convergence of the unknown parameters in a simulation. In this simulation, the choke position input was held constant at 30% open and the mud pump flow was held constant at 1000 l/min. From Figure 3-4 it is clear that the estimated parameters converge quickly to steady-state values and this confirms the theory described above. The estimated annulus density, reservoir influx and bottomhole flowrate have converged within 30 seconds. Convergence of the BHP takes longer due to initial conditions but is also shown in this graph.

3-2-4 Tuning the gain matrix

Since there is no straightforward method to determine appropiate values for the gain constant, L, and the gain matrix, Γ, a comparison with various gains will be made. The gain constant, L, determines the speed of adapting q_{bit} and will be set to 0.5. An appropriate and matching gain matrix should now be found. Γ is used to adapt the unknown values $\theta_1 = \frac{(\rho_a - \rho_d)g}{M}$, $\theta_2 = \frac{F_a\rho_a}{M}q_{res}$ and $\theta_3 = \frac{F_a\rho_a}{M}q_{res}^2$. Intuitively, it is evident that θ_1 is small compared to θ_2 and θ_3 since the difference between the annular and drillstring density is generally low, compared to the frictional components in θ_2 and θ_3. Furthermore at least θ_2 or θ_3 should respond quickly to potential reservoir influx. Knowing this information, various sets for the gain matrix were simulated using the situations described in Section 2-4. The root mean square error (RMSE) is used to indicate the differences between the predicted values of the BHP by the observer

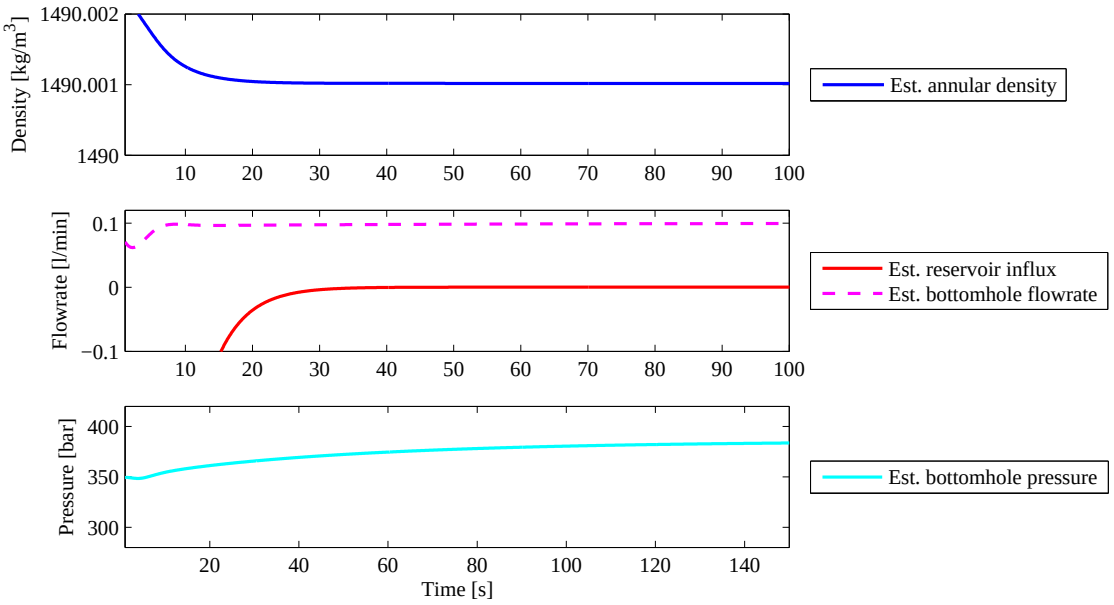

Figure 3-4: Convergence of the uncertain parameters for the adaptive observer, the bottomhole flowrate is scaled to 0.1 l/min for figure readability.

and the values actually observed (in this case the BHP from the model). It is calculated for each set according to [34]:

$$RMSE = \sqrt{\frac{\sum_{i=1}^{n}(\hat{y}_i - y_i)^2}{n}}, \tag{3-50}$$

where $\hat{y}$ is the estimated BHP from the observer and y is the BHP from the simplified model and n is the number of predictions. The results are shown in table 3-2.

From the Table 3-2 it is seen that the set of $\Gamma_1 = 1 \cdot 10^{-11}$, $\Gamma_2 = 1 \cdot 10^{5}$, $\Gamma_3 = 1 \cdot 10^{-4}$ provides the lowest RMSE (0.075). Therefore, this set will be applied in the continuation of this chapter, in order to examine the performance of the observer. Since the RMSE is determined based on the BHP of approximately 400 bar, a RMSE of 0.075 bar is presumed

Table 3-2: The root mean square error for various sets of the gain matrix, Γ.

Γ_1	Γ_2	Γ_3	RMSE (bar)
$1 \cdot 10^{-11}$	$1 \cdot 10^{5}$	$1 \cdot 10^{-4}$	0.075
$1 \cdot 10^{-9}$	$1 \cdot 10^{5}$	$1 \cdot 10^{-4}$	0.075
$1 \cdot 10^{-5}$	$1 \cdot 10^{5}$	$1 \cdot 10^{-4}$	0.96
$1 \cdot 10^{-9}$	$1 \cdot 10^{7}$	$1 \cdot 10^{-4}$	3.90
$1 \cdot 10^{-9}$	$1 \cdot 10^{3}$	$1 \cdot 10^{-4}$	1.43
$1 \cdot 10^{-9}$	$1 \cdot 10^{5}$	$1 \cdot 10^{-2}$	0.079
$1 \cdot 10^{-9}$	$1 \cdot 10^{5}$	$1 \cdot 10^{-7}$	0.076
$1 \cdot 10^{-9}$	$1 \cdot 10^{-4}$	$1 \cdot 10^{5}$	38.64

to be a very small error. As aforementioned, the set of gains was tested on different well parameters as well. It was uncovered that these gains are suitable to estimate the variables within a wide range of parameters.

3-3 Estimator performance

In the previous sections, an EKBF and an adaptive observer were proposed to estimate the BHP. Results of estimator performance will be shown in this section.

Performance during drilling situations To show that not only the estimated parameters converge but also the flow and pressure at the bit are calculated correctly with the estimators, the drilling procedures from Section 2-4 are simulated. The estimators should be able to estimate the BHP during various situations. Results of the pressure, flow and choke opening behaviour are depicted in Figures 3-5 and 3-6 and the corresponding observer error (error between the estimated BHP and 'measured' BHP from the model) is shown along with these dynamics. The estimated variables are not examined here since it is not proven that $\tilde{\theta} \to 0$, thus the estimated parameters might not converge to 'true' values during the situations (where 'true' means the value that is expected for the estimated parameter). Only convergence of $\tilde{q}_{bit} \to 0$ and $\tilde{p}_{bit} \to 0$ was shown, which will be confirmed in the following results.

From Figures 3-5 and 3-6 it is seen that both estimators are able to track the BHP accurately during most situations. It is clear that the EKBF is not able to make correct estimations once there is loss of flow ($q_{bit} = 0$), caused by the fact that the Jacobian of f will not be observable anymore. For the EKBF it is also seen that reservoir influx and change in annular density result in a small error, hereafter the observer estimations converge again to true values. The adaptive observer was designed by using the assumption that $q_{bit} > 0$, therefore the observer will be slightly off when there is no bottomhole flow, which is hardly seen in Figure 3-6. Further, it is visible that the estimated BHP deviates a little at the moment reservoir influx occurs and deviates approximately 1 bar at the moment the annular density rises, though in both cases the error converges to zero again after a few seconds. A remark is made that the oscillation in q_{bit} during pump shutoff with backpressure pump is caused by the implementation of the non-return valve.

Performance during noise Aside from the situations that could happen during drilling operations, the observers robustness during noise will be tested. Process and measurement noise are applied to the main mud pump and the pump pressure sensor as explained in Section 2-4. In Figure 3-7a the error between estimated and measured BHP from both the EKBF and the adaptive observer during process and measurement noise are shown. The property of the EKBF to reduce noise is shown in Figure 3-7b, where the estimated pump pressure of the EKBF and the adaptive observer are compared to the unfiltered pump pressure measurement signal.

From Figure 3-7a it is visible that process noise (simulated between 200 and 400 seconds) does not cause an estimation error for both estimators and both are able to track the BHP and do not become unstable. As far as measurement noise (simulated between 600 and 800 seconds), the EKBF has the property to account for this (by putting more or less weight on

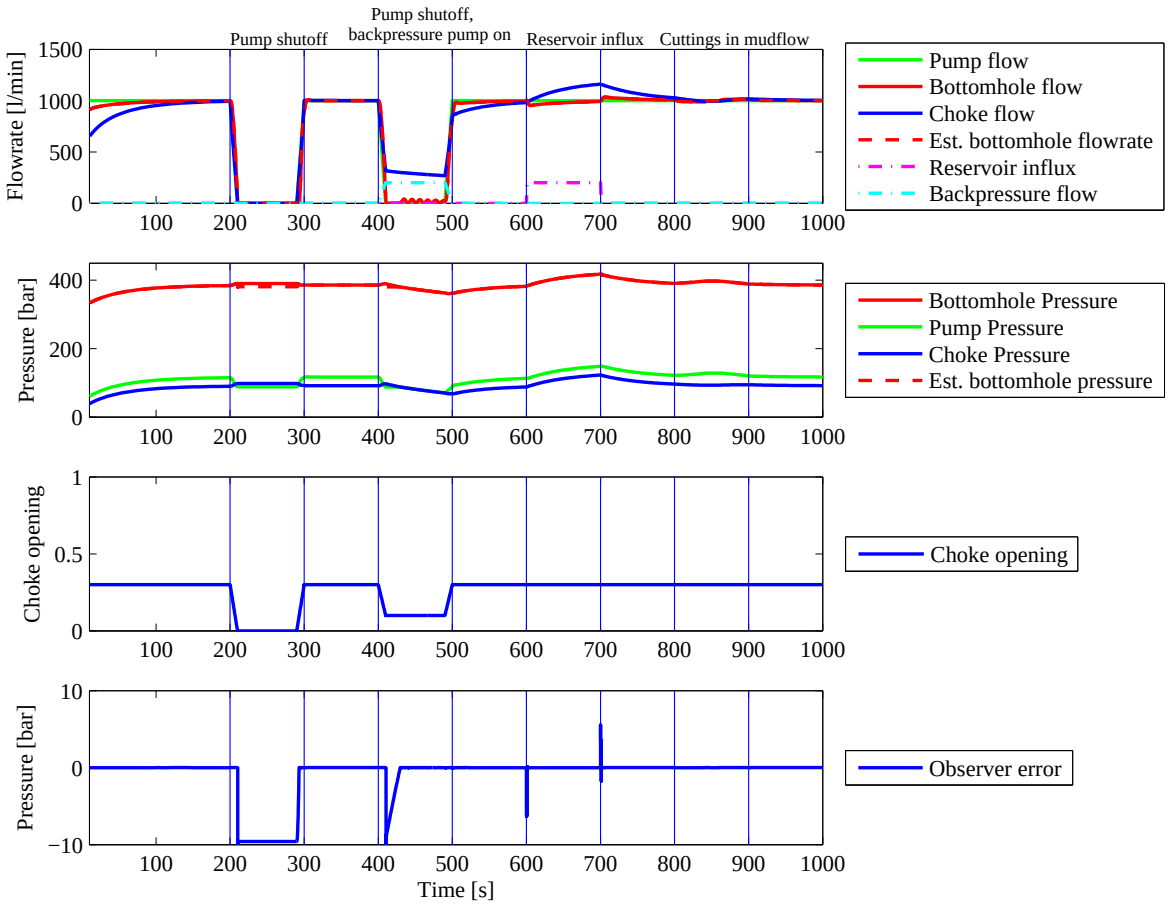

Figure 3-5: Open-loop system performance during simulations of the case study on the EKBF.

the measurement or process signal), which is seen in the estimator error, that is clearly smaller than the observer error for the adaptive observer. In Figure 3-7b where the pump pressure is shown it is seen that estimated pump pressure by the EKBF contains a lot less noise since it is filtered out. This is regarded a beneficial property of the EKBF compared to the adaptive observer. The adaptive observer gains can be chosen differently, which could improve the robustness to noise but will decrease the convergence time. Nevertheless, although the adaptive observer with current gain is not able to filter signals, it is important to notice that the observer is still stable and no signs of divergence of estimations are detected.

A remark should be made here, that a low-pass filter for the sensors in the adaptive observer was considered to obtain the same results as the EKBF. This filtered out other desired dynamics of the system as well and will thus result in model-observer mismatch in other situations. Therefore, the low-pass filter was disregarded.

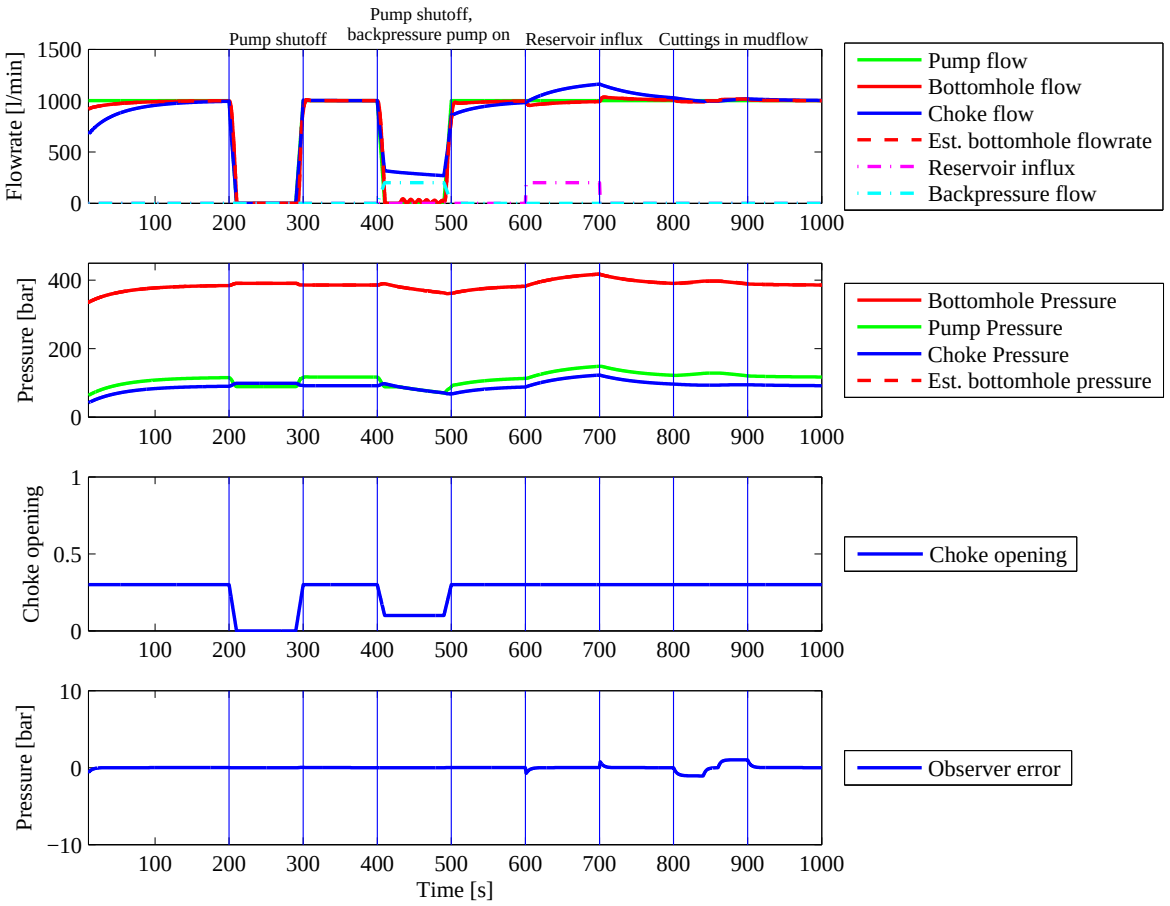

Figure 3-6: Open-loop system performance during simulations of the case study on the adaptive observer.

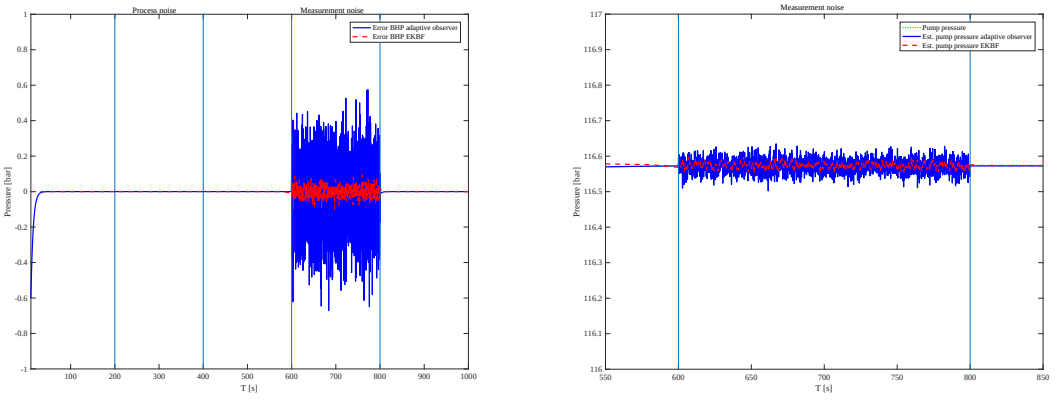

(a) BHP error during process and measurement noise for EKBF and adaptive observer.

(b) Pump pressure measurement and estimated pump pressure by EKBF and adaptive observer.

Figure 3-7: Process and measurement noise on the estimators.

3-4 Summary and concluding remarks

In this chapter, two solutions were proposed for estimating the BHP from surface measurements and known information about well parameters. Firstly, an EKBF was introduced that can be used in nonlinear continuous-time processes. Secondly, an adaptive observer was suggested using a change of coordinates to estimate the unknown state and parameters. It is discussed that global stability of the EKBF is hard to proof, nevertheless local stability and convergence is shown. Proof of convergence of the estimations of the adaptive observer, based on current literature [29], [30], was shown.

Afterwards, the performance of both estimators was examined by simulating typical drilling situations and process and measurement noise. It was observed that the adaptive observer has better performance in various situations and the unknown values converge faster. The EKBF is able to reject Gaussian white noise, which is not a property of the adaptive observer. However, the influence of the noise on the estimation error of the observer is not substantially large and moreover, the observer estimations remain stable (bounded within an error region). Therefore, it is chosen to proceed using the adaptive observer in order to design a suitable controller. The EKBF is kept as a back-up in the continuation of this research in case the adaptive observer might not respond as expected.

Another remark should be made concerning both observers which might not directly stand out from the theory described above. As the goal is to design a control system that would be easy to use for the operator, the estimator must fit this requirement as well. Currently, both estimators require tuning parameters that are not found in a straightforward manner. Namely, the Q-matrix in the EKBF and the adaptive gain matrix Γ in the adaptive observer. The Q-matrix consists of 5 tuning parameters that depend on the uncertainty of the systems states. The adaptive gain matrix consist of three parameters, that can be set for a wide range for the parameters. This brings another advantage of the adaptive observer since user convenience will be better.

Chapter 4

Controller design

This chapter is concerned with the aim to design a controller for the MPD system. Now a solution has been found to retrieve bottomhole information, control of the BHP is still pending. Sections 4-1 and 4-2 present two control solutions, suitable for industrial applications. The typical situations during drilling operations from Section 2-4 are applied here as well to examine the performance of the controller. Note that the usability for the operator is important, so the required control parameters are analysed as well.

In order to evaluate the control performance, a drilling window of 10 bar ($\pm$ 5 bar) is assumed. Thus, the controlled BHP needs to stay within 5 bar of its setpoint. Throughout this section, the BHP setpoint is set to 350 bar. Therefore upper and lower bounds are equal to 355 bar (fracture pressure) and 345 bar (pore pressure).

4-1 PI control

A common solution for industrial operations and likewise for MPD systems is PI(D) control. Therefore, the performance of a Proportional Integral (PI) controller will first be examined. The derivative term is left out since its impact on system stability might not be as expected in real-world applications [35]. The control vector, u, is calculated with the general PI equation:

$$u_{PI} = K_p(e + \frac{1}{T_i}\int_0^t e\,dt), \tag{4-1}$$

where u_{PI} is in this case the choke position z. e is the error, namely the difference between the estimated BHP and the setpoint for the BHP, e=p_{setp}−$\hat{p}_{bit}$. K_p is the proportional gain and T_i is the integral time. The controller variables were tuned by using the Ziegler-Nichols method. These were set to K_p=-0.5 and T_i=10 s. Note that a negative K_p is required since a positive error means the BHP is below setpoint. Therefore, to keep the BHP near its setpoint (and increase the BHP), the choke opening must smaller (thus a positive error requires a lower control signal).

Integrator anti-windup The choke valve in the control loop imposes a problem on the integral term of the PI controller. For instance, if the valve is closed too slow during pump shutoff, pressure will be lost and the BHP will be below its setpoint. This results in a constant error during the period that the valve is closed. In this case the valve is saturated since it is fully closed. Whenever actuator saturation happens the control signal stops changing and the stored integrator value will grow, until the sign of the error changes and the integration reverses. This process is called *integrator windup* [36]. It can lead to large overshoots and poor transient responses. Therefore, integrator anti-windup is added to the control system.

The anti-windup scheme is implemented by using the valve's saturation in the loop. As soon as the actuator is saturated, a feedback loop around the integrator becomes active and starts to keep the integrator input small by using the anti-windup gain, K_a. By applying this anti-windup scheme, both the overshoot and control effort are reduced. Implementation of the anti-windup scheme in an example control scheme is shown in Figure 4-1.

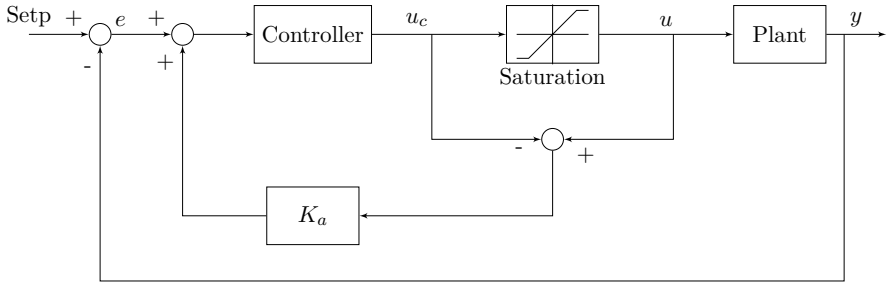

Figure 4-1: Block scheme of integrator anti-windup.

Applying this PI controller in combination with the adaptive observer of Section 3-2 and the anti-windup scheme leads to the performance results seen in Figure 4-2.

In Figure 4-2 the *observer error* is the error between the simulated BHP from the model and the estimated BHP from the observer. The *control error* is the error between the setpoint for the BHP and the estimated BHP, since this is the value that is controlled. The *system error* is the error between the setpoint for the BHP and simulated BHP from the model. A remark should be made that these error notations will be used in the continuations of this chapter and in Chapter 5. As is seen, a simple PI controller is able the control the 'measured' BHP (BHP from the well model) within less than 1 bar difference to the setpoint (so within the required drilling window). A small impediment is found in the fact that the controller is late in reacting when the pump is turned off between t=200-300 s. A solution is required to compensate for the flow from the main mud pump and from the backpressure pump in order to minimize the error during pump shutoff.

4-1-1 PI and feedforward control

In this section, feedforward gain is added to the PI feedback control loop to account for the mud flow from the pumps. It is used to improve the response, for instance when making new drillstring connections or when tripping, if the pump flowrate changes. In order to take the changing flowrate into account, the feedforward gain is multiplied by the flow input from the main mud pump. If the feedforward control action is close to the required control output,

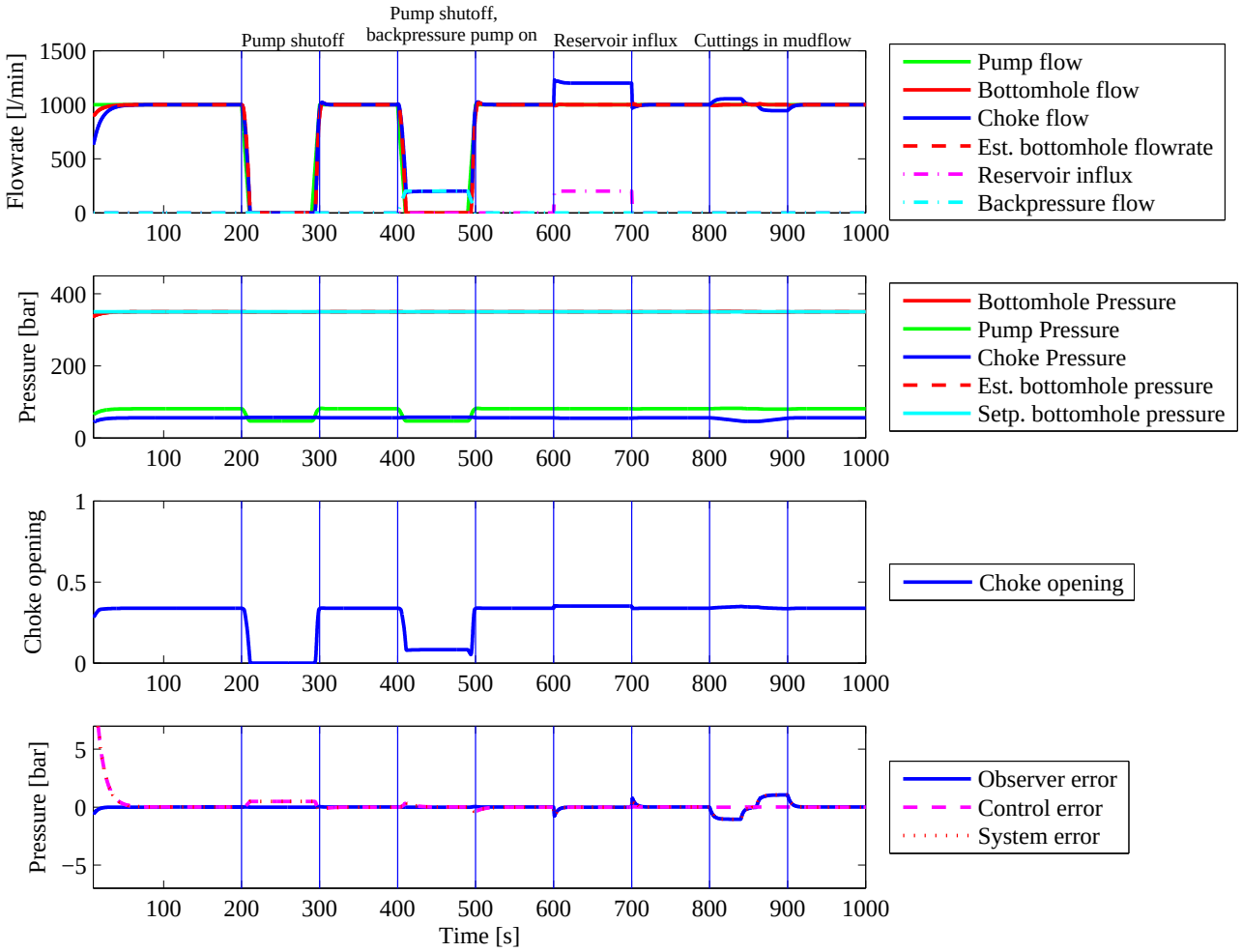

Figure 4-2: Closed-loop system performance of PI control with adaptive observer.

less control effort from the PI controller is required. Therefore, faster error reduction is achieved and the system does not rely solely on the PI controller. Note that the flow from the backpressure pump is taken into account as well to capture the changes in flowrate if the backpressure pump is turned on. Therefore, the backpressure pump is added to the flow from the main mud pump before the feedforward gain is applied. A control scheme of the PI and feedforward controller (with integrator anti-windup) is found in Figure 4-3.

It is now presented how the feedforward gain, K_f, is calculated to account for the flow from the main mud pump (and backpressure pump). At first, a setpoint for the choke pressure is determined by using the setpoint for the BHP in the following equation:

$$p_{bit} = p_c + \rho_a g h_{bit} + F_a \rho_a (q_{bit} + q_{res})^2. \tag{4-2}$$

Here, the parameters from Appendix A are filled in and, as mentioned earlier; q_{bit}=1000 l/min and p_{bit}=p_{setp}=350 bar. A choke pressure setpoint, $p_{c_{setp}}$, of approximately 55 bar is required to achieve a BHP of 350 bar.

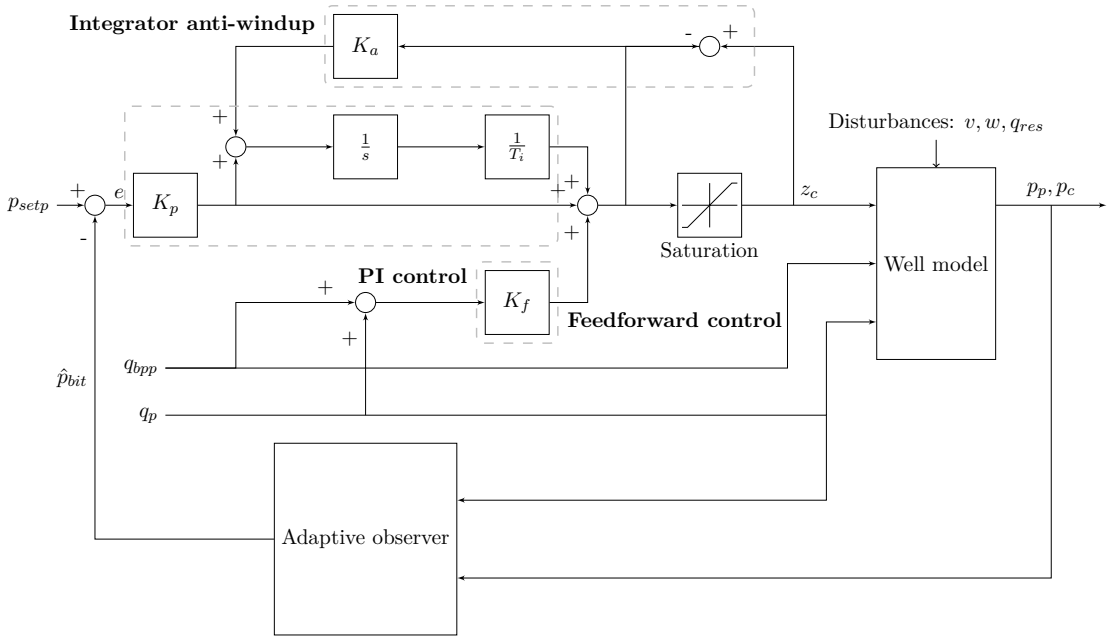

Figure 4-3: Block scheme of feedback control with PI-controller and feedforward control on adaptive observer.

The setpoint for the choke pressure is applied in the following equation to acquire a setpoint for the valve's position:

$$\dot{p}_c = \frac{\beta_a}{V_a}\left(q_{bit} + q_{res} + q_{bpp} - C_v(z)\sqrt{\frac{p_{c_{setp}} - p_0}{SG}}\right). \tag{4-3}$$

Here $\dot{p}_c$ is zero since a steady-state situation in the well is assumed (at 1000 l/min) and q_{res} and q_{bpp} are assumed zero as well. This leaves the equation to $q_{bit} = C_v(z)\sqrt{\frac{p_{c_{setp}} - p_0}{SG}}$. The setpoint for the choke pressure, $p_{c_{setp}}$, is filled in and a desired setpoint for the valve can be calculated, which is approximately, z_{setp}=0.3. The feedforward gain is used as: $z_c = u_f = K_f(q_p + q_{bpp})$, so the gain can be determined by dividing the desired choke position by the steady-state pump flow of 1000 l/min as:

$$K_f = \frac{z_{setp}}{q_p} \tag{4-4}$$

In this steady-state situation, the feedforward gain of 20 is required to keep the BHP at its setpoint. Adding this controller to the earlier defined PI controller results in the following control law:

$$u_{PI} = K_p(e + \frac{1}{T_i}\int_0^t edt) + K_f(q_p + q_{bpp}). \tag{4-5}$$

The performance results of using the feedforward and PI controller (in combination with the integrator anti-windup) on the well is shown in Figure 4-4. It is observed that the PI and feedforward controller performs better during pump shut-off and start up than solely the PI controller. This is coherent with expectations, since the controller now takes the flow from the main mud pump directly into account. Now, the error throughout the simulation stays below 1 bar which is when the annular density changes and this is due to convergence time

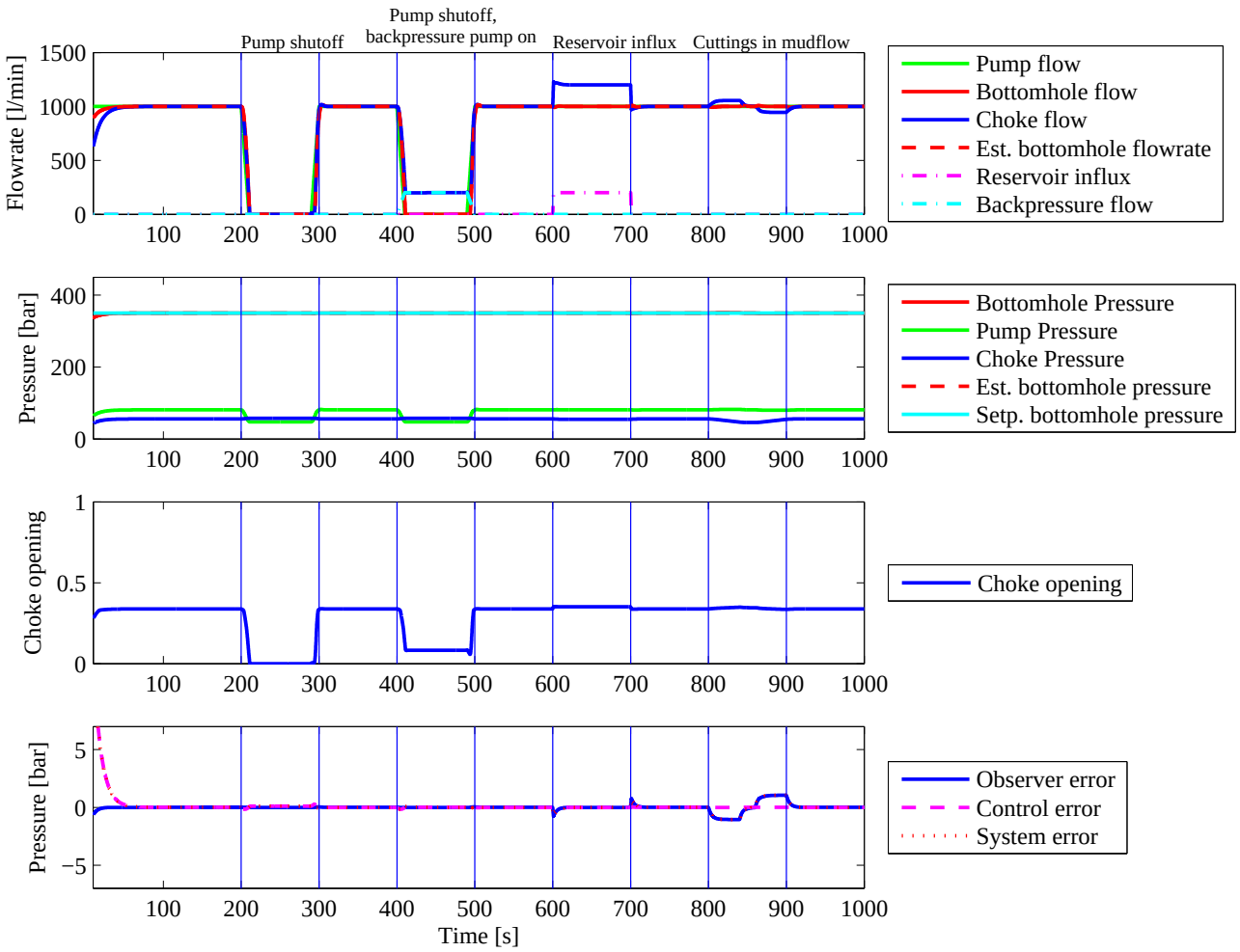

Figure 4-4: Closed-loop system performance of PI control and feedforward with adaptive observer.

of the observer (thus not a controller issue). A big advantage of the PI controller is that it is easily build and that the values for K_p and T_i are determined relatively easy. A downside is that this PI controller only depends on the error of the estimated BHP, which might be less robust if the observer provides deviating results. In the continuation of this thesis, if the term *PI controller* is used, it implies that feedforward control and integral anti-windup are also implemented in the control loop.

4-2 Linear quadratic regulator control

Another control design technique from industry is the *linear quadratic regulator* (LQR) [37]. It uses a static gain matrix and full state feedback from the model. One should be aware that full state feedback is not possible with the MPD well model since the flow through the bit, q_{bit}, is unmeasured. Therefore, the state measurements from the system, p_p and p_c, will be used together with the estimated flow, $\hat{q}_{bit}$. Note that in this research, an adaptive observer

is used instead of a Kalman filter for the estimated q_{bit}. This is regarded a modified form of the Linear Quadratic Gaussian which is a combination of an LQR and a Kalman filter [37].

LQR is a linear optimal controller based on a state-space of the system's model:

$$\begin{cases} \dot{x} &= Ax + Bu + w, \\ y &= Cx + v \end{cases}. \tag{4-6}$$

Since our system is nonlinear, the model from Section 2-1-2 with states $\dot{x}=\begin{bmatrix} p_p & p_c & \hat{q}_{bit} \end{bmatrix}^T$ will be linearised to:

$$A = \begin{bmatrix} 0 & 0 & \frac{-\beta_d}{V_d} \\ 0 & 0 & \frac{\beta_a}{V_a} \\ \frac{1}{M} & -\frac{1}{M} & 0 \end{bmatrix} \qquad B = \begin{bmatrix} 0 \\ \frac{\beta_a}{V_a} \\ 0 \end{bmatrix} \qquad C = \begin{bmatrix} 1 & 1 & 1 \end{bmatrix}. \tag{4-7}$$

Note that, here again, the bit flow q_{bit} will normally not be measured but the estimated flow from the observer, $\hat{q}_{bit}$, is used.

The performance index, J, of the LQR is defined as

$$J = \frac{1}{2}\int_0^T (x^T Q x + u^T R u) dt, \tag{4-8}$$

where $Q \geq 0$ and $R > 0$ are symmetric, positive (semi-) definite weighting matrices. Also, u is the input (the valve's position) and x is the state feedback from the plant. The performance index is minimized in MATLAB and the LQR gain, K_r, for linear-state feedback is found and applied in the control law as:

$$u = -K_r x. \tag{4-9}$$

In this set-up the state feedback vector will thus be:$x = \begin{bmatrix} p_p & p_c & \hat{q}_{bit} \end{bmatrix}^T$. The LQR gain, K_r, has the following form:

$$K_r = -R^{-1}B^T P \tag{4-10}$$

Where P is the solution to the algebraic Ricatti equation (which is solved in MATLAB):

$$A^T P + PA - PBR^{-1}B^T P + Q = 0. \tag{4-11}$$

The term 'regulator' in LQR refers to the fact that this controller regulates the states to zero. Thus the LQR controller is only able to act as a disturbance rejector. In order to track the setpoint for the BHP, an integral term is added to the LQR controller. This is done by adding a new state, z_e, to the LQR controller:

$$\begin{bmatrix} \dot{x} \\ \dot{z_e} \end{bmatrix} = \begin{bmatrix} Ax + Bu \\ e \end{bmatrix}, \tag{4-12}$$

where the error is, $e = p_{setp} - \hat{p}_{bit}$. If a regulator is found that stabilizes the system, then $\dot{z} = 0$ in steady state.

For the same reasons that are mentioned in Section 4-1, feedforward control and integrator anti-windup are implemented in the LQR control loop as well. The control law with the LQR controller is now defined as:

$$u = -K_r \begin{bmatrix} x \\ z_e \end{bmatrix} + K_f(q_p + q_{bpp}) = -K_r \begin{bmatrix} p_p \\ p_c \\ q_{bit} \\ \int_0^t (p_{setp} - \hat{p}_{bit})dt \end{bmatrix} + K_f(q_p + q_{bpp}). \tag{4-13}$$

This LQR controller is shown in a control scheme in Figure 4-5.

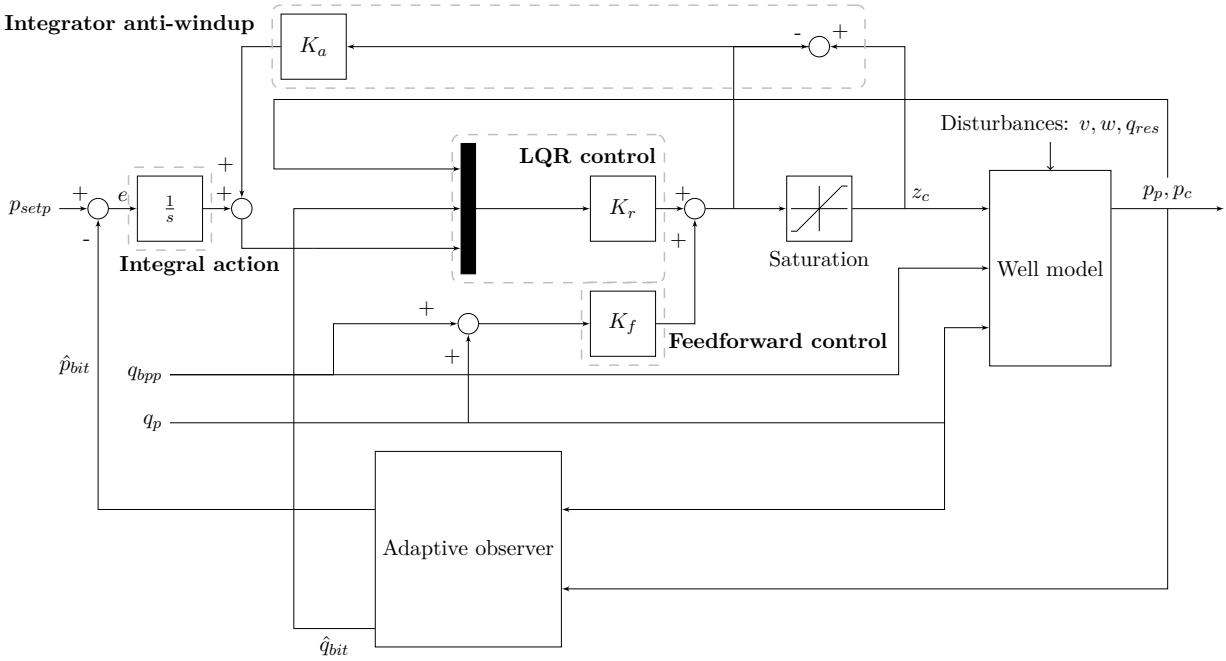

Figure 4-5: Block scheme of the LQR controller with feedforward and integrator anti-windup.

Applying the LQR controller combined with feedforward gain and the integral anti-windup, as described in Section 4-1, gives the results shown in Figure 4-6. From Figure 4-6 it is seen that the LQR is able to control the BHP accurately. The only error that occurs is during change of annular density which is due to convergence time of the observer. As is seen the performance of the LQR controller is very resemblant to the performance of the PI controller. In order to examine the control error closely, the estimated BHP of the PI and LQR are compared to the BHP setpoint in Figure 4-7. Note that the estimated pressure is taken since the control error is examined. From Figure 4-7 it is visible that the PI controller performs better than the LQR controller during pump shutoff and start up and during changes in annular density. The LQR controller performs better during reservoir influx.

In practice, the LQR controller is expected to outperform the PI controller during noise since it uses real-time plant measurement as well. This presumption will be tested in Chapter 5 on the validation model. On the other hand, implementation is slightly harder since the Q and R values need to be found and a (linearised) model of the system is required. In the continuation of this thesis, if the term *LQR controller* is used, it implies that feedforward control and integral anti-windup are also implemented in the control loop.

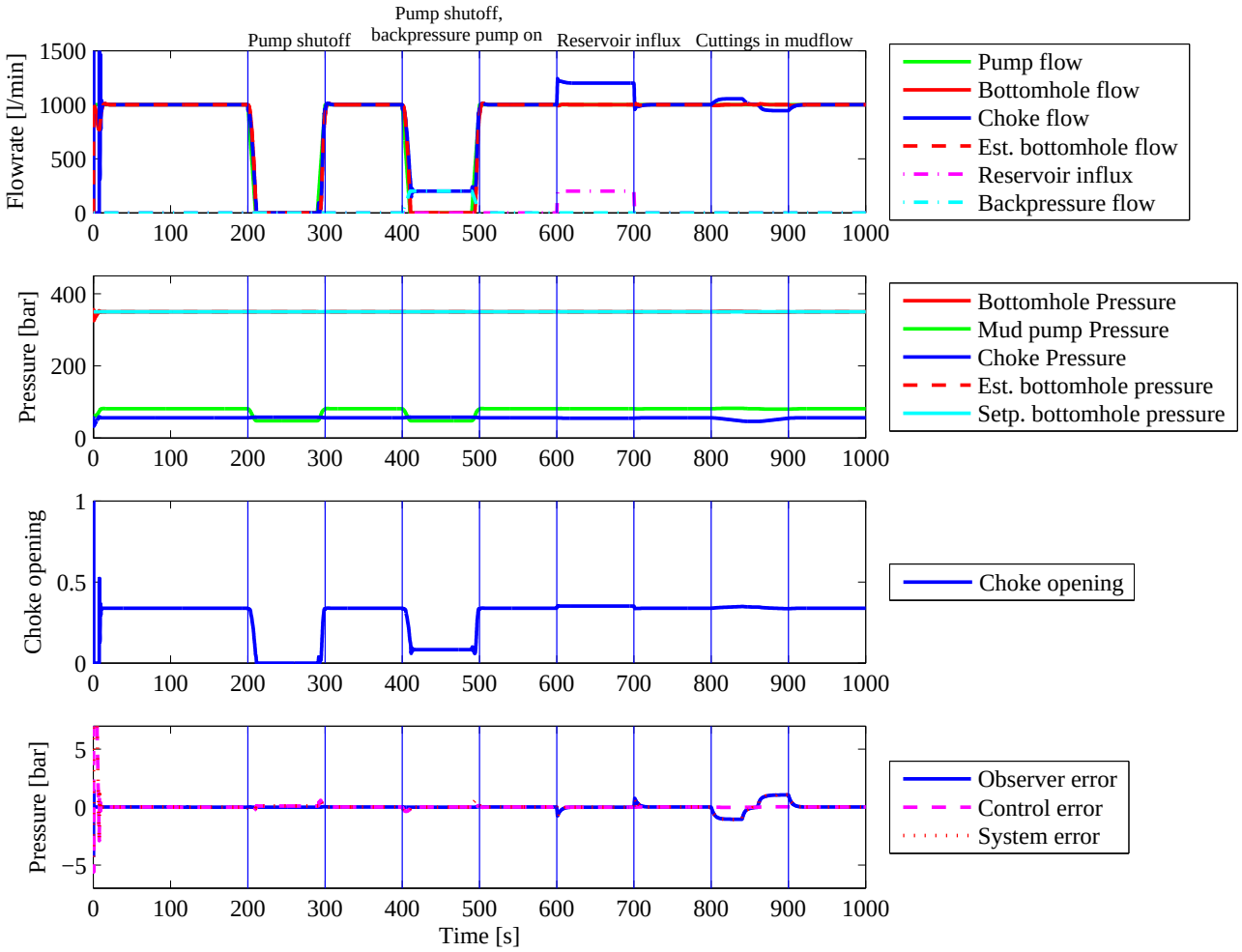

Figure 4-6: Closed-loop system performance of LQR control with adaptive observer.

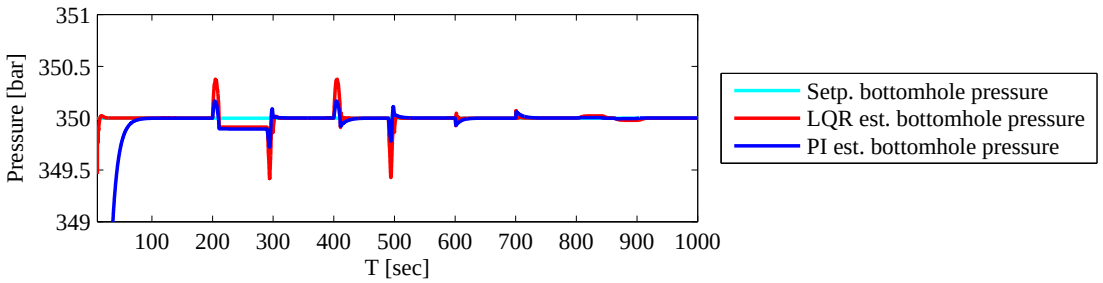

Figure 4-7: Closed-loop system performance of PI and LQR controller.

4-3 Operator usage of the control system

As mentioned in Chapter 1, one of the sub-objectives states that the automated MPD control system should be easy to operate; thus little or no input parameters should be required from the operator during drilling. This requirement will be discussed in this section. In Figure 4-8

all required input parameters for the automated MPD control system are visualized.

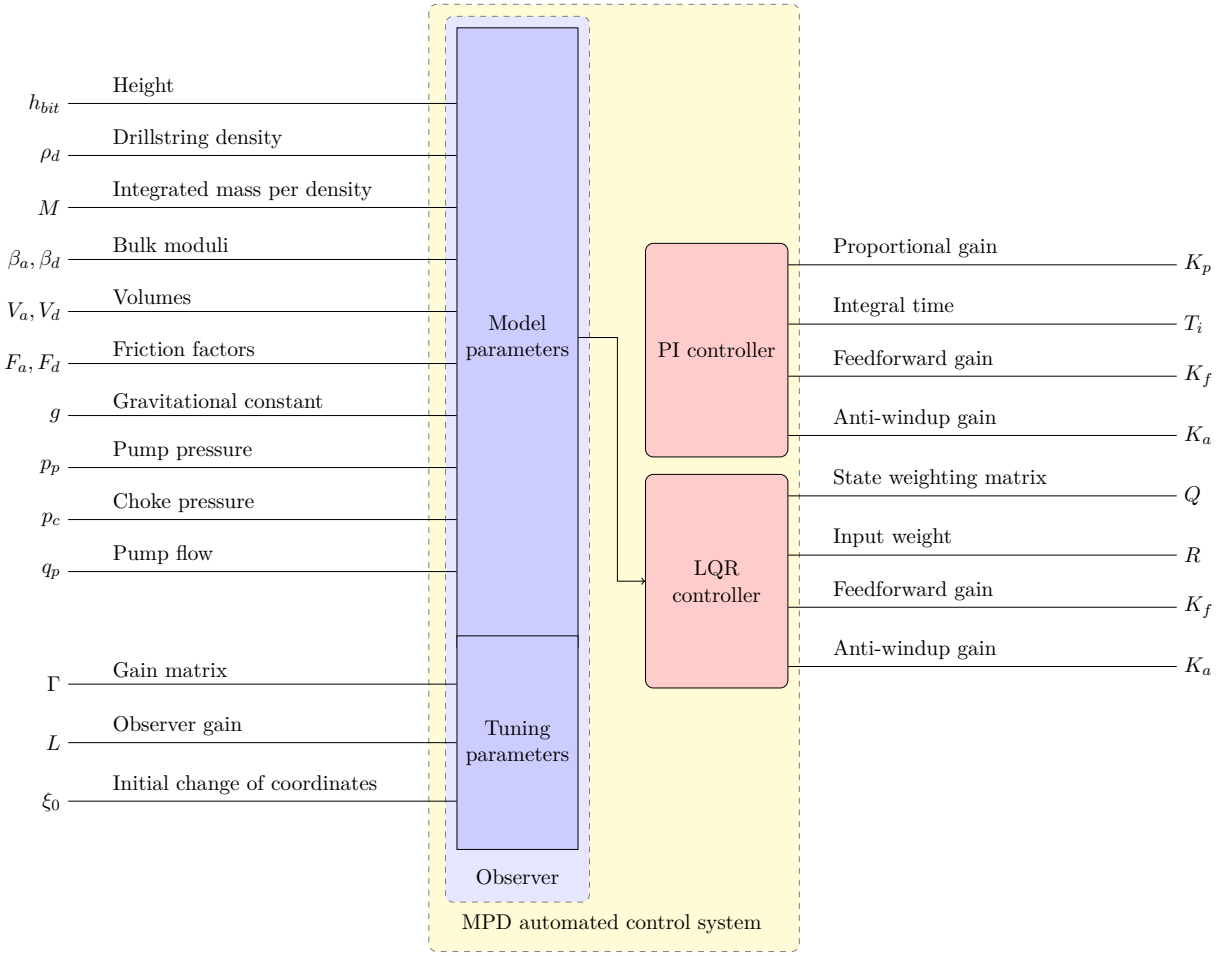

Figure 4-8: Required parameters for the MPD automated control system split into observer and control parameters.

Now that all the required parameters are defined, every parameter has to be investigated to see if it is computed or measured by the automated MPD system itself, can be pre-set as a fixed value in the control system or need to be provided by the operator (or, less desirable, by a specialist). If input from the operator is required, it should preferably be comprehensible parameters for the operator that can be filled in directly. Each parameter and how it is provided to or by the system is defined in Table 4-1. Afterwards, the tuning parameters from the observer and control parameters will be further discussed since they require some additional explanation.

The tuning parameters determined in this research are usably for any general MPD well. The gain matrix, Γ, observer gain, L and initial change of coordinates, ξ_0 are all suitable within a wide range of well parameters. Unless faster or slower changes in density or reservoir influx are expected, these tuning parameters will be able to estimate the BHP. Otherwise, the observer can be simulated offline, determining the observer tuning parameters beforehand, so no adjustments to the observer parameters are required from the operator during drilling.

Table 4-1: Control system parameters and how it is provided to/by the control system.

Model parameters	
Height	Depth measurement by system
Drillstring density	Online measurement from the Coriolis meter, measured by system
Integrated mass per density	Computed by system from density/height measurement and volumes
Bulk moduli	Offline measurements by a mud engineer, filled in by the operator
Volumes	Drillstring & annulus volumes required from operator, found in pipetally
Friction factor	Computed by system from system parameters, offline mud measurements and required flow by the operator
Gravitational constant	Pre-set in system
Pump pressure	Pump pressure measurement by system
Choke pressure	Choke pressure measurement by system
Pump flow	Required from operator
Tuning parameters	
Gain matrix	Computed by system using the well parameters
Observer gain	Computed by system using the well parameters
Initial change of coordinates	Computed by system using the well parameters
PI control parameters	
Proportional gain	Tuned during start-up of project
Integral time	Computed by system based on bulk modulus, density, height and lag time of choke valve
Feedforward gain	Computed by system based on desired mud flow and well parameters
Anti wind-up gain	Fixed value
LQR control parameters	
State weighting matrix	Tuned during project
Input weight	Pre-set in system
feedforward gain	Computed by system based on desired mud flow
Anti wind-up gain	Fixed value

In general, the PI control parameters, K_p and T_i, should be tuned by a control engineer (specialist). During first trials with the MPD control system it is suggested that a control engineer is always present in order to examine the performance of these parameters. Nevertheless, a suggestion is given now on how the PI controller could be implemented so that it does not need to be adjusted during drilling. A suitable K_p can be found in the trials, tuning the gain in order to maximize the performance whilst making sure that the system does not become unstable. Subsequently, the integral time, T_i, can be calculated online by making use of the propagation speed of the mud. For this purpose, the bulk modulus, density and height are necessary to calculate the time it takes before a pulse has travelled from the choke to the bottomhole. Furthermore, it is essential to take some lag time into account, since the choke valve might have backlash and delay. From the calculated propagation time

and lag time for the choke valve, the integral time can be determined by the control system. The feedforward gain, K_f, is computed by the control system if the required drilling flow is filled in by the operator and well parameters are known. A fixed value is chosen for the anti wind-up gain, K_a. Choosing a K_a that is equal to or larger than the integral time, will make sure the anti-windup scheme is activated fast and no windup occurs (for instance K_a=10 will provide accurate results).

Determining the LQR control parameters is slightly more complicated. The feedforward gain and anti-windup gain are found in the same way as described for the PI controller. The weight on the input R can be set to 1, then only the matching Q should be tuned. This should be done according to the scale of the parameters and the expected deviations. Here, a control engineer needs to tune the state weighting matrix depending on the well parameters. Furthermore, the model parameters are also required for the linearised model to determine the LQR gain, this can be computed by the control system. In general, the same could done as described above by trying to calculate the gains during drilling so that no changes are required from the operator. Nevertheless, tuning the Q and R matrix is less straightforward and therefore also harder to implement in the system if one wants to keep high performance with different well parameters.

4-4 Summary and concluding remarks

In this chapter, two solutions are proposed to control the estimated BHP from the adaptive observer that was designed in Chapter 3. PI control has earlier proven to be successful in industrial applications, whereas LQR control is a new suggestion.

A PI controller (combined with integrator anti-windup) is first proposed, which is able to control the BHP during various situations. Two drawbacks of this controller are noted; the BHP is not accurately controlled during pump shut-off or start up and during increase and decrease of density in the annulus. In order to solve the first issue, feedforward control is added to compensate for the flow from the main mud pump. The error during pump shut-off and start up is now reduced to a large extent. The little variation during annular density change is left unsolved, since this is an observer fault (due to convergence time) and cannot be solved by adjusting the controller.

Secondly, an LQR controller was proposed. The LQR controller was also applied in combination with integrator anti-windup and feedforward control. It is seen that the performance is approximately the same for the LQR and PI controller. The LQR controller provides full state feedback and uses direct measurements from the system and is therefore expected to be more robust during noise. On the other hand, if the linearised model turns out not to match the plants model this could give false results.

Furthermore, the required parameters for the automated MPD control system are provided. Every parameter is examined to see if it needs to be provided by the operator, is calculated by the system or it is given as a measurement output. For the PI controller a suggestion was given on how to implement the controller so that no adjustments from the operator during drilling are required. The LQR controller is a little harder to implement since a linearised model and weighting matrices are required.

Lastly, it is important to notice that both the PI and LQR controller are linear control methods, these control methods were chosen since they have proven succesfull in industrial applications and will be easy for the operator to use. As mentioned earlier, the MPD well model is nonlinear. In this control loop, where the well and the observer use the same model, the nonlinearities apparently do not have an effect on the controller performance. In practice however, the dynamics of the well might be more nonlinear and this could potentially decrease the controllers performance.

Chapter 5

Validation

In the previous chapter, two controllers have been designed to control BHP. It is shown that both the PI and LQR controller are able to keep the error of the BHP setpoint and the measured BHP (from the well model) between the defined drilling window of $\pm$ 5 bar. However, in Chapter 4, a 'perfect world' was used, indicating that the model used to simulate the real well was the same as the model implemented in the adaptive observer (namely the drillstring and annulus model).

In order to validate if the designed control system is able to control the BHP in a well with differing transient responses, the validation model from Section 2-2 is used. This validation model differs in terms of transient responses, since pressures and flows are calculated in each section. To verify whether the control system is robust in various circumstances, it will now be applied in a control loop with the validation model and its performance will be analyzed on various aspects:

- drilling situations
- noise
- varying friction

Here again, a drilling window of $\pm$ 5 bar is assumed to asses the ability to control the BHP.

5-1 Simulations

5-1-1 Drilling situations

In order to validate the model, several drilling situations have been defined in Section 2-4. These situations during drilling are: tripping (shutting off the pump and shutting of the pump simultaneously with starting up the backpressure pump), reservoir influx and drilling

cuttings. The situations are simulated on the validation model and the observer and controller implemented in the loop to control the BHP. The observation was made earlier that the multiple compartment model captures fast pressure changes by calculating the flow and pressure at each section. In order to make sure that observer and control error will not influence each other, low gains for the controller should be chosen. Therefore, the proportional gain, K_p, is re-adjusted to $K_p = -1 \cdot 10^{-2}$. Performance results of the PI controller on the flow, pressure and choke position of the well and a PI/LQR comparison is shown in Figure 5-1.

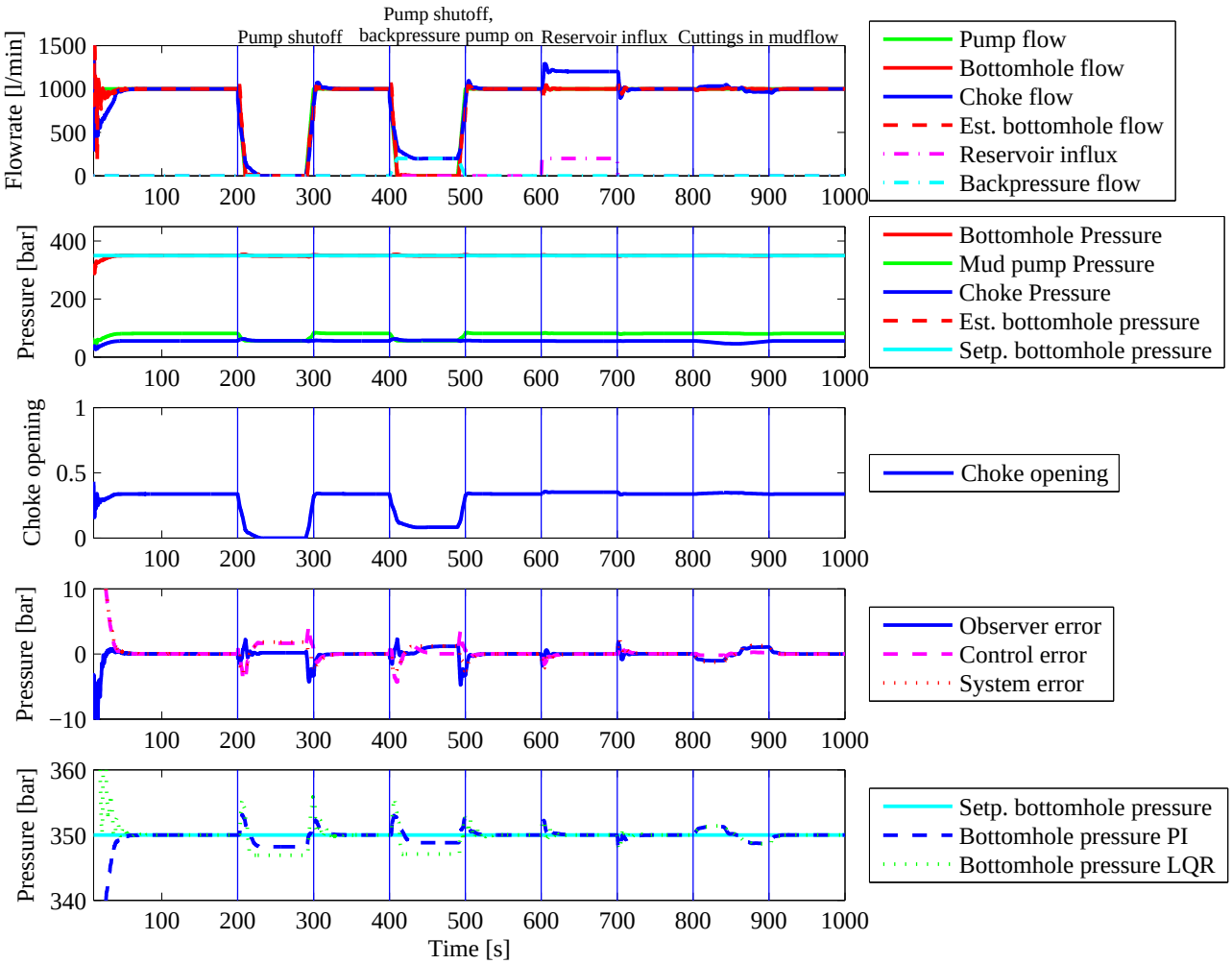

Figure 5-1: Closed-loop system performance PI control with adaptive observer on the validation model and a PI/LQR comparison during various drilling situations.

As is seen, the PI controller is able to control the BHP to within the drilling window. During pump shutoff and start up, a small error arises (of approximately 4 bar), however, in all other situations, the BHP is controlled very well. The difference in performance compared to the simple model in Chapter 4 is caused by the fact that transient responses are now included to a higher extent in the models. In the last subfigure of Figure 5-1 the performance of the PI and LQR controller are compared. It is seen that both controllers are able to control the BHP within the drilling window. Nevertheless, the LQR controller performs slightly worse than

the PI controller at the moment that the pump is off. This is explained by the fact that the linearised model to determine the LQR gains assumes a (positive) non-zero $\hat{q}_{bit}$. When loss of flow occurs, the flow through the bit is zero and therefore there is no full-state feedback. The state feedback from $\hat{q}_{bit}$ is lost, which causes a control error. Since results on the system dynamics are approximately the same for both controllers, the performance results for the LQR controller (flow, pressure, choke position and errors) are shown in Appendix C.

A worst-case scenario All possible drilling situations are treated separately in the section above. During a real MPD operation, it is a possibility that some situations happen simultaneously. Therefore, a worst-case scenario is now described. The pump is shutoff to make a new drillstring connection and suddenly reservoir influx enters the annulus. The control system should then still be able to detect the influx and control the BHP. This situation is simulated on the validation model and the results are shown in Figure 5-2. Pump shut down is simulated at t=200-300 s and reservoir influx occurs at t=250 s.

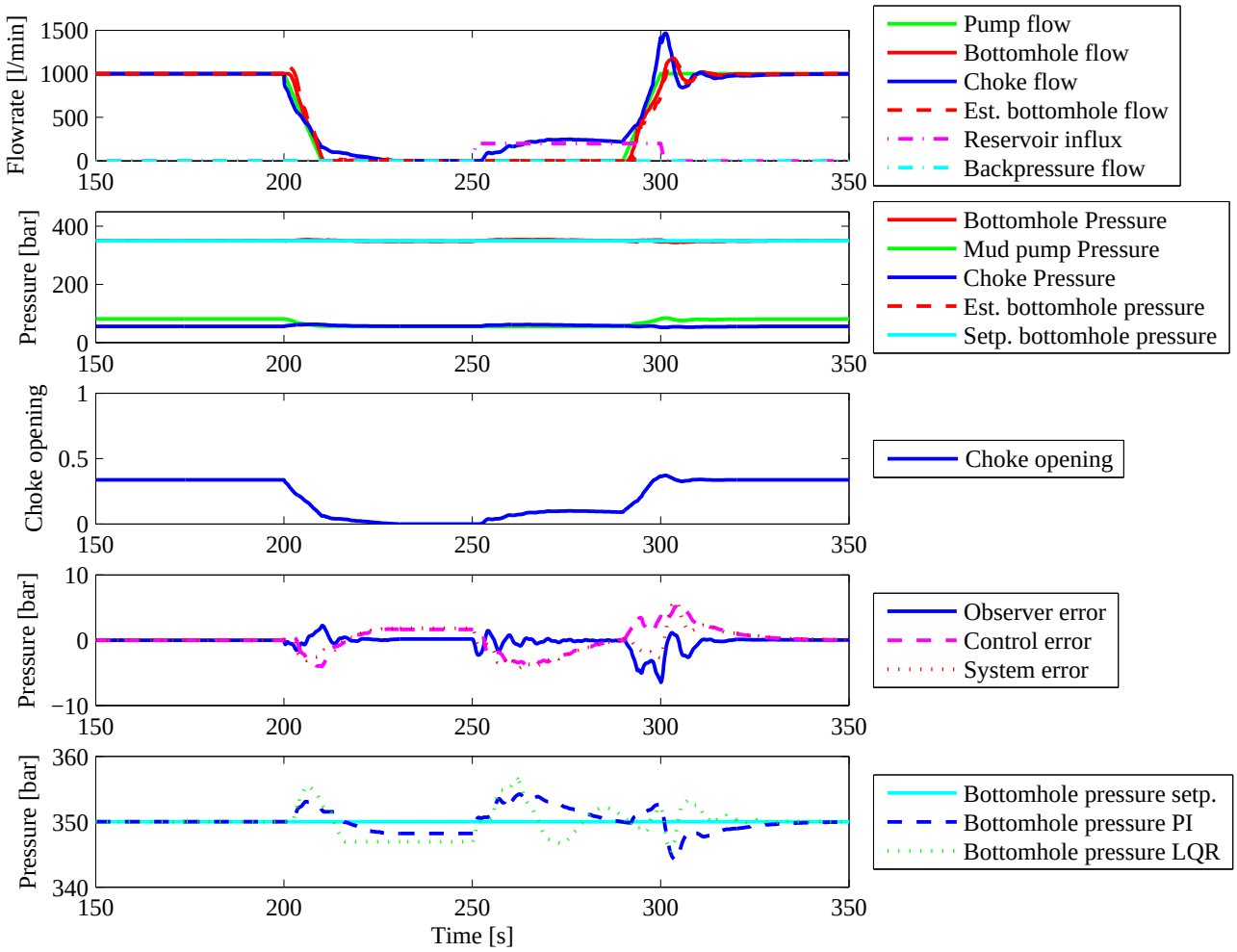

Figure 5-2: Closed-loop system performance of PI control with adaptive observer on the validation model and a PI/LQR comparison during a worst-case scenario.

It is seen that even this situation is handled properly by the control system, the BHP is kept within the drilling window. The observer is able to detect the reservoir influx when the pump is off and the observer estimations converge to zero. Also the controller is able to control the BHP within the drilling window. The last subfigure is shown to compare the performance of the PI and LQR controller. It is seen that the LQR controller does not perform as desired since the BHP error is 6 bar, so it is outside the ±5 bar range of the drilling window. This is caused again by the fact that loss of low decreases the LQR controller's performance. As aforementioned, LQR results are shown in Appendix C.

5-1-2 Noise

Furthermore, as described in Section 2-4, noise will be applied to the validation model. The process noise is applied on the mud pump flowrate and the measurement noise is applied on the pump pressure output of the validation model. Both process and measurement noise are implemented. As earlier indicated in Section 3-2, the adaptive observer (with earlier determined gains) does not filter any noise. Thus it is not expected that the noise is absent or reduced in the estimated BHP signal, but it will be examined if the control system is still stable and handles noise to the extend that the control output will not diverge or blow-up. In order to examine the effect of noise on the control system, the choke opening (control signal) and BHP are analyzed. These results are shown in Figure 5-3.

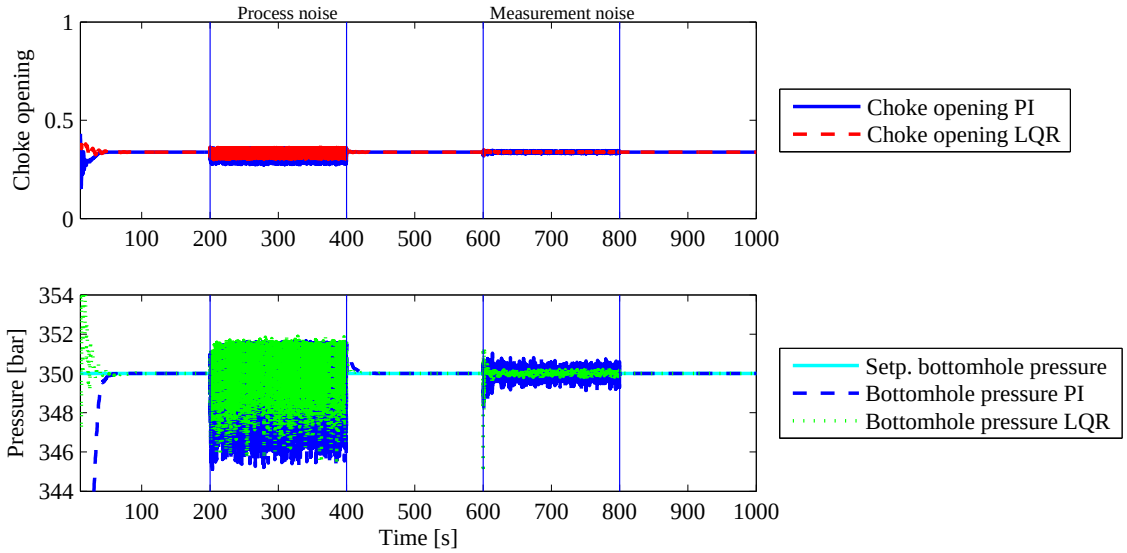

Figure 5-3: Closed-loop system performance of PI and LQR control with adaptive observer on the validation model during process and measurement noise.

The results show that both control systems are able to accurately control the BHP during process and measurement noise. The choke openings for both control systems show that the control signals oscillate, nevertheless the signals do not become unstable. In both noise situations the BHP is kept within the drilling window and it can be concluded that the control system are robust to noise and stay in a stable region. In the last subfigure of Figure 5-3 the results of process and measurement noise on the controlled BHP are shown. It is seen that

LQR controller performs better during process noise. This is expected since the LQR takes multiple states into account to compute the gains so different weights are given the states to anticipate on expected process or measurement noise. The PI controller can be adjusted to noise if K_p and T_i are tuned differently but this will significantly reduce the controllers performance during other situations.

5-1-3 Varying friction

At last, the effect of varying the frictional pressure drop will be examined. In the simple drillstring and annulus model, a Newtonian fluid in a smooth pipe and a generalized Reynolds number (for a flow of 1000 l/min) were assumed, in order to estimate the frictional pressure drop in the well. During actual drilling, the friction might behave differently from this simple Newtonian fluid. Therefore, two different types of pressure drops are presented in Section 2-4. The second friction model assumes a rough pipe and the third friction model assumes an offset in the frictional pressure drop to account for drillstring rotation. Note that the pressure drop with an offset for drillstring rotation is not implemented in the model of the adaptive observer. Hence, a model mismatch is present between the plant and the observer's model thus an observer error is expected. Nevertheless, it is interesting to see how the control system handles unmodelled pressure losses. The different frictional pressure drops are applied to the validation model during the drilling situations from Section 5-1-1, the results are shown in Figure 5-4.

Applying a Newtonian fluid with a rough pipe friction factor results in a small observer error but does not significantly reduce the MPD control system's performance. This is expected since frictional pressure losses in smooth and rough pipes differ only 0.5 bar. From friction model 3 it is seen that putting an offset on the friction has a great effect on the performance of the control system. When a 30% higher pressure drop is applied, the observer does not detect this, this is clarified by the fact that a 30% higher pressure drop is not accounted for in the model in the observer. The pressure drop at steady-state flow of 1000 l/min is higher (6 bar and 1 bar higher). If frictional pressure drops from the bottomhole to the surface are higher, lower pump and choke pressures are measured at the surface. Subsequently a lower estimation for the BHP is made and thus a larger error arises. The observer error is approximately 7 bar which coincides with expectations from the measurements. Still, for all three friction models, the control error is kept close to zero.

The intention of modelling varying friction behaviour was to examine the observer performance (and not necessarily control performance). Therefore, the results for the LQR controller are not shown since they are approximately equal to the results shown with the PI controller.

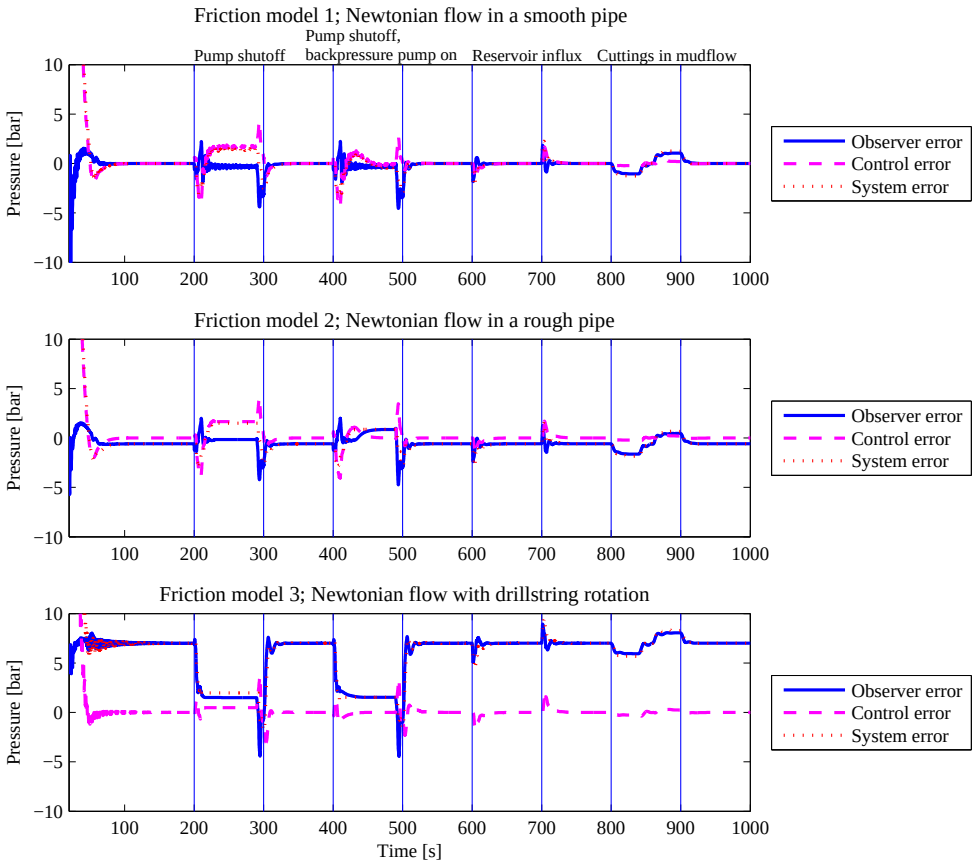

Figure 5-4: Closed-loop system performance of PI control with adaptive observer on the validation model during various drilling situations with different friction behaviour.

5-2 Summary and concluding remarks

In this chapter, two control systems are tested with the validation model simulating drilling situations, noise and varying friction behaviour. For the various drilling situations both the PI and LQR controller are able to control the BHP to its setpoint and keep the BHP within the drilling window. Furthermore, a worst-case scenario is simulated and both controllers are still able to detect influx and control the BHP. During the various situations and the worst-case scenario, it was seen that the performance of the PI controller was slightly better than the LQR controller during pump shut down. This is due to the fact that full state feedback is no longer possible at that instance. The BHP controlled with LQR controller was slightly outside the range of the drilling window.

Secondly, process and measurement noise are introduced and simulated on the validation model. The BHP is still controlled with an error less than 5 bar and both control systems did not become unstable due to the noise. It is seen that the LQR controller is able to reduce the influence of noise slightly by anticipating on the noise through adjusting the state weighting matrix. The PI gains could also be adjusted to the noise but this will significantly reduce the controllers performance.

Finally, different frictional pressure drops are applied on the validation model. It is shown that for Newtonian fluids in a rough pipe, the control system is able to control the BHP accurately within the drilling window. However, if an offset in the friction is introduced to simulate the frictional pressure drop due to drillstring rotation, the BHP is not estimated correctly anymore by the observer. The BHP is therefore also not controlled to its setpoint. This is thus an observer issue, the control error is (as is shown) still near zero throughout the drilling situations. A remark should be made here that it is important to have the right friction model implemented in the observer in order to make correct BHP estimations.

From this chapter, where the controllers were tested on a validation model, it can be concluded that the PI and LQR controller both have advantageous characteristics. The PI controller performs better during loss of flow, since the controlled BHP by LQR controller becomes erroneous at that instance. On the other hand, the LQR controller performs better during noise by adjusting the weighting matrix to the potential noise. A summary of characteristics of the PI and LQR controller found in Chapter 4 and this chapter is listed in Table 5-1. From the results that are achieved in this research and the fact that the PI controller requires no adjustments during drilling, the PI controller is currently preferred. A remark should be made here that more research could be done in practical implementation of the LQR controller and perhaps a solution can be found to decrease the error during loss of flow.

Table 5-1: PI and LQR characteristics.

	PI	**LQR**
Operator usage	Tuning can be done beforehand, no adjustments required	Q matrix needs to be tuned according to system parameters
Overal performance	BHP is kept within drilling window	BHP is kept within drilling window, except during worst-case scenario
Drilling situations	Robust to drilling situations	Error during loss of bottomhole flow
Noise	Stable during noise	Performs better during noise by adjusting the weighting matrix

Chapter 6

Conclusions and recommendations

6-1 Conclusions

In this thesis, a control system is designed for MPD. Therefore, two models are presented to model the well. The first one simplifies the well by dividing it into a drillstring and an annulus section and is used to design the estimator. The other is designed to serve as a validation model, simulating the well dynamics more realistically by discretising the well into multiple sections. Furthermore, a case study is defined in order to simulate drilling situations, noise and varying frictional pressure drops on the validation model. Also, an investigation is done on the estimation problem of the well. Parametric uncertainties and their influence on the BHP are investigated. It was determined that reservoir influx and annular density need to be estimated simultaneously with the bottomhole flowrate (and pressure).

After a model of the well is defined, two estimators are proposed that are able to deal with the nonlinearities of the system and predict unknown and uncertain parameters. An EKBF and an adaptive observer are designed to serve as a solution to overcome the problem of having no real-time bottomhole measurements. Both proved to estimate the BHP accurately, however, during loss of flow, convergence is not guaranteed anymore for the EKBF. On the other hand, the EKBF has the advantage that it is able to filter noise. The adaptive observer estimates the BHP accurately during different drilling situations and convergence is shown. For these reasons, the adaptive observer was used in the continuation of the research.

Now that the BHP can be estimated by using surface measurements, known information and estimated uncertain values, the BHP should be controlled as well. In order to do so, two practical control methods, namely PI and LQR control, are applied. Both controllers are combined with feedforward control and integrator anti-windup. It is shown that these control methods are sufficient to control the BHP within 1 bar of its setpoint. Now that the MPD control system is complete, all required parameters are defined and it is investigated if these are provided as a measurement by the system, should be pre-set in the control system or have to be provided by the operator. This is done to examine if system is easy to use for operators on the rig. A suggestion is given on how the PI controller can be implemented so that it does not need adjustments to its control parameters during drilling.

The MPD control system is validated against the earlier defined multiple compartment model. Various drilling situations, noise and different frictional pressure drops are simulated on the validation model to examine the performance and robustness of the control system. It is shown that both the PI and LQR controller are able to control the BHP within the drilling window (of $\pm$ 5 bar). Simulating an offset on the frictional pressure drop in the well causes a problem for the control systems. A solution for this issue will be recommended in the next section.

To conclude, a control system for MPD is developed that is able to control the BHP within the drilling window by using only surface measurements. In addition, the developed control system is easy to use for operators.

6-2 Recommendations

Before being able to apply the MPD control system to drill a well, more research is required and several issues are left pending. There are many interesting questions to be dealt with for any future work on this subject. Therefore, several recommendations for future work are made.

- Big improvements regarding the reliability of this estimator and control strategy can be made by validating the developed control strategy to more realistic validation models. The validation model used in this research is ultimately still a simplification, since ODE's are used instead of PDE's. Thus a more complicated model, such as the full flow model developed by SINTEF [38] which also includes temperature effects, could be used. Also, the currently used adaptive observer should be validated against real well data, which were not available during this research project.

- Analyze the suitability of the developed control strategy to wells that have more nonlinear dynamic effects. Even though the current control strategy has proven to be robust in estimating and controlling the BHP during various situations, investigations can be done in both the observer and controllers under more nonlinear circumstances. Since, in practice, the dynamics behavior of the well could be more nonlinear than is currently simulated with the models used. In terms of a nonlinear observer, some research has already been done by developing an Unscented Kalman Filter, that is able to estimate the BHP under high nonlinearities [39]. It could be useful to examine if this estimator improves the observer performance in a real drilling scenario. With respect to nonlinear control it should be noted that both the current control solutions (PI and LQR) are linear control methods thus their robustness to more nonlinear conditions should be tested.

- Further investigation could be done on friction data from real wells. If the frictional pressure drop is indeed behaving as the modelled Newtonian fluid, the current adaptive observer will be able to make a good estimation of the BHP. However, if the fluid behaves for instance as a different type of fluid (e.g. Herschel-Bulkley fluid) or an unexpected offset in pressures losses is present, the observer needs to be redesigned in order to estimate the BHP.

- As mentioned in the introduction of this research there is another way to receive information about the bottomhole than using an estimator, namely mud pulse telemetry. As explained, data from mud pulse telemetry is slow, nevertheless, measurements can be made, for instance every 30 seconds. In order to improve the observers outcomes, these downhole measurements could be fed to the observer to update the estimation.
- Another option to consider is to include the backpressure pump in the control system. The backpressure pump is now actuated but it is not included in the feedback loop. It could be implemented in the feedback loop, giving a control signal for both the choke valve and the backpressure pump simultaneously (multiple-input control). Once the backpressure pump is included in the closed loop, better performance might be obtained in case of low flow from the main mud pump.
- An aspect that is now left out of this research are the nonlinearities of the choke valve. In practice, the choke valve will have (mechanical) backlash and there is a delay between sending the control signal and actual movement of the valve. This could delay the response to disturbances and decrease the system's performance. A remark should be made that it is uncertain if this will actually decrease the control systems performance, since the well itself has propagation delays as well. So if the response time of the well to pressure changes is slower than the choke valve's, the influence of nonlinearities of the choke might be small. Nevertheless, it is suggested to research this topic as well.

Appendix A

Base case parameters

Table A-1: Base case parameters and descriptions.

Parameter	Unit	Value	Scaled value	Description
β_a	Pa	$1.4 \cdot 10^9$	$1.4 \cdot 10^4$	Bulk modulus in annulus
β_d	Pa	$1.4 \cdot 10^9$	$1.4 \cdot 10^4$	Bulk modulus in drillstring
δ	mm	$3 \cdot 10^{-6}$	-	Absolute roughness
d_{ai}	m	0.216	-	Inner diameter annulus
d_{di}	m	0.097	-	Inner diameter drillstring
d_{do}	m	0.114	-	Outer diameter drillstring
g	m/s^2	9.81	-	Gravitational acceleration
F_a	-	$4.75 \cdot 10^5$	-	Friction factor annulus
F_d	-	$5.63 \cdot 10^6$	-	Friction factor drillstring
h_{bit}	m	$2 \cdot 10^3$	-	Vertical depth of bit
M_a	kg/m^4	$8 \cdot 10^7$	$8 \cdot 10^2$	Integrated density per cross section
M_d	kg/m^4	$2.7 \cdot 10^8$	$2.7 \cdot 10^3$	Integrated density per cross section
p_0	Pa	$1 \cdot 10^5$	1	Atmospheric pressure
ρ_a	kg/m^3	1490	$1.49 \cdot 10^{-2}$	Density in annulus
ρ_d	kg/m^3	1490	$1.49 \cdot 10^{-2}$	Density in drillstring
SG	-	1.49	$1.49 \cdot 10^{-5}$	Specific gravity
V_a	m^3	52.7	-	Volume annulus
V_d	m^3	14.8	-	Volume drillstring
Initial conditions				
p_c	Pa	$50 \cdot 10^5$	50	Choke pressure
p_p	Pa	$80 \cdot 10^5$	80	Pump pressure
q_{bit}	m^3/s	$1.67 \cdot 10^{-2}$	-	Flow through bit at bottomhole
q_p	m^3/s	$1.67 \cdot 10^{-2}$	-	Flow through pump

Appendix B

Multiple compartment model plots

In this appendix, additional plots of the multiple compartment model are shown in order to visualize the compartments. The multiple compartment model is discussed in Chapter 2-2.

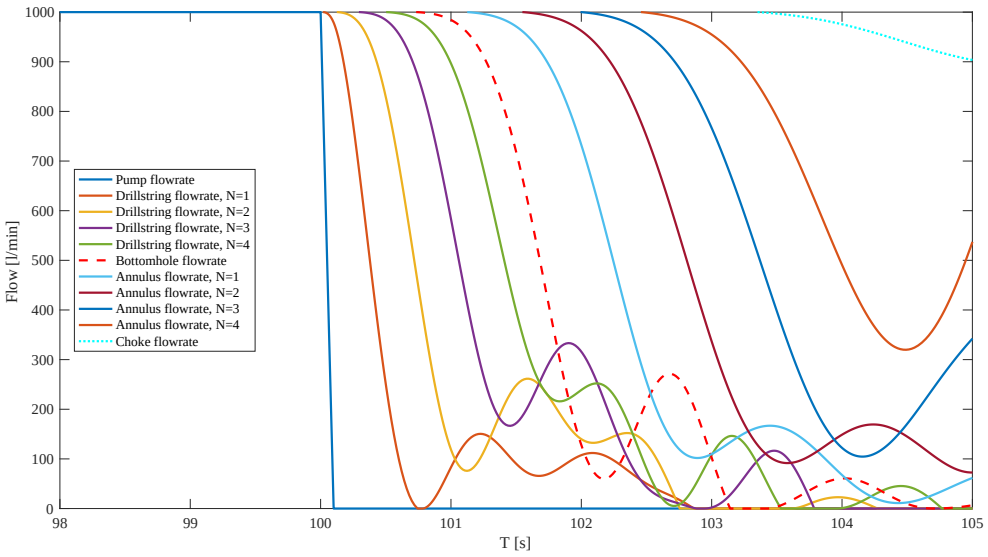

Figure B-1: Pulse propagation in the flow of the validation model after pump shut down.

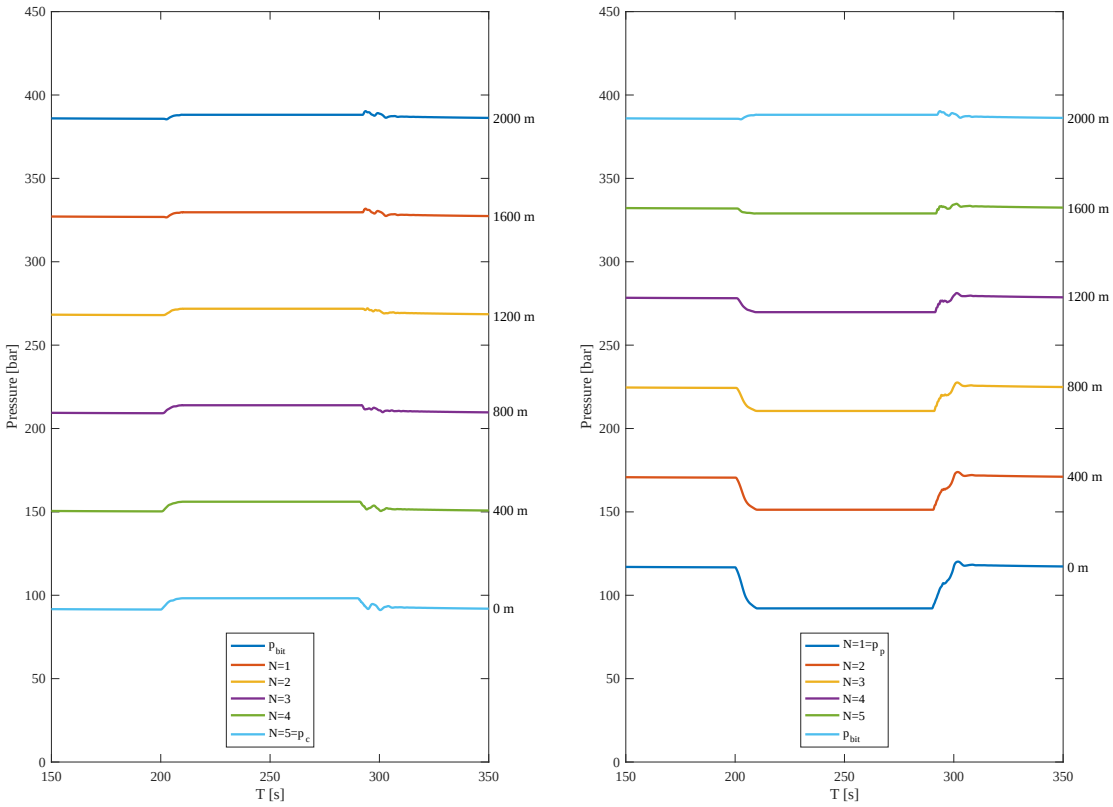

(a) Pressures in the annulus.

(b) Pressures in the drillstring.

Figure B-2: Pressures at control volumes during pump shut-off at t=200 s and start up at t=400 s distributed over well depth.

Appendix C

LQR validation results

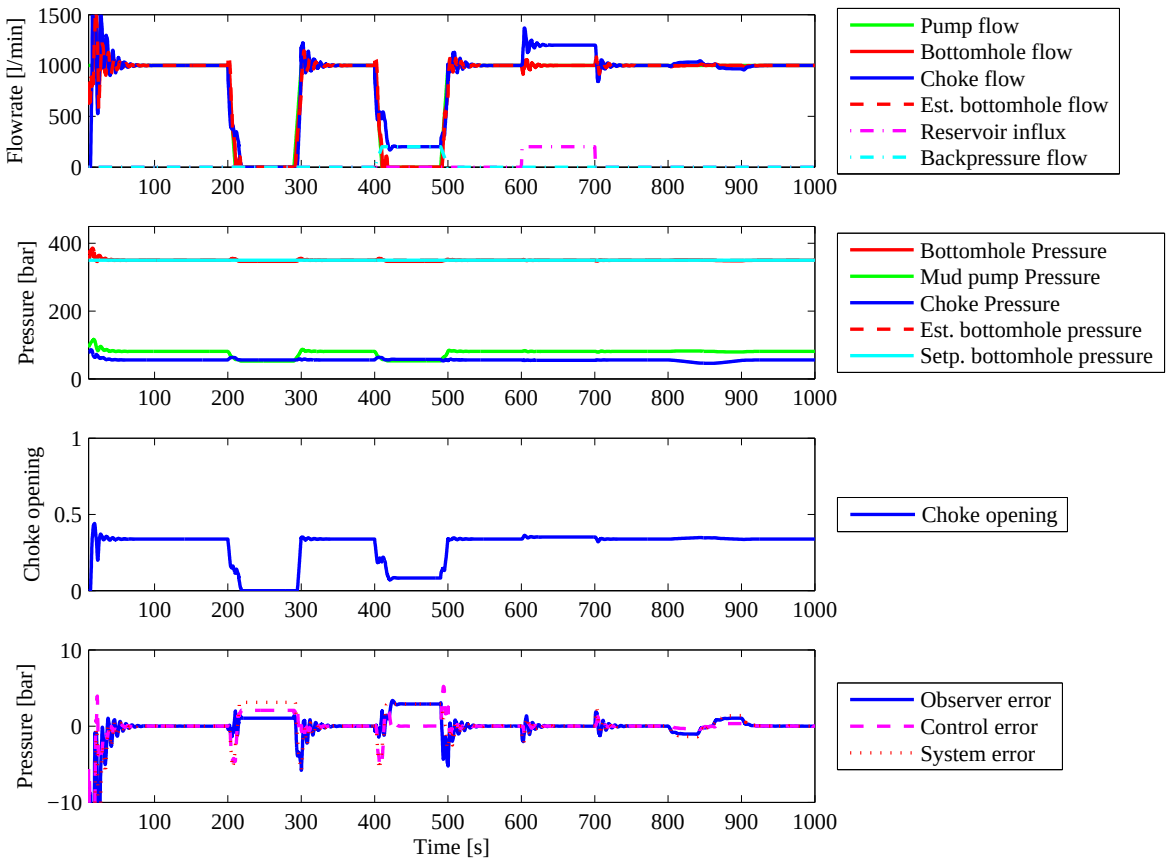

Figure C-1: Closed-loop system performance of LQR controller with adaptive observer on the validation model during various drilling situations.

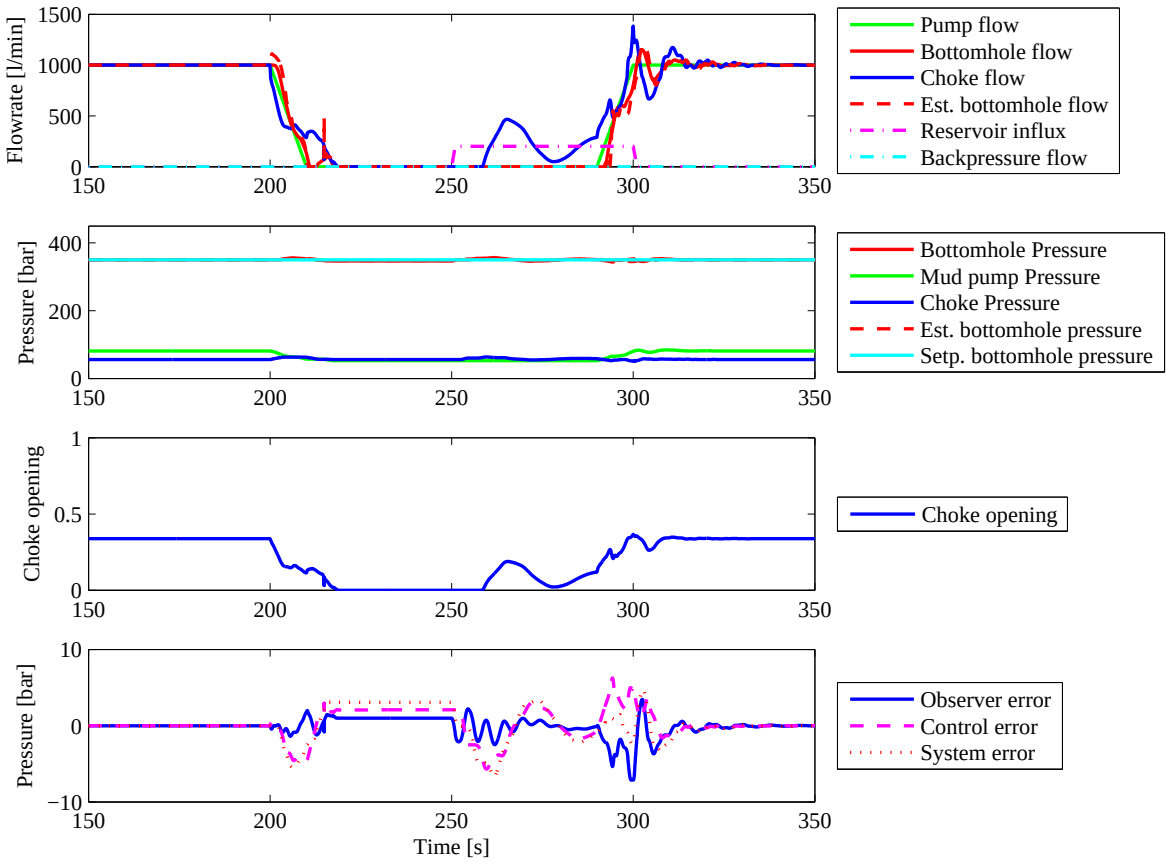

Figure C-2: Closed-loop system performance of LQR controller with adaptive observer on the validation model during various drilling a worst-case scenario.

Bibliography

[1] B. Rehm, A. Haghshenas, A. S. Paknejad, and J. Hughes, *Managed Pressure Drilling*. Gulf Publishing Company, 2008.

[2] Ø. Breyholtz, G. Nygaard, H. Siahaan, and M. Nikolau, "Managed Pressure Drilling: A Multi-Level Control Approach," *SPE Intelligent Energy Conference and Exhibition*, 2010.

[3] J. Godhavn, A. Pavlov, G. Kaasa, and N. Rolland, "Drilling seeking automatic control solutions," *18th IFAC World Congress*, 2011.

[4] "Axon energy products, chokemaster drilling choke." http://www.axonep.com/chokemaster%E2%84%A2-drilling-choke, 2016-11-05.

[5] O. A. I.S. Landet, A. Pavlov and H. Mahdianfar, "Control of Heave-Induced Pressure Fluctuations in Managed Pressure Drilling," *American Control Conference*, 2012.

[6] M. Rohani, "Managed Pressure Drilling; Techniques and options for improving operational safety and efficiency," *Petroleum & Coal*, vol. 54, 2012.

[7] F. Bartlit, S. Sankar, and S. Grimsley, "Chief Counsel Report," 2011.

[8] "Managed Pressure Drilling." http://www.iadclexicon.org/managed-pressure-drilling-mpd. Accessed: 2016-02-17.

[9] P. Fredericks and D. Reitsma, "MPD automation adresses drilling challenges in conventional, unconventional resources," *Drilling Contractor*, 2006.

[10] D. Hannegan, "Offshore drilling hazard mitigation: Controlled pressure drilling redefines what is drillable," *Drilling Contractor*, 2009.

[11] J. McCaskill and B. Goodwin, "Managing wellbore pressure while drilling," *Drilling Contractor*, 2006.

[12] D. Gala and J. Toralde, "Managed Pressure Drilling 101: Moving Beyond 'it's Always Been Done That Way'," *the Way Ahead*, vol. 7, 2011.

[13] G. Kaasa, Ø. Stamnes, L. Imslanda, and O. Aamo, "Simplfied Hydraulics Model Used for Intelligent Estimation of Downhole Pressure for a Managed-Pressure-Drilling Control System," *SPE/IADC Drilling Conference*, 2012.

[14] B. Guo and G. Liu, *Applied Drilling Circulation Systems: Hydraulics, Calculations and Models*. GPP, 2011.

[15] Ø. Stamnes, *Nonlinear Estimation with Applications to Drilling*. PhD thesis, Norwegian University of Science and Technology, April 2011.

[16] H. Mahdianfar and A. Pavlov, "Adaptive output regulation for offshore managed pressure drilling," *International journal of adaptive control and signal processing*, 2016.

[17] R. Caenn, H. C. Darley, and G. R. Gray, *Composition and properties of drilling and completion fluids*. Gulf professional publishing, 2011.

[18] M. Verhaegen and V. Verdult, *Filtering and System Identification*. Cambridge, 2011.

[19] R. Kalman and R. Bucy, "New Results in Linear Filtering and Prediction Theory," *Journal of Basic Engineering*, 1961.

[20] L. Ray, A. Ramasubramanian, and J. Townsend, "Adaptive friction compensation using extended Kalman-Bucy filter friction estimation," *Control engineering practice*, 2001.

[21] Y. Wang and M. Papageorgiou, "Real-time freeway traffic state estimation based on extended kalman filter: a general approach," *Transportation Research Part B: Methodological*, vol. 39, no. 2, pp. 141–167, 2005.

[22] E. Wan and R. van der Merwe, "The Unscented Kalman Filter for Nonlinear Estimation," *Oregon Graduate Institute of Science & Technology*, 2000.

[23] R. Van Der Merwe and E. A. Wan, "The square-root unscented kalman filter for state and parameter-estimation," in *Acoustics, Speech, and Signal Processing, 2001. Proceedings.(ICASSP'01). 2001 IEEE International Conference on*, vol. 6, pp. 3461–3464, IEEE, 2001.

[24] G. Welch and G. Bishop, "An Introduction to the Kalman Filter," *University of North Carolina at Chapel Hill*, 2001.

[25] K. Reif, S. Gunther, and E. Yaz, "Stochastic Stability of the Discrete-Time Extended Kalman Filter," *IEEE Transactions on automatic control*, 1999.

[26] J. Walrand and A. Dimakis, *Random Processes in Systems - Lecture Notes*. University of Californa, 2006.

[27] Y. Tan and I. Kanellakopoulos, "Adaptive nonlinear friction compensation with parametric uncertainties," *American Control Conference*, 1999.

[28] N. Jo and Y. Son, "Adaptive Observer Design for Nonlinear Systems Using Generalized Nonlinear Observer Canonical Form," *KSME International Journal*, 2004.

[29] J. Zhou, O. N. Stamnes, O. M. Aamo, and G.-O. Kaasa, "Adaptive output feedback control of a managed pressure drilling system," in *Decision and Control, 2008. CDC 2008. 47th IEEE Conference on*, pp. 3008–3013, IEEE, 2008.

[30] O. N. Stamnes, J. Zhou, G.-O. Kaasa, and O. M. Aamo, "Adaptive observer design for the bottomhole pressure of a managed pressure drilling system," in *Decision and Control, 2008. CDC 2008. 47th IEEE Conference on*, pp. 2961–2966, IEEE, 2008.

[31] A. Mecaelli and C. Samson, "Trajectory tracking for unicycle-type and two-steering-wheels mobile robots," *Rapport de recherche 2097*, 1993.

[32] A. Lefeber, "Tracking control of nonlinear mechanical systems," *Universiteit Twente*, 2000.

[33] W. E. Dixon, A. Behal, D. M. Dawson, and S. P. Nagarkatti, *Nonlinear control of engineering systems: A Lyapunov-based approach*. Springer Science & Business Media, 2013.

[34] C. Willmott, "Some Comments on the Evaluation of Model Performance," *Bulletin of the American Meteorological Society*, 1982.

[35] K. H. Ang, G. Chong, and Y. Li, "Pid control system analysis, design, and technology," *IEEE transactions on control systems technology*, 2005.

[36] G. F. Franklin, J. D. Powell, and A. Emami-Naeini, *Feedback control of dynamic systems*, vol. 4. Prentice Hall, 2002.

[37] J. Hespanha, "Lecture notes on lqr/lqg controller design," 2005.

[38] J. Petersen, R. Rommetveit, K. S. Bjorkevoll, J. Froyen, *et al.*, "A general dynamic model for single and multi-phase flow operations during drilling, completion, well control and intervention," in *IADC/SPE Asia Pacific Drilling Technology Conference and Exhibition*, Society of Petroleum Engineers, 2008.

[39] H. Mahdianfar, A. Pavlov, and O. M. Aamo, "Joint unscented kalman filter for state and parameter estimation in managed pressure drilling," in *European Control Conference, IEEE*, 2013.

Glossary

List of Acronyms

BOP	Blowout Preventer
BHP	Bottomhole Pressure
EKBF	Extended Kalman-Bucy Filter
LQR	Linear quadratic regulator
MPD	Managed Pressure Drilling
NPT	Non-productive Time
ODE	Ordinary Differential Equation
PDE	Partial Differential Equation
PI	Proportional Integral
RCD	Rotating Control Device
RMSE	Root Mean Squared Error
VAF	Variance Accounted For

List of Symbols

α	Cubical expansion coefficient [$^{\circ}C^{-1}$]
β	Bulk modulus [Pa]
β_a	Bulk modulus annulus [Pa]
β_d	Bulk modulus drillstring [Pa]

δ	Absolute roughness [mm]
ϵ	Relative roughness
η	Vector function based on known parameters
Γ	Gain matrix
γ	Angle [°]
μ	Viscosity [kg/(ms)]
ϕ	Regressor
ρ	Density [kg/m^3]
ρ_a	Density in annulus [kg/m^3]
ρ_d	Density in drillstring [kg/m^3]
ρ_w	Density water [kg/m^3]
σ	Second change of coordinates
τ	Lumped friction term
Θ	Vector of unknown variables
θ	Unknown variable
ξ	New coordinate of adaptive observer
Δp_f	Friction along flow path [Pa]
$_n$	New scaled parameter
A	State matrix
A_s	Area [m^2]
B	Input matrix
C	Measurement matrix
c	Speed of sound [m/s]
C_v	Valve sizing coefficient
d	Diameter [m]
d_{ai}	Inner diameter annulus [m]
d_{di}	Inner diameter drillstring [m]
d_{do}	Outer diameter drillstring [m]
e	Error
F	Friction factor containing known parameters
f	Nonlinear system dynamics
F_a	Annulus friction factor
f_b	Blasius friction factor
F_d	Drillstring friction factor
f_c	Chen's friction factor
G	Gravitational component affecting the fluid
g	Acceleration of gravity [m/s^2]
h	Nonlinear output function
h_{bit}	Vertical depth [m]
J	Performance index

k	Time step
K_a	Anti-windup gain
K_e	Kalman-Bucy gain
K_p	Proportional gain
K_r	LQR gain
K_f	Feedforward gain
L	Observer gain
l	Length of flow path [m]
M	Integrated density per cross section [kg/m^4]
M_a	Integrated mass over annular cross section [kg/m^4]
M_d	Integrated mass over drillstring cross section [kg/m^4]
N	Number of compartments
N_v	Number of VAF data samples
P	Covariance of measurement error/LQR Riccati solution
p	Pressure [Pa]
p_c	Choke pressure [Pa]
p_p	Pump pressure [Pa]
p_{bit}	Bottomhole pressure [Pa]
p_{setp}	Bottomhole pressure setpoint [Pa]
Q	Covariance matrix of process noise/LQR state weighting matrix
q	Flow rate [m^3/s]
q_c	Choke flowrate [m^3/s]
q_p	Main mud pump flowrate [m^3/s]
q_{bit}	Bottomhole flowrate [m^3/s]
q_{bpp}	Backpressure flowrate [m^3/s]
q_{res}	Reservoir flowrate [m^3/s]
R	Covariance matrix of measurement noise/LQR control input weight
Re	Reynolds number
S	Scaling factor
SG	Specific gravity
T	Temperature [°C]
t	Time [s]
T_i	Integral time [s]
u	Control vector
V	Volume [m^3]
v	Process noise
V_a	Volume drillstring [m^3]
V_d	Volume drillstring [m^3]
V_l	Lyapunov function
v_s	Velocity [m/s]

w	Process noise
x	State vector
x_s	Spatial coordinate [m]
y	Output vector
z	Choke position
z_e	Additional integral LQR state